LECTURE NOTES

ON

ADVANCED COMPUTATIONAL AERODYNAMICS

IV B. Tech I semester (JNTUH-R15)

Ms. D.ANITHA
Assistant Professor

AERONAUTICAL ENGINEERING
INSTITUTE OF AERONAUTICAL ENGINEERING
(Autonomous)
DUNDIGAL, HYDERABAD - 500 043

UNIT – I

Panel Methods

In most of these cases the geometry was approximated by flat, zero-thickness surfaces and for additional simplicity the boundary conditions were transferred, too, these simplified surfaces (e.g., at $z = 0$).
The application of numerical techniques allows the treatment of more realistic geometries and the fulfillment of the boundary conditions on the actual surface. In this the methodology of some numerical solutions will be examined and applied to various problems. The methods presented here are based on the surface distribution of singularity elements, which is a logical extension of the analytical methods presented in the earlier chapters. Since the solution is now reduced to finding the strength of the singularity elements distributed on the body's surface this approach seems to be more economical, from the computational point of view, than methods that solve for the flow field in the whole fluid volume (e.g., finite difference methods). Of course this comparison holds for inviscid incompressible flows only, whereas numerical methods such as finite difference methods were basically developed to solve the more complex flow fields where compressibility and viscous effects are not negligible.

1.1 Basic Formulation

Consider a body with known boundaries S_B , submerged in a potential flow, as shown in Fig. 1.1. The flow of interest is in the outer region V where the incompressible, irrotational continuity equation, in the body's frame of reference, in terms of the total potential $\mathcal{B}^*$ is

$$\nabla^2 \mathcal{B}^* = 0 \qquad (1.1)$$

Following Green's identity, as presented in Section 3.2, we can construct the general solution to Eq. (1.1) by a sum of source σ and doublet μ distributions placed on the boundary S_B

Here the vector **n** points in the direction of the potential jump μ, which is normal to S_B and positive outside of V (Fig. 1.1), and $\mathcal{B}_\infty$ is the free-stream potential written as

$$\mathcal{B}_\infty = U_\infty x + V_\infty y + W_\infty z \qquad (1.2)$$

This formulation does not uniquely describe a solution since a large number of source and doublet distributions will satisfy a given set of boundary conditions. Therefore, a choice has to be made in order to select the desirable combination.

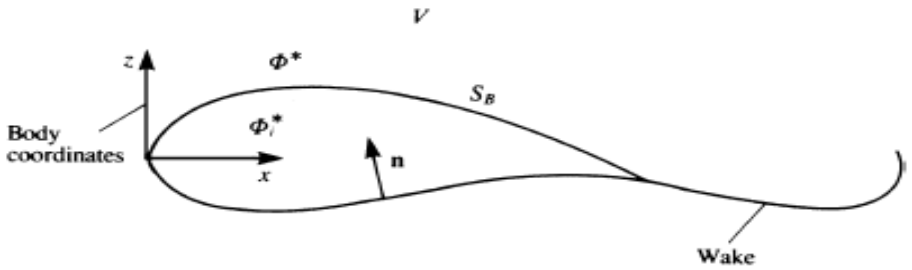

Figure 1.1 Potential flow over a closed body.

It is clear from the previous examples that for simulating the effect of thickness, source elements can be used, whereas for lifting problems, antisymmetric terms such as the doublet (or vortex) can be used. To uniquely define the solution of this problem, first the boundary conditions of zero flow normal to the surface must be applied. In the general case of three-dimensional flows, specifying the boundary conditions will not immediately yield a unique solution because of two problems. First, a decision has to be made in regard to the "right" combination of source and doublet distributions. Second, some *physical* considerations need to be introduced to fix the amount of circulation around the surface S_B . These considerations deal mainly with the modeling of the wakes and fixing the wake shedding lines and their initial orientation and geometry. (This is the three-dimensional equivalent of a two-dimensional Kutta condition.)

1.2 The Boundary Conditions

The boundary condition for Eq. (1.1) can directly specify a zero normal velocity component $\partial\delta^*/\partial n = 0$ on the surface S_B, in which case this "direct" formulation is called the Neumann problem. It is possible to specify δ^* on the boundary, so that indirectly the zero normal flow condition will be met, and this "indirect" formulation is called the Dirichlet problem. Of course, a combination of the above boundary conditions is possible, too, and this is called a mixed boundary condition problem.

An additional approach would be to search for a singularity distribution that creates enclosed streamlines, equivalent to the geometry of the surface S_B. This method is useful in two dimensions, where the stream function W is well defined but for complex, three-dimensional geometries the implementation of this method is difficult and will not be dealt with here.

1.2.1 Physical Considerations

The above mathematical formulation, even after selecting a desirable combination of sources and doublets, and after fulfilling the boundary conditions on the surface S_B, is not unique. Previous examples showed that for describing the flow over thick bodies without lift the source distribution was sufficient, but for the lifting cases the amount of the circulation was not uniquely defined.

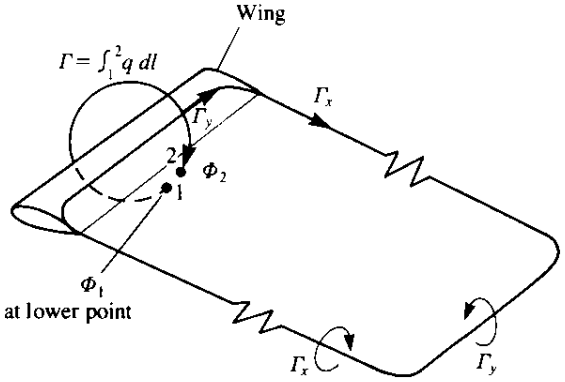

Figure 1.2 Vorticity system created by a finite wing in steady forward flight.

Let us examine the case of a lifting wing, as viewed from a large distance (Fig. 1.2). For simplicity, the bound vortex is represented by a concentrated vortex line with the strength T ($=T_X = T_Y$). According to the Helmholtz theorems a vortex line cannot start in a fluid and we can write which for the simple case of Fig. 1.2 implies that the problem is modeled by one constant- strength, closed vortex line. Also, the amount of the bound circulation is where point 1 lies under and point 2 is above the (very) thin wake. These two arguments clearly demonstrate that for the three dimensional lifting problem there is a need to model a wake, since the bound vorticity needs to be continued beyond the wing. Also, as shown in Fig. 1.2, for the wing to have circulation T at a spanwise location, a discontinuity in the velocity potential near the trailing edge must exist:

$$\delta_2 - \delta_1 = T$$

where δ_1 is under and δ_2 is above the wake. Now we are in a position where the additional *physical* conditions, required for a unique solution, can be established in relation to a *wake model*. This model has to specify two additional conditions:

1. To set the wake strength at the trailing edge.
2. To set its shape and location.

a. *Wake Strength*

The simplest solution to this problem is to apply the two-dimensional Kutta con- dition along the three-dimensional trailing edge (as shown in Fig. 1.3) such that

$$\gamma_{T.E.} = 0 \qquad (1.4)$$

Since, for example, in the two-dimensional case $\partial\mu(x)/\partial x = -\gamma(x)$ the above condition can be rewritten for the trailing-edge line, such that μ is constant in the

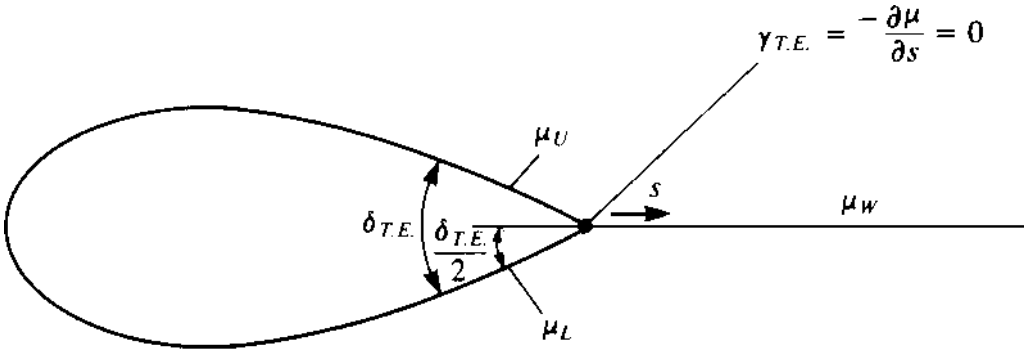

Figure 1.3 Implementation of the Kutta condition when using surface doublet distribution.

wake (μW) and equals the value at the trailing-edge ($\mu T.E.$), that is,

$$\mu T.E. = \text{const.} \equiv \mu W$$

or

$$\mu U - \mu L - \mu W = 0 \qquad (1.5)$$

where μU and μL are the corresponding upper and lower surface doublet strengths at the trailing edge, as shown in Fig. 1.3 This formulation is more useful for airfoils with very thin or even cusped trailing edges. As an example, the specification of the Kutta condition in terms of constant-strength doublet elements (or vortex rings) is shown in Fig. 1.4 (here for convenience a positive doublet points into the wing). At the wing's trailing edge, the trailing segment of the upper doublet will have a strength of $-TU$, the leading vortex segment of the lower surface (which is now inverted) will be $+TL$, and the leading segment of the wake vortex is $+TW$.

Thus, the strength of the wake panel in terms of the local circulation T is again

$$-TU + TL + TW = 0$$

or, exactly as in Eq. (1.5*a*),

$$TW = TU - TL \qquad (1.6)$$

In certain situations the shape of the trailing edge is also important. For example, Fig. 1.5a shows a situation where the flow leaves the trailing edge smoothly and parallel to the cusped trailing edge.

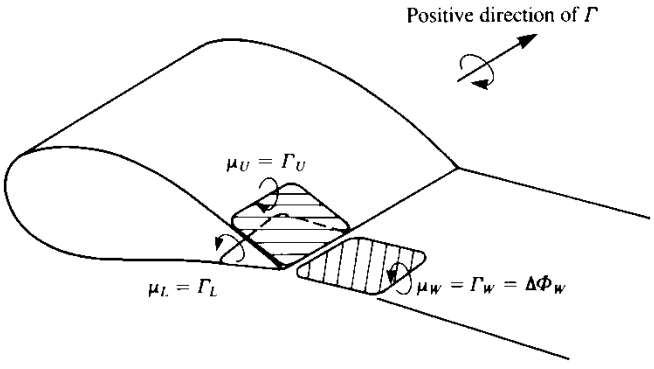

Figure 1.4 Implementation of the Kutta condition when using vortex ring elements.

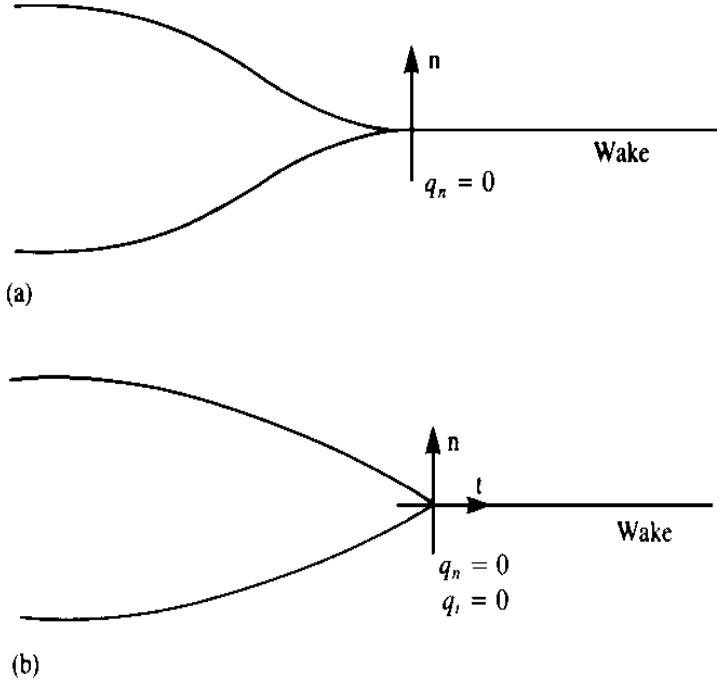

Figure 1.5 Possible conditions that can be applied at (a) cusp and (b) finite angle trailing edges.

In such situations this point is not necessarily a stagnation point and if the velocity formulation is used then only the $q_n = 0$ condition can be used. In the case that the trailing edge has a finite angle (Fig. 1.5b), then in order to have a continuous velocity at this point the condition $q_t = 0$ can also be used.

b. *Wake Shape*

In two dimensions, the trailing vortex segment of the wake is ignored since it has zero vorticity (in steady flow) and it is sufficient to specify the location of the trailing edge where the Kutta condition is met. In three dimensions, the wake influence is more dominant and its geometry clearly affects the solution. To distinguish between the models for bound circulation (which generate the lift) and the circulation shed into the wake, it is logical to assume that the wake should not produce lift – since it is not a solid surface. As an example, let us recall the formulation for the force **F** generated by a vortex sheet γ. The Kutta–Joukowski theorem for lift (Section 3.11) states that

$$\mathbf{F} = \rho \mathbf{q} \times \gamma \qquad (1.7)$$

For a three-dimensional case 6**F** = 0 only if the local flow is parallel to γ (we assume γ /=0). So the condition for the wake geometry is

$$\mathbf{q} \times \gamma_W = 0 \qquad (1.8)$$

or

$$\gamma_W \text{ "} \mathbf{q} \qquad (1.8a)$$

that is, the vorticity vector is parallel to the local velocity vector.

An equivalent representation of the wake by a thin doublet sheet is obtained by noting that $\gamma_W = -\nabla \mu_W$. If no force is produced by this lifting surface then Eq. (9.18) becomes

$$\mathbf{q} \times \nabla \mu_W = 0 \qquad (1.9)$$

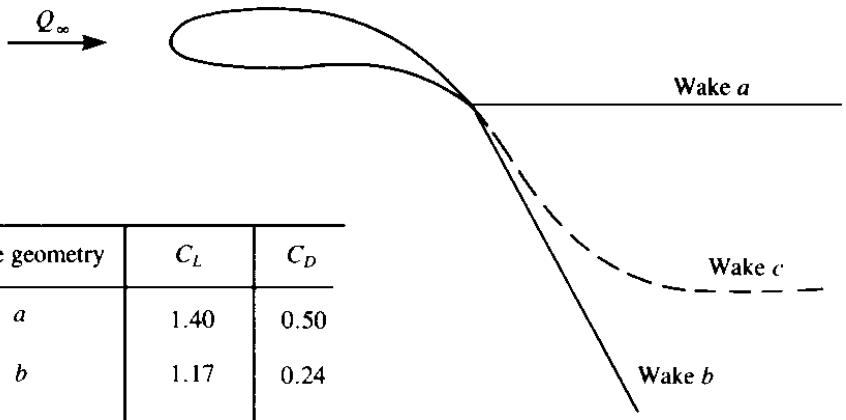

Wake geometry	C_L	C_D
a	1.40	0.50
b	1.17	0.24
c	1.22	0.33

Figure 1.6 Effect of prescribed wake geometry on the aerodynamics of an = 1.5 wing.

So the condition for the wake panels, in terms of doublets, is

$$\mu W = \text{const.} \qquad (1.9a)$$

and the boundaries of these elements (which are really the vortex lines) should be parallel to the local streamlines, as in Eq. (1.8*a*). This condition (Eq. (1.8*a*)) is difficult to satisfy exactly since the wake location is not known in advance. In most cases it is sufficient to assume that the wake leaves the trailing edge at a median angle $\delta T.E./2$, as shown in Figs. 1.3 and 1.4, whereas for portions of the wake far from the trailing edge, additional effort is required to satisfy the condition of Eq. (1.8).

As an example of the dependence of the solution on the wake initial geometry, the results for a cambered rectangular wing of aspect ratio 1.5 are shown in Fig. 1.6. The solution was obtained by a first-order panel method (VSAERO[9.3]) with 600 panels per semi span and the corresponding lift and drag coefficients are tabulated in the inset to the figure (incidentally, case *c* is the closest to experimental results).

1.2.2 Reduction of the Problem to a Set of Linear Algebraic Equations

At this point it is assumed that the problem is unique and that a combination of source/doublet distributions has been selected along with a wake model and the Kutta condition. For the following example $\delta = \delta\infty$ along with Eq. (1.2) for the source strength will be used and a constant-strength rectilinear panel is assumed. The body's surface (see Fig. 1.7) is now divided into N surface panels and into NW additional wake panels. The boundary condition (either Neumann or Dirichlet) will be specified at each of these elements at a collocation point (which for the Dirichlet boundary condition must be specified inside the body where $\mathcal{B}^* = \mathcal{B}\infty$, e.g., at a point under the center of the panel). In most cases, though, the point may be left on the surface without moving it inside the body. Rewriting, for example, the Dirichlet boundary condition for each of the N collocation points.

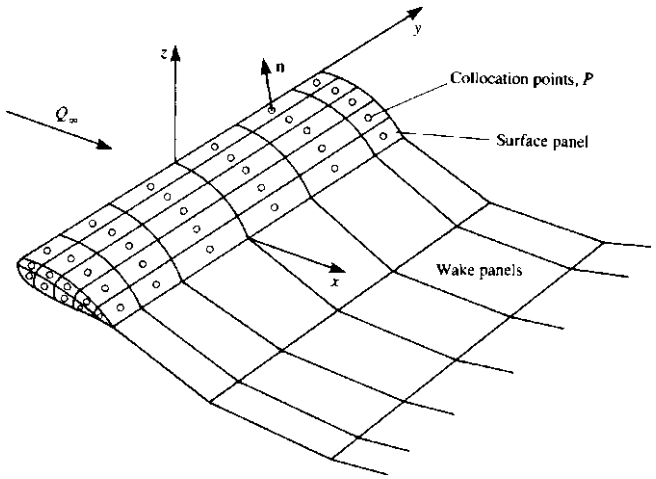

Figure 1.7 Approximation of the body surface by panel elements.

That is, for each collocation point *P* (shown in Fig. 1.7) the summation of the influences of all *k* body panels and *4* wake panels is needed. The integration in Equation is limited now to each individual panel element representing the influence of this panel on point *P*. For a unit singularity element (σ or μ), this influence depends on the panel's geometry only. The integration can be performed analytically or numerically, prior to this calculation, and for example for a constant-strength μ element shown in Fig. 1.8 the influence of panel *k* (defined by the four corners 1, 2, 3, and 4) at point *P* is and for a constant-strength σ element

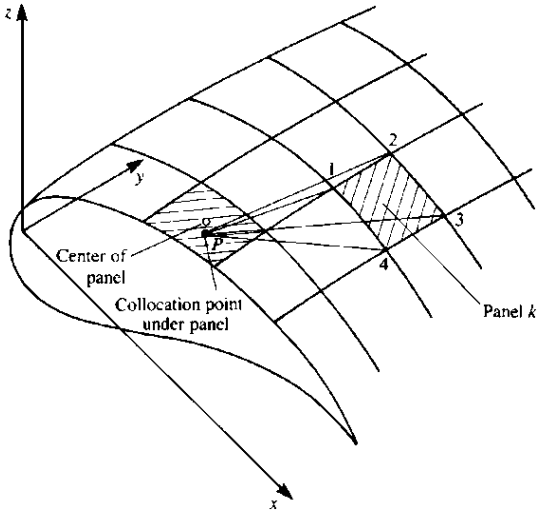

Figure 1.8 Influence of panel *k* on point *P*.

Also, by using the Kutta condition, the wake doublets can be expressed in terms of the unknown surface doublets μk . For example, in Fig. 1.9 two of the trailing edge (T.E.) doublets μr and μs (here *r, s,* and *t* are some arbitrary counters) are related to the corresponding wake doublet μt.

$$\mu t = \mu r - \mu s$$

and hence the influence of the wake element becomes

$$C t \mu t = C t \, (\mu r - \mu s)$$

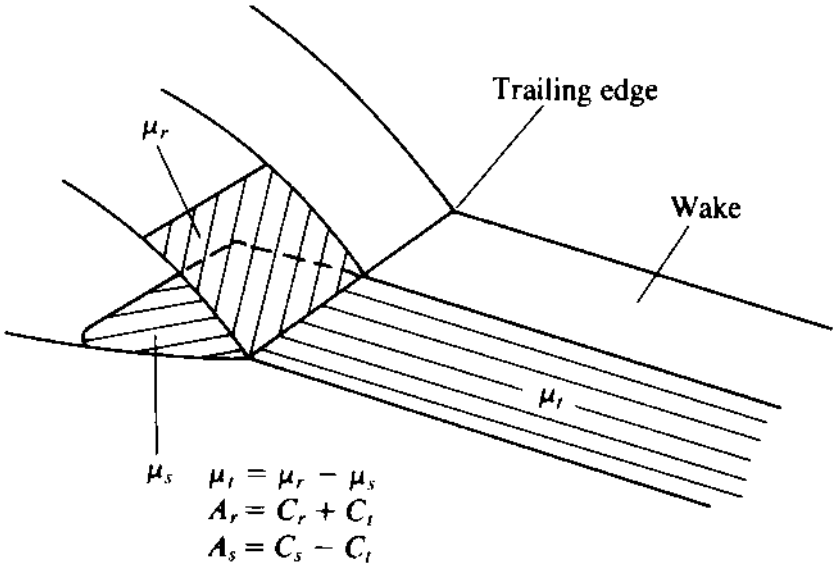

Figure 1.9 Relation between trailing edge upper and lower panel doublet strength and the corresponding wake doublet strength.

This algebraic relation can be substituted into the Ck coefficients of the unknown surface doublet such that

$Ak = Ck$ if panel is not at T.E.

$Ak = Ck \pm Ct$ if panel is at T.E.

where the ± sign depends on whether the panel is at the upper or the lower side of the trailing edge (Fig. 1.9).

Consequently, for each collocation point P, a linear algebraic equation containing N unknown singularity variables μ_k can be derived.

The derivation of the influence coefficient integrals depends on the shape of the panel element (e.g., planar, curved, etc.) and on the singularity distribution (constant or linearly varying strength, etc.). Some examples will be presented in the following chapters.

1.3 Aerodynamic Loads

Once Equation is solved the unknown singularity values are obtained (μ_k in this example). The velocity components are evaluated now in terms of the panel local coordinates (l, m, n) shown in Fig. 1.10. The two tangential perturbation velocity components are where the differentiation is done numerically using the values on the neighbor panels.

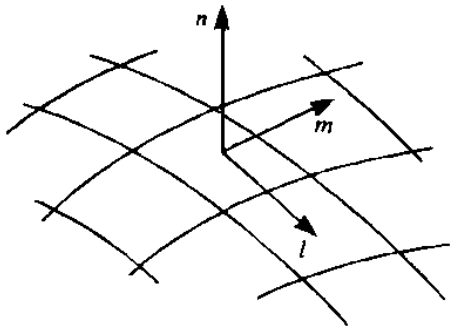

Figure 1.10 Panel local coordinate system for evaluating the tangential velocity components.

Strength:

$$q_n = -\sigma$$

The total velocity in the local (l, m, n) direction of panel k is

$$\mathbf{Q}k = (Q\infty_l, Q\infty_m, Q\infty_n)k + (ql, qm, qn)k$$

and of course the normal velocity component on a solid boundary is zero. The pressure coefficient can now be computed for each panel.

The contribution of this element to the nondimensional fluid dynamic loads is normal to the panel surface

In terms of the pressure coefficient the vector form for the panel contribution to the fluid dynamic load becomes

The individual contributions of the panel elements now can be summed to compute the desired aerodynamic forces and moments.

1.4 Preliminary Considerations, Prior to Establishing, Numerical Solutions Prior to establishing a numerical solution

a. *Type of singularity that will be used*: The options usually include sources, doublets, and vortices or any combination of the above.
b. *Type of boundary conditions*: Velocity or velocity-potential formulation may be used and the corresponding Neumann, Dirichlet, or a combination of such boundary conditions must be selected.
c. *Wake models*: How and where the Kutta condition will be specified. Also, the shape of the wake is controlled by Equation and can be set by Programmer-specified shape based on intuition or on flow visualizations.

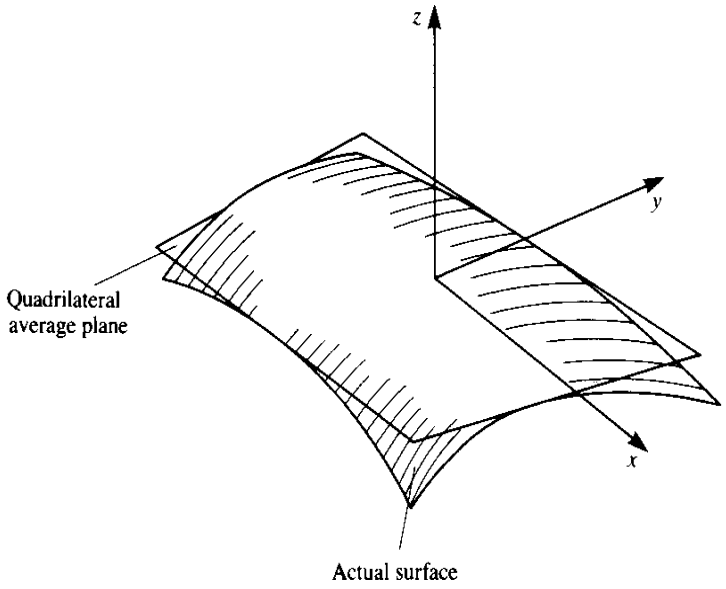

Figure 1.11 Nonplanar surface element and its quadrilateral approximation.

1. Wake relaxation (where the wake points are moved with the local induced velocity).

2. Time stepping (where the wake shape is developed by moving the wing from an initial stand-still position).

d. *Method of discretizing surface and singularity distributions*:

1. Discretization of geometry: The placing of a simple panel element on an arbitrary three-dimensional configuration is rather difficult. Figure 1.11 describes such a curved surface element with a local coordinate system x, y, z. The shape of the surface can be described as $z = f(x, y)$, but for simplicity it is usually approximated by a piecewise polynomial approximation. For example, if a first- order polynomial is used then the average surface can be described by

   $$z = a0 + b1x + b2\,y$$

   and for a second-order polynomial approximation

   $$z = a0 + b1x + b2\,y + c1x^2 + c2xy + c3\,y^2$$

   and so on (where the coefficients a, b, c are constants). Figure 1.11 shows the result of approximating a curved surface element by a first-order plane, while Fig. 1.12 shows the possible consequence of representing a three-dimensional curved surface by such quadrilateral elements. This representation of the geometry may result in difficulties in specifying the boundary conditions, since the "leakage" between the panels can weaken the satisfaction of the zero flow through the boundaries requirement. One possible solution is shown in Fig. 1.13 where the surface is described by five flat sub elements (as in the PANAIR code[9.4])

2. Discretization of singularity distribution: The strength of the surface distribution of the singularity elements can be represented, too, in terms of a piecewise polynomial approximation. For example, if the doublet distribution on the element of Fig. 1.11 is constant such that

   $$\mu = a0 = \text{const.}$$

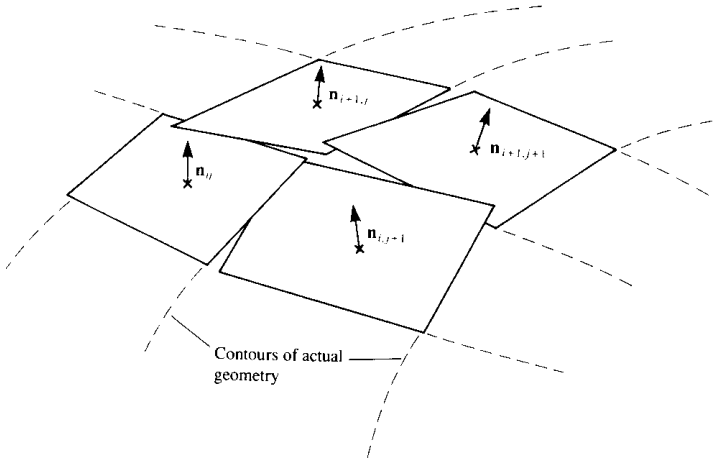

Figure 1.12 Possible difficulty in representing a three-dimensional surface by an array of quadrilateral surface elements.

then this is a zero-order approximation of μ. Similarly, a first-order (or linear) approximation is

$$\mu = a0 + b1x + b2\,y$$

and a second-order (or parabolic) polynomial approximation is

$$\mu = a0 + b1x + b2\,y + c1x^2 + c2xy + c3\,y^2$$

(Here the coefficients a, b, c are constants, too, and of course are different from the coefficients of the surface approximation).

e. *Considerations of numerical efficiency:* It is clear from the brief discussion on discretization that the computation of the influence coefficients is elaborate. Many methods divide such calculations into near and far field where the far field calculation treats the element as a point singularity (and not as a surface distribution).

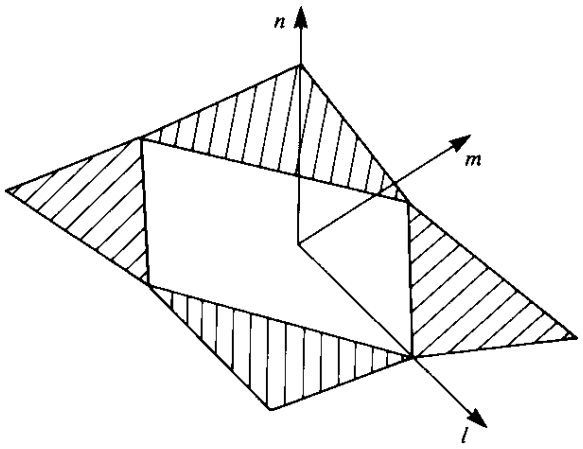

Figure 1.13 Description of a nonplanar panel element by a set of flat sub elements.

Typically, the near field is assumed if the distance to a point P is less than 2.5–5 times the larger diagonal of the panel. On the other hand because of the $1/r$ characteristics of the singularity elements, when $r \to 0$ the value of $1/r \to \infty$; therefore, when the point P is too close to the panel (or to a vortex line) cutoff distances are usually applied. (Only the aerodynamic aspects of the numerics are discussed here; other important aspects, e.g., the matrix solver efficiency, are not.)

1.5 Steps toward Constructing a Numerical Solution

When establishing a numerical solution for potential flow a sequence similar to the following is recommended.

a. Selection of Singularity Element

The first and one of the most important decisions is the type of singularity element or elements that will be used. This includes the selection of source, doublet, or vortex representation and the method of discretizing these distributions (zero-, first-, second-order, etc.). Also, all of the questions raised in the previous section need to be answered before the actual formulation of the solution can be constructed. Once these decisions have been made an influence routine, similar to the model needs to be established. This influence computation is a direct function of the element geometry and such a routine outputs the velocity components and the potential ($6u, 6v, 6w, 68$) induced by the element. In general, the implementation which represents the core of most numerical solutions. Therefore, in the next chapter some of the more frequently used singularity elements will be formulated.

b. Discretization of Geometry (and Grid Generation)

Once the basic solution element is selected, the geometry of the problem has to be subdivided (or discretized), such that it will consist of those basic solution elements. In this grid generating process, the elements' corner points and collocation points are defined. The collocation points are points where the boundary conditions, such as the zero normal flow on a solid surface, will be enforced. Figure 1.14a shows how the cambered thin airfoil at an angle of attack can be discretized by using the lumped-vortex element. In this case the camberline is divided into five panels and the locations of the collocation points and of the vortex points are shown in the figure. Similarly, the subdivision of a three-dimensional body into planar surface elements is shown in Fig. 1.14b. (The collocation points are not shown but they are at the center of the panel and may be slightly under the surface.) It is very important to realize that the grid *does* have an effect on the solution. Typically, a good grid selection will enable convergence to a certain solution when the density is increased (within reason). Moreover, a good grid selection usually will require some pre- liminary understanding of the problem's fluid dynamics, as will be shown in some of the forthcoming examples.

c. Influence Coefficients

In this phase, for each of the elements, an algebraic equation (based on the boundary condition) is derived at the collocation point. To generate the coefficients in an automatic manner, a unit singularity strength is assumed and the element influence routine is called at each of the collocation points (by a DO loop).

d. Establish RHS

The right-hand side of the matrix equation is the known portion of the free-stream velocity or the potential and requires mainly the computation of geometric quantities (e.g., $-Q_\infty \alpha$).

e. Solve Linear Set of Equations

The coefficients and the RHS of the algebraic equations were obtained in the previous steps and now the equations are solved by standard matrix techniques.

***f**. Secondary Computations: Pressures, Loads, Off-Body Velocity, Etc.*

The solution of the matrix equation results in the singularity strengths and the velocity field and any secondary information can be computed now. The pressures will be computed by Bernoulli's equation, and the loads and aerodynamic coefficients by adding up the contributions of the elements. A typical flowchart for such a computer program is shown in Fig. 1.15 where the sequence of computations is close to the above described methodology.

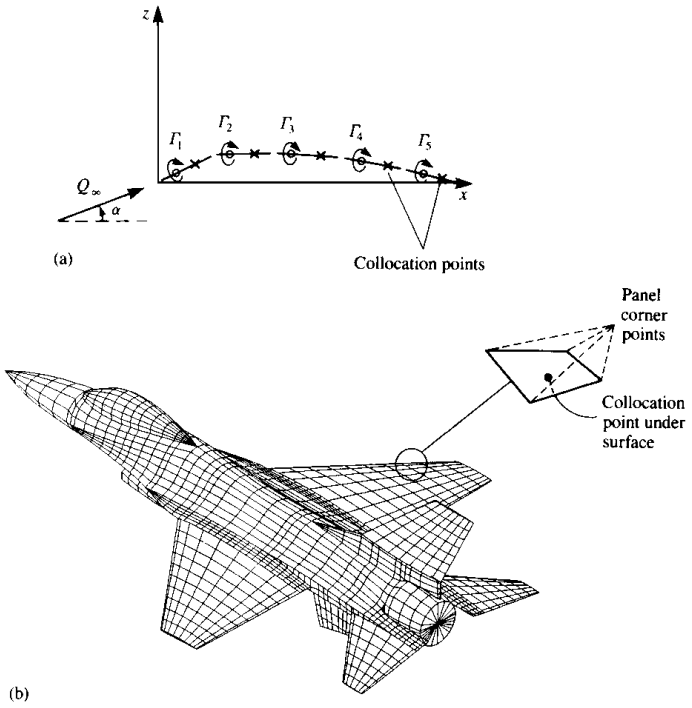

Figure 1.14 Discretization of (a) the geometry of a thin airfoil by using the lumped vortex element and of (b) a three-dimensional body using constant-strength surface doublets and sources.

In the following example, the essence of the above steps will be clarified.

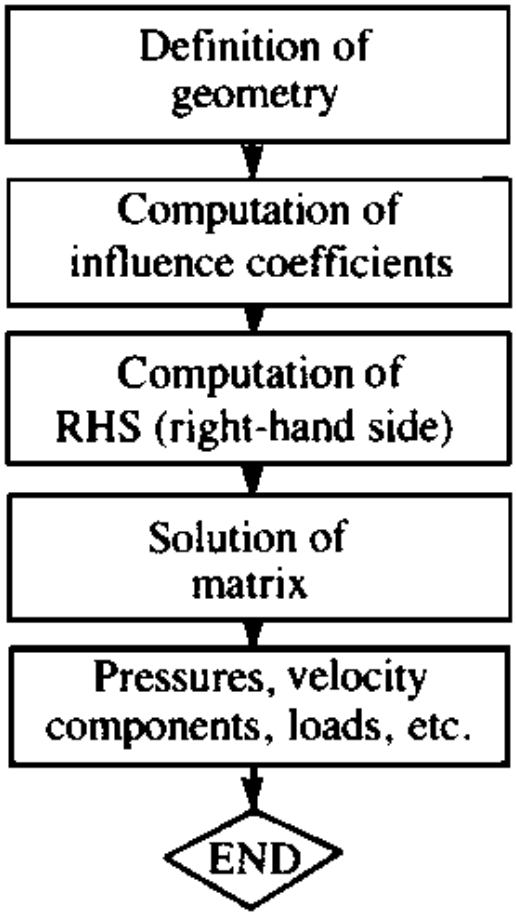

Figure 1.15 Typical flowchart for the numerical solution of the surface singularity distribution problem.

1.6 Example: Solution of Thin Airfoil with the Lumped-Vortex Element

As a first example for demonstrating the principle of numerical solutions, let us consider the solution for the symmetric, thin airfoil. Because the airfoil is thin, no sources will be used, while the doublet distribution will be approximated by two constant- strength doublet elements ($\mu 1$, $\mu 2$ pointing in the $-z$ direction). This element is equivalent to two concentrated vortices at the panel edges (see Fig. 1.16). However, the geometry of the "lumped-vortex" model was developed in Chapter 5, and by placing the vortex at the quarter chord and the collocation point at the three-quarter chord point of the panel the Kutta condition is automatically satisfied. Using this knowledge the equivalent discrete- vortex model (with only two elements) for the airfoil is shown in Fig. 1.17. Also, for the thin lifting surface only the Neumann (velocity) boundary condition can be used, because of the zero thickness of the airfoil. (Note that the doublet representation in Fig. 1.16 clearly indicates the existence of a starting vortex, also shown in Fig. 1.17, at a large distance behind the airfoil.)

a. *Selection of Singularity Element*

For this very simple example the lumped-vortex element is selected and its influence is derived in terms of the geometry involved. Such an element is depicted in Fig. 1.18a; it consists of a concentrated vortex at the panel quarter chord and a collocation point and normal vector **n** at the three-quarter chord.

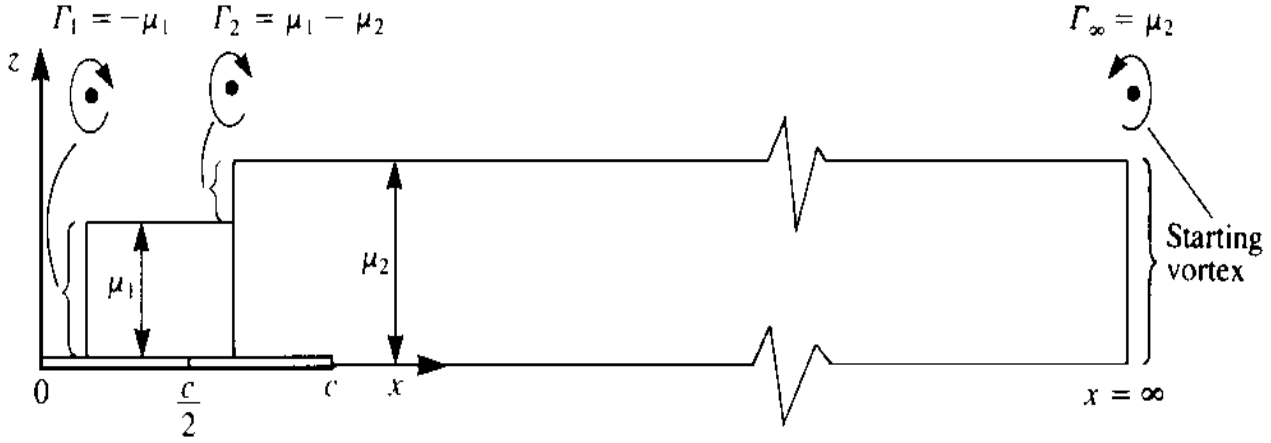

Figure 1.16 Constant-strength doublet element representation of the flat plate at an angle of attack (using two doublet panels pointing in the $-z$ direction).

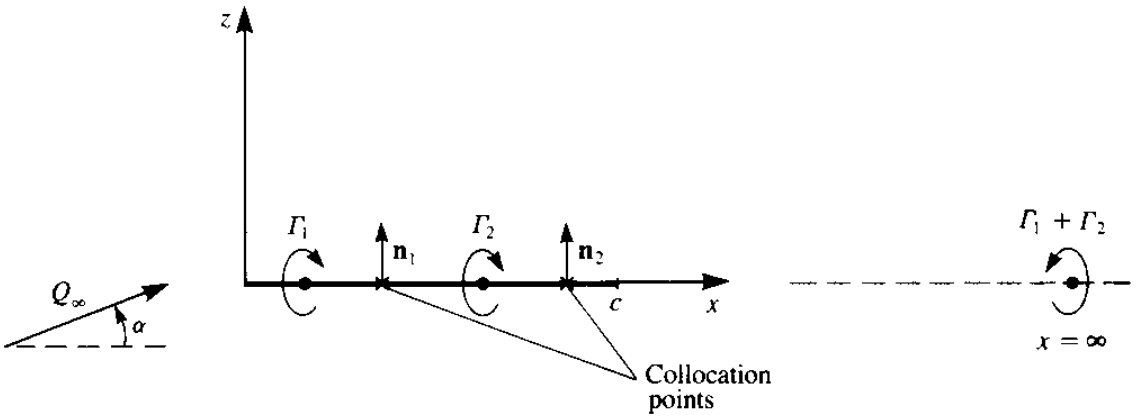

Figure 1.17 Equivalent discrete-vortex model for the flow over a flat plate at an angle of attack (using two elements).

It is important to remember that this element is a simplification of the two-dimensional continuous solution and therefore accounts for the Kutta condition at the trailing edge of the airfoil.

If the vortex element of circulation T is located at $(x0, z0)$, then the velocity induced by this element at an

arbitrary point $P(x, z)$, according to the analysis.

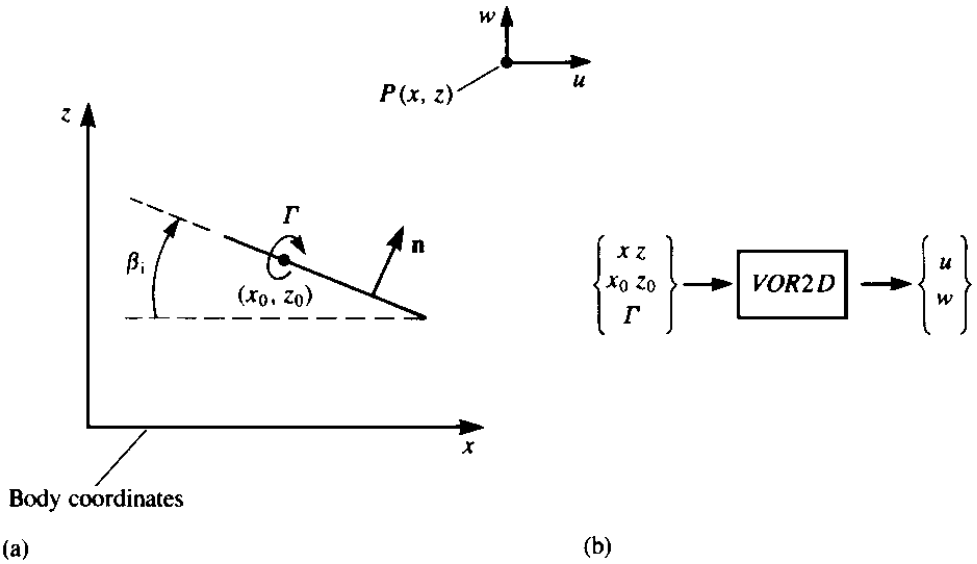

Figure 1.18 Nomenclature and flowchart for the influence of a panel element at a point *P*.

This can be programmed as an influence coefficient subroutine in the manner shown in Fig. 1.18b. Let us call this routine VOR2D.

$$(u, w) = VOR2D(T, x, z, x0, z0)$$

b. *Discretization of Geometry and Grid Generation*

For this example, the thin airfoil case is being solved (Fig. 1.17). For simplicity, only two elements will be used so that no computations are necessary. At this phase the geometrical information on the grid has to be derived. This can be automated by computer routines for more complex situations, but for this case the vortex point locations are

$$(x01, z01) = (c/8, 0)$$
$$(x02, z02) = (5c/8, 0)$$

and the collocation points are

$$(xc1, zc1) = (3c/8, 0)$$
$$(xc2, zc2) = (7c/8, 0)$$

The normal vectors **n** must be evaluated at the collocation points, and for an arbitrary element i we write

$$\mathbf{n}_i = (\sin\beta_i, \cos\beta_i)$$

where the angle β_i is defined in Fig. 1.18a. In this particular case, when the airfoil has no camber and is placed on the $z = 0$ plane, both normals are identical:

$$\mathbf{n}1 = \mathbf{n}2 = (0, 1)$$

c. *Influence Coefficients*

Here the condition requiring zero velocity normal to the airfoil will be enforced.

This boundary condition, according to Eq. (9.4), is

$$(\mathbf{q} + \mathbf{Q}_\infty) \cdot \mathbf{n} = 0$$

The velocity **q** is induced by the unknown vortices, whereas the free-stream normal com- ponent can be calculated directly and hence is moved to the right-hand side of the equation:

$$\mathbf{q} \cdot \mathbf{n} = -\mathbf{Q}_\infty \cdot \mathbf{n}$$

Because, in this case, the airfoil was divided into two elements with two unknown vortices of circulation $T1$, $T2$, two equations based on the zero flow normal to the airfoil boundary condition will be derived at the collocation points.

We define as positive T a clockwise rotation, and calculate the velocity induced by a unit strength vortex at point 1 on collocation point 1.

$$(u11, w11) = VOR2D(1.0, xc1, zc1, x01, \quad z \quad 01)$$

and the velocity induced at collocation point 1, by a unit vortex at point 2, is

$$(u12, w12) = VOR2D(1.0, xc1, zc1, x02, z02)$$

The velocity induced at collocation point 2, by a unit vortex at point 1, is

$$(u21, w21) = VOR2D(1.0, xc2, zc2, x01, \quad z \quad 01)$$

and the velocity induced at collocation point 2, by a unit vortex at point 2, is

$$(u22, w22) = VOR2D(1.0, xc2, zc2, x02, \quad z \quad 02)$$

The influence coefficients aij are really the normal component of the flow velocity induced by a unit strength vortex element Tj at collocation point i :

$$aij = \mathbf{q}ij\ (Tj = 1) \cdot \mathbf{n}i$$

For the current problem, Equation is applied to collocation point 1 and to vortex point 1. Thus $a11 = (u11, w11) \cdot \mathbf{n}1$ similarly, for the second vortex, we have

$$a12 = (u12, w12) \cdot (0, 1)$$

and for the second collocation point, we get

$$a21 = (u21, w21) \cdot (0, 1)$$

Note that the left-hand side of Eq. (9.34a) can be described now as

$$\mathbf{q} \cdot \mathbf{n} = aij\ Tj \qquad \text{for} \quad i = 1, 2;\ j = 1,2$$

d. *Establish RHS*

The solution is based on enforcing the boundary condition of Equation at the collocation points. Since the product $\mathbf{Q}\infty \cdot \mathbf{n}$ is known it is transferred to the right-hand side of the equation:

$$\mathbf{q} \cdot \mathbf{n} = -\mathbf{Q}\infty \cdot \mathbf{n} \equiv \text{RHS}$$

It is useful to express the component of the free stream in vector form to allow easy vector operations; for this particular case the right-hand side (RHS) is

$$\text{RHS}i = -(U\infty, W\infty) \cdot \mathbf{n}i$$

where $(U\infty, W\infty) = Q\infty(\cos \alpha, \sin \alpha)$. Computing the RHS vector for the two collocation points results in

$$\text{RHS}1 = -Q\infty \sin \alpha$$

$$\text{RHS}2 = -Q\infty \sin \alpha$$

e. *Solve Linear Set of Equations*

The results of the previous computations can be summarized as

$$aij\ Tj = \text{RHS}i \quad i = 1, 2;\ j = 1$$

and explicitly, for this particular case, which can be solved by standard matrix methods

f. *Secondary Computations: Pressures, Loads, Etc.*

The resulting pressures and loads can be computed by using the Kutta–Joukowski theorem

$$6Li = \rho\ Q\infty Ti$$

and by assuming a constant pressure distribution along the element, the pressure difference becomes

$$6pi = \rho\ Q\infty Ti/a$$

where a is the panel length. The lift and moment about the airfoil leading edge are then non dimensional aerodynamic coefficients are $\sin \alpha$.

These results are similar to those for a zero-thickness symmetrical airfoil and equal to the exact flat plate solution. The method can easily be extended to various camber line shapes and even multi element lifting airfoils.

1.7 Accounting for Effects of Compressibility and Viscosity

The potential flow model presented in this chapter results in a very simple mathematical model that can be transformed into a very efficient and economical numerical solution. This led to the development of three-dimensional "panel codes" for arbitrary geometries, and naturally, modifications were sought to improve these methods beyond the limits of incompressible inviscid flows. Some of these modifications are listed here.

a. *Effects of Compressibility*

The first and most straightforward modification to an incompressible potential-flow based method is to incorporate the effects of "low-speed compressibility" (e.g., for $M_\infty < 0.6$). This modification can be obtained by using the Prandtl–Glauert rule, as developed in Section 4.8. Thus, small-disturbance flow is assumed, and a compressibility factor β

If the free stream is parallel to the x coordinate then the x coordinate is being stretched with increased Mach number while the y and z coordinates remain unchanged. Consequently, an equivalent incompressible potential $8M$ =0 can be defined such that

Once the x coordinate is transformed, the equivalent incompressible potential problem is solved as described previously.

b. *Effects of Thin Boundary Layers*

When analyzing high Reynolds number flows in Section 1.8, it was assumed that the boundary layer is thin and that the boundary conditions are specified on the actual surface of the body. However, by neglecting the viscosity terms in the momentum equation, the information for calculating the viscous surface friction drag is lost too.

It is possible to account for the viscosity effects such as displacement thickness and friction drag by using a boundary layer solution that can be matched with the potential-flow solution. Two of the most common methods for combining these two solutions are as follows.

1. The first approach is to use a boundary layer solution, usually a two-dimensional model along a streamline, which is quite effective for simple wings and bodies. The solution begins by solving the inviscid potential flow, which results in the velocity field and the pressure distribution. These data are fed into two-dimensional boundary layer solutions that provide the local wall friction coefficient and the boundary layer thickness. The friction coefficient can then be integrated over the body surface for computing the friction drag. If the displacement thickness effect is sought, then a second iteration of the potential flow computation is needed, but now with modified surface geometry. This modification can be obtained by displacing the body panels according to the local boundary layer displacement, and the procedure can be reiterated until a satisfactory solution is obtained. Some of the principles of a computer program (e.g., the MCAIR panel code).
2. The second approach to incorporate boundary layer solutions into panel codes is to follow the procedure described above, but to account for the displacement effects by a modification of the boundary conditions instead of a change of the surface geometry. In this case, at each panel the normal flow is given a certain blowing value that accounts for the local boundary layer displacement thickness δ^*. The formulation can be derived using the properties of the source distribution of Section 4.4, and the incremental "transpiration velocity" is simply added to the source strength obtained from the inviscid model. Here q is the local streamwise velocity component of the potential flow (outside the boundary layer) and the differentiation takes place along a streamlines. Note that as a result of the added transpiration velocity $q_{ni} = 6\sigma i$, the normal velocity component on the actual surface of the body is nonzero.

c. *Models for Wake Rollup, Jets, and Flow Separations*

The vortices in the thin wake behind lifting wings tend to follow the local velocity induced by the lifting surface and its wakes. Consequently, the condition stated by results in the wake rollup. This condition causes the shape of the wake to be unknown when the boundary conditions for the potential flow are established. Traditionally, the shape of the wake is assumed to be known (e.g., planar vortex sheet) and after the solution is obtained, the validity of the initial wake shape can be rechecked. Two methods used by two panel codes will be presented to calculate the wake shape (VSAERO-wake relaxation[9.3] and PMARC-time stepping[9.7,9.8]). Since the wake is modeled by a doublet/vortex distribution, it is possible to extend this method for modeling jets and even shear layers of separated flows.

It was demonstrated in the previous chapters that the solution of potential flow problems over bodies and wings can be obtained by the distribution of elementary solutions. The strengths of these elementary solutions of Laplace's equation are obtained by enforcing the zero normal flow condition on the solid boundaries. In general, as the complexity of the method is increased, the "element's influence" calculation becomes more elaborate. Therefore, in this chapter, emphasis is placed on presenting some of the typical numerical elements upon which some numerical solutions are based (the list is not complete and an infinite number of elements can be developed). A generic element is shown schematically in Fig.1.19. To calculate the induced potential and velocity increments at an arbitrary point $P(x_P, y_P, z_P)$ requires information on the element geometry and strength of singularity.

However, it must be clear that the values of the velocity potential and velocity components are incremental values and can be added up according to the principle of superposition.

Three-dimensional elements will be presented later and their complexity increases with the order of the polynomial approximation of the singularity strength. Also, the formulation is derived in the panel frame of reference and when these formulas are used in any other "global coordinate system," the corresponding coordinate transformations must be used (for rotations and translations).

1.8 Two-Dimensional Point Singularity Elements

These elements are probably the simplest and easiest to use and also the most efficient in terms of computational effort. Consequently, even when higher order elements are used, if the point of interest is considered to be far from the element, then point ele- ments can be used to describe the "far field" effect. The three point elements that will be discussed are source, doublet and vortex, and their formulation is given in the following sections.

1.8.1 Two-Dimensional Point Source

Consider a point source singularity at $(x0, z0)$, with a strength σ, as shown in Fig. 1.19. The increment to the velocity potential at a point P is then

$$\begin{pmatrix} x_P, y_P, z_P \\ \text{Panel geometry} \\ \text{Singularity strength} \end{pmatrix} \Rightarrow \begin{pmatrix} \text{influence} \\ \text{coefficient} \\ \text{calculation} \end{pmatrix} \Rightarrow \begin{pmatrix} \Delta u, \Delta v, \Delta w \\ \Delta \Phi \end{pmatrix}_P$$

Figure 1.19 Schematic description of a generic panel influence coefficient calculation.

and after differentiation of the potential, the velocity components are

$$u = \frac{\partial \Phi}{\partial x} = \frac{\sigma}{2\pi} \frac{x - x_0}{(x - x_0)^2 + (z - z_0)^2}$$

$$w = \frac{\partial \Phi}{\partial z} = \frac{\sigma}{2\pi} \frac{z - z_0}{(x - x_0)^2 + (z - z_0)^2}$$

1.8.2 Two-Dimensional Point Doublet

Consider a doublet that is oriented in the z direction [$\boldsymbol{\mu} = (0, \mu)$]. If the doublet is located at the point $(x0, z0)$, then its incremental influence at point P is

$$\delta(x, z) = -\frac{\mu}{2\pi} \frac{z - z0}{(x - x0)^2 + (z - z0)^2}$$

and the velocity component increments are

$$\frac{\partial \Phi}{\partial x} = u = -\frac{\mu}{\pi} \frac{(x - x0)(z - z0)}{[(x - x0)^2 + (z - z0)^2]^2}$$

In the case when the basic singularity element is given in a system (x, z) rotated by the angle β relative to the (x^*, z^*) system, as shown in Fig. 1.19, then the velocity components can be found by the transformation.

1.8.3 Two-Dimensional Point Vortex

Consider a point vortex with the strength T located at $(x0, z0)$. Again using the definitions of the points, as in Fig. 1.20, and the results.

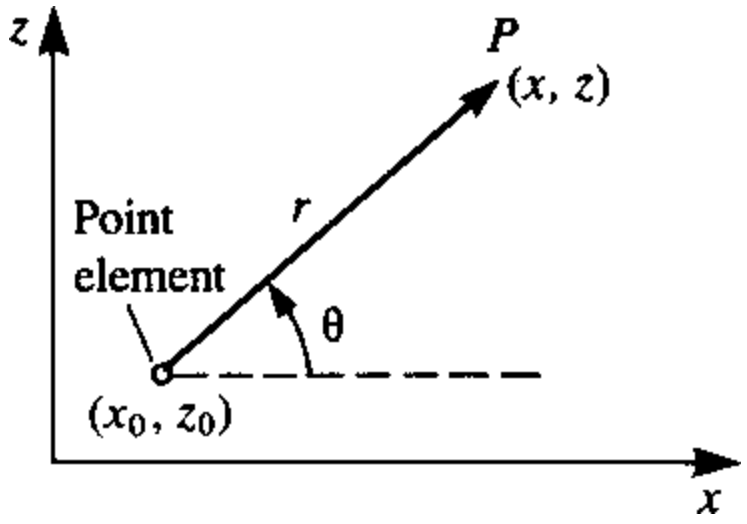

Figure 1.20 The influence of a point singularity element at point P.

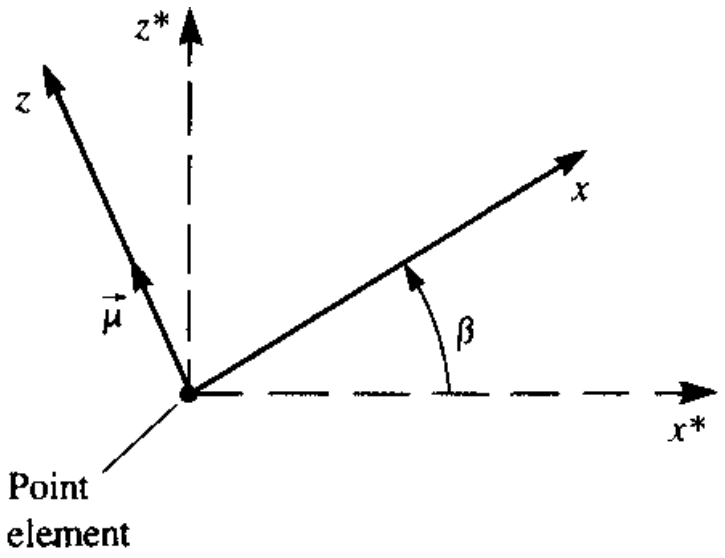

Figure 1.21 Transformation from panel to global coordinate system.

Note that all these point elements fulfill the requirements presented in Fig. 1.21. That is, the increments of the velocity components and potential at P depend on the geometry (x, z, x_0, z_0) and the strength of the element.

1.8.4 Two-Dimensional Constant-Strength Singularity Elements

The discretization of the source, doublet, or vortex distributions in the previous section led to discrete singularity elements that are clearly not a continuous surface representation. A more refined representation of these singularity element distributions can be obtained by dividing the solid surface boundary into elements (panels). One such element is shown schematically in Fig. 1.22, and both the surface shape and the shape of the singularity strength distribution are approximated by a polynomial. In this section, for the surface representation, a straight line will be used. For the singularity strength, only the constant, linearly varying, and quadratically varying strength cases are presented, but the methodology of this section can be applied to higher order elements.

In this section, too, three examples will be presented (source, doublet, and vortex) for evaluating the influence of the generic panel of Fig. 1.22 at an arbitrary point P.

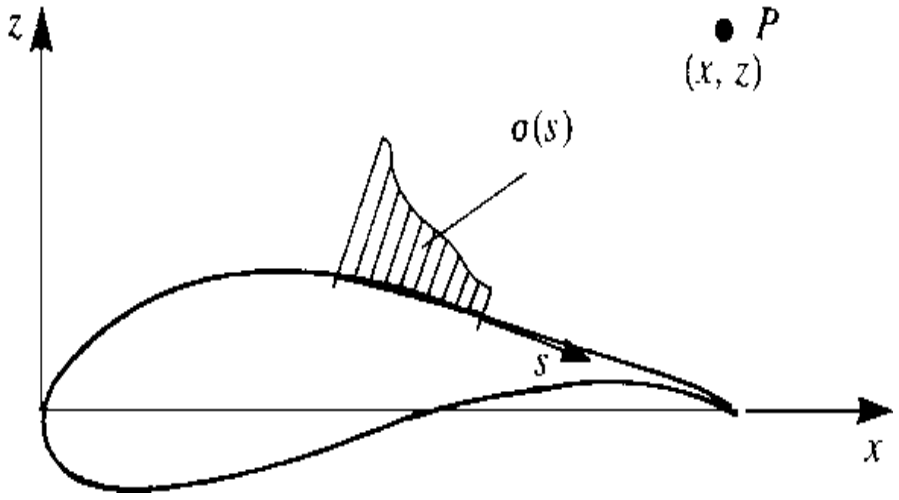

Figure 1.22 A generic surface distribution element.

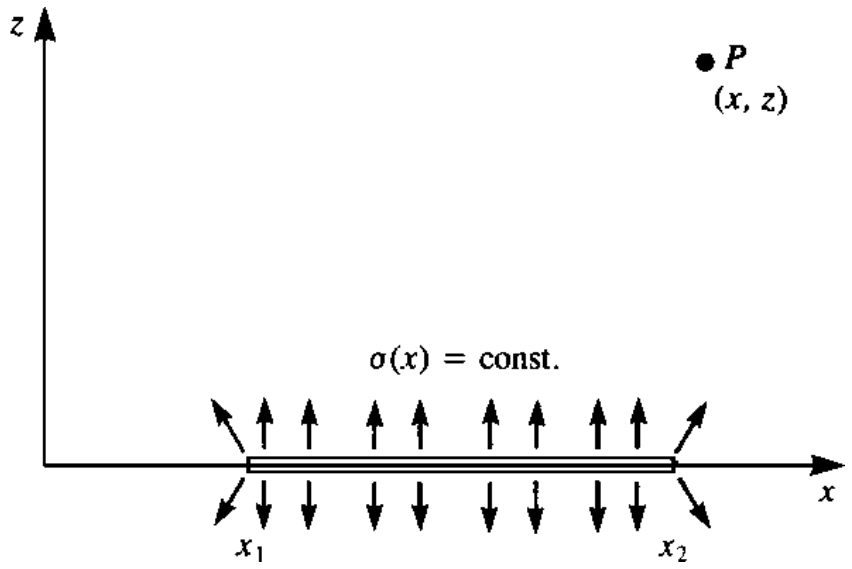

Figure 1.23 Constant-strength source distribution along the *x* axis.

For simplicity, the formulation is derived in a panel-attached coordinate system, and the results need to be transformed back into the global coordinate system of the problem.

1.8.5 Constant-Strength Source Distribution

Consider a source distribution along the *x* axis as shown in Fig. 1.23. It is assumed that the source strength per length is constant such that $\sigma(x) = \sigma$ = const. The influence of this distribution at a point *P* is an integral of the influences of the point elements (described in the previous section) along the segment $x1 \rightarrow x2$:

The integral for the velocity potential (note that $\ln r^2 = 2 \ln r$ is used in the derivation) and in terms of the corner points $(x1, 0)$, $(x2, 0)$ of a generic panel element (Fig. 10.6), the distances $r1$, $r2$, and the angles $\theta1$, $\theta2$

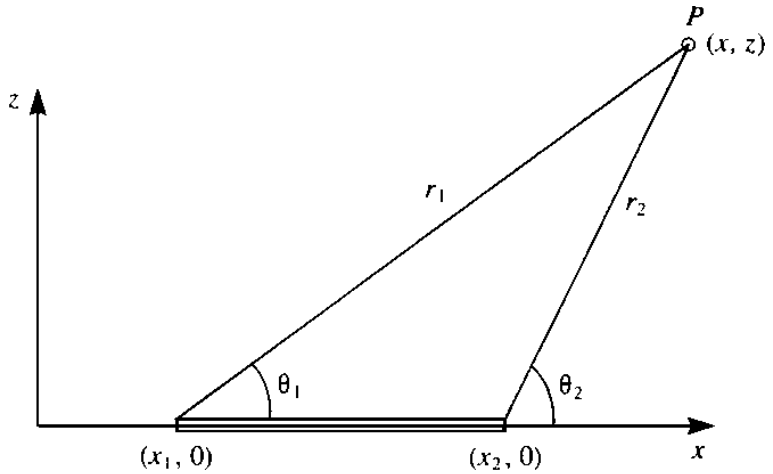

Figure 1.24 Nomenclature for the panel influence coefficient derivation.

Of particular interest is the case when the point *P* is on the element (usually at the center).
In this case $z = 0\pm$ and the potential becomes
For evaluating the *w* component of the velocity, it is important to distinguish between the conditions when the panel is approached from its upper or from its lower side. For the case of *P* being above the panel, $\theta1 = 0$, while $\theta2 = \pi$. These conditions are reversed on the lower side.

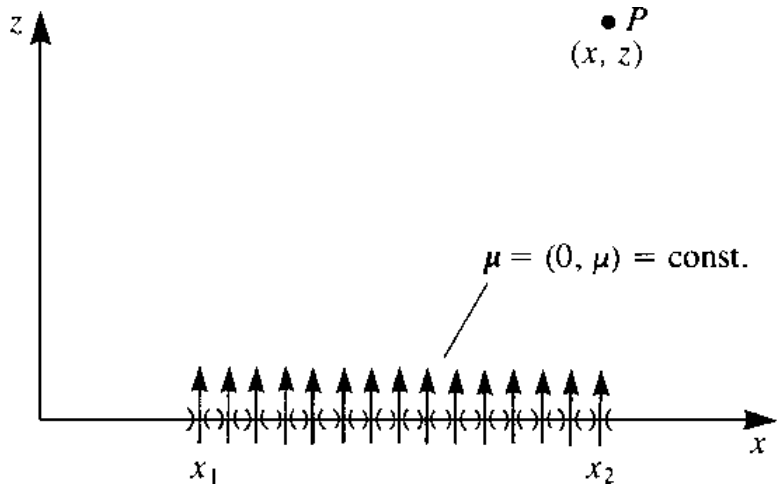

Figure 1.25 Constant-strength doublet distributions along the *x* axis.

1.8.6 Constant-Strength Doublet Distribution

Consider a doublet distribution along the *x* axis consisting of elements pointing in the *z* direction [$\boldsymbol{\mu} = (0, \mu)$], as shown in Fig. 1.25. The influence at a point $P(x, z)$ is an integral of the influences of the point elements between $x1$ and $x2$. Note that the integral for the *w* component of the source distribution is similar to the potential integral of the doublet. Therefore, the potential at *P*. Comparison of this expression to the potential of a point vortex indicates that this constant doublet distribution is equivalent to two point vortices with opposite sign at the panel edge such that $T = -\mu$ (see Fig. 1.26). Consequently, the velocity components

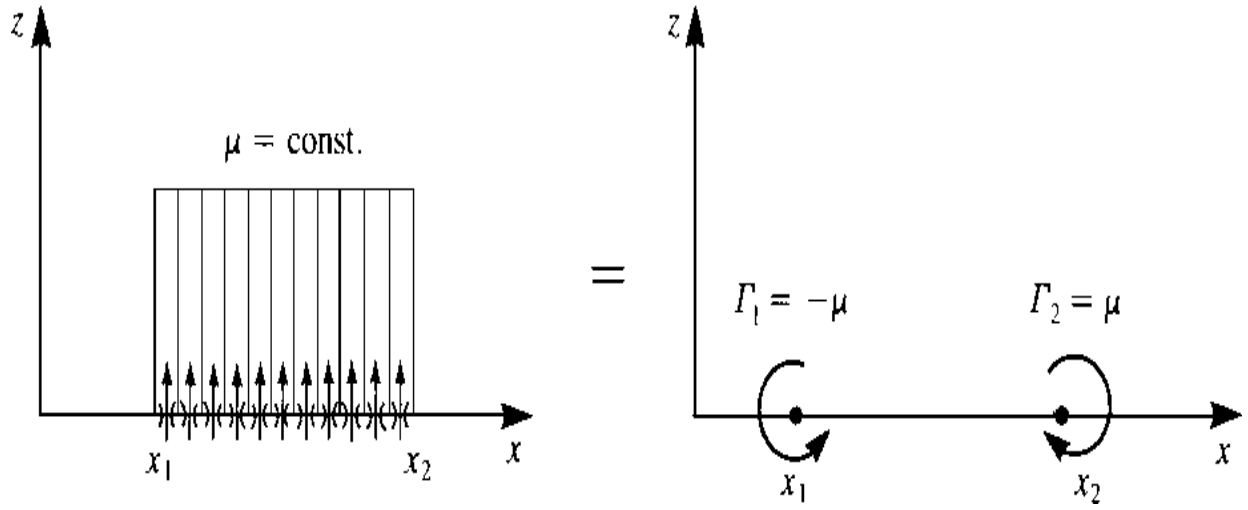

Figure 1.26 Equivalence between a constant-strength doublet panel and two point vortices at the edge of the panel.

1.8.7 Constant-Strength Vortex Distribution

Once the influence terms of the constant-strength source element are obtained, owing to the similarity between the source and the vortex distributions, the formulation for
this element becomes simple. The constant-strength vortex distribution $\gamma(x) = \gamma = \text{const.}$ is placed along the *x* axis as shown in Fig. 1.27. The influence of this distribution at a
point *P* is an integral of the influences of the point elements between $x1$ and $x2$. So we have

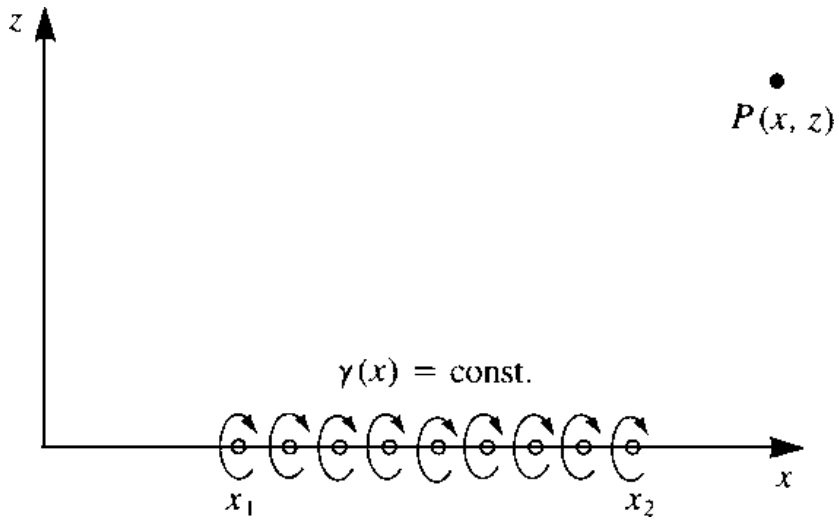

Figure 1.27 Constant-strength vortex distribution along the *x* axis

Following the formulation used for the constant-source element, and observing that the *u* and *w* velocity components for the vortex distribution are the same as the corresponding *w* and *u* components of the source distribution.

In most situations the influence is sought at the center of the element where |r1|= |r2| and consequently *w*(panel − center, 0±) = 0.

1.9 Two-Dimensional Linear-Strength Singularity Elements

The representation of a continuous singularity distribution by a series of constant- strength elements results in a discontinuity of the singularity strength at the panel edges. To overcome this problem, a linearly varying strength singularity element can be used. The requirement that the strength of the singularity remains the same at the edge of two neighbor elements results in an additional equation.

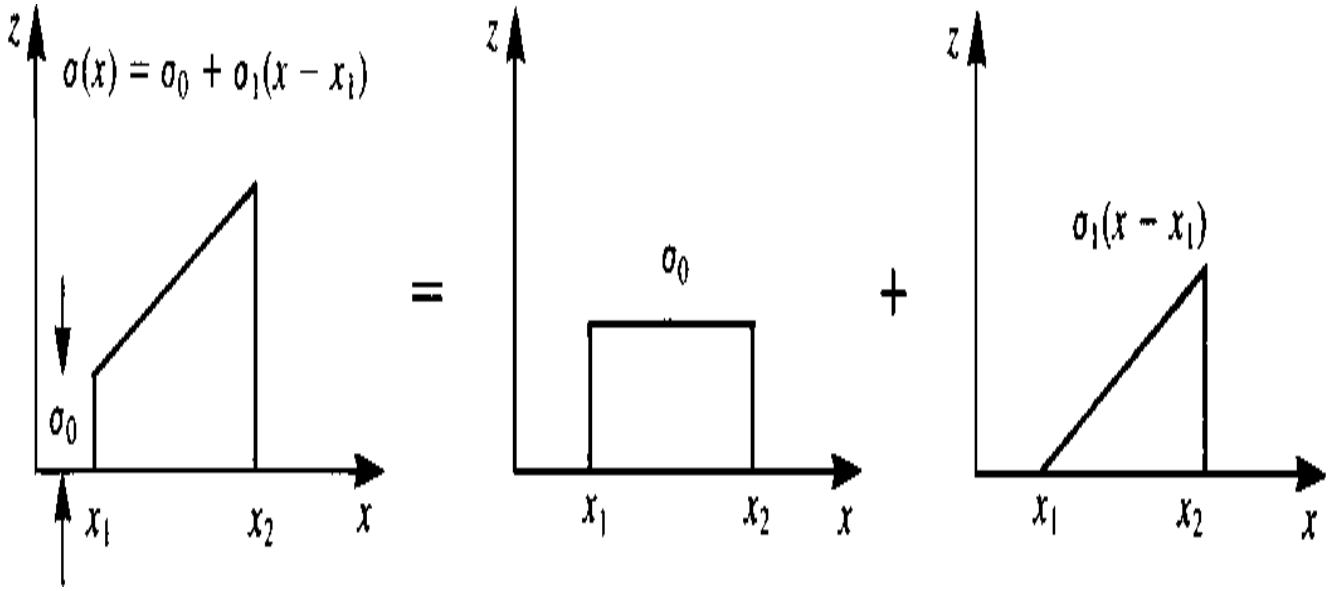

Figure 1.28 Decomposition of a generic linear strength element to constant-strength and linearly varying strength elements.

1.9.1 Linear Source Distribution

Consider a linear source distribution along the x axis ($x1 < x < x2$) with a source strength of $\sigma(x) = \sigma 0 + \sigma 1(x - x1)$, as shown in Fig. 1.29. Based on the principle of superposition, this can be divided into a constant-strength element and a linearly varying strength element with the strength $\sigma(x) = \sigma 1 x$. Therefore, for the general case (as shown in the left-hand side of Fig. 10.10) the results of this section must be added to the results of
the constant-strength source element.

The influence of the simplified linear distribution source element, where $\sigma(x) = \sigma 1 x$, at a point P is obtained by integrating the influences of the point elements between $x1$ and $x2$.

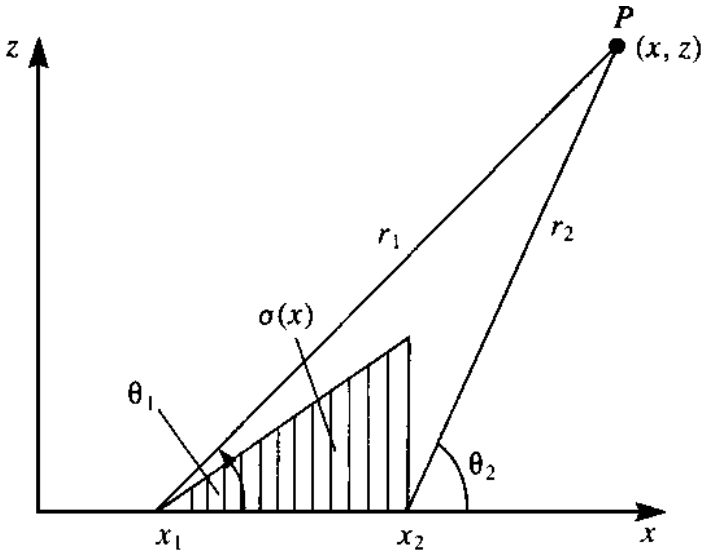

Figure 1.29 Nomenclature for calculating the influence of linearly varying strength source.

1.9.2 Linear Doublet Distribution

Consider a doublet distribution along the x axis with a strength $\mu(x) = \mu 0 + \mu 1(x - x1)$, consisting of elements pointing in the z direction [$\boldsymbol{\mu} = (0, \mu)$], as shown in Fig. 1.30. In this case, too, only the linear term ($\mu(x) = \mu 1 x$) is considered and the influence at a point $P(x, z)$ is an integral of the influences of the point elements between $x1$ and $x2$:

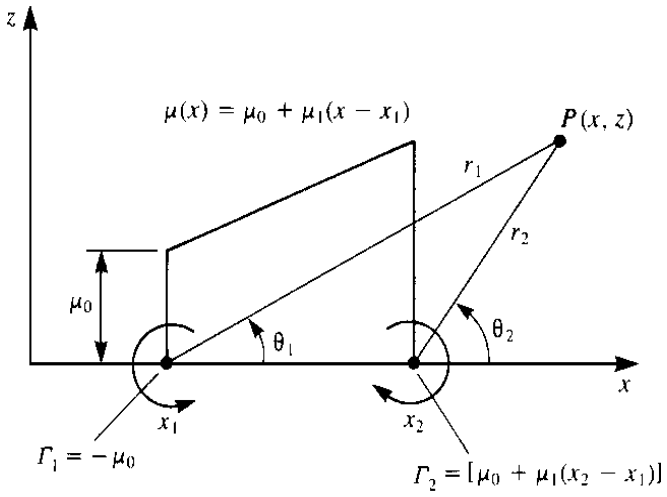

Figure 1.30 Linearly varying strength doublet element.

1.9.3 Linear Vortex Distribution

In this case the strength of the vortex distribution varies linearly along the element,

$\gamma(x) = \gamma 0 + \gamma 1(x - x1)$

Again, for simplicity consider only the linear portion where $\gamma(x) = \gamma 1 x$ and $\gamma 1$ is a constant. The influence of this vortex distribution at a point P in the x –z plane is obtained by integrating the influences of the point elements between $x1$ and $x2$.

1.9.4 Quadratic Doublet Distribution

A quadratic doublet distribution can be replaced by an equivalent linear vortex distribution presented in the previous section. However, in situations when the Dirichlet type boundary condition is applied, it is more convenient to use the corresponding doublet distribution (instead of the linear vortex distribution). Thus, a quadratic doublet distribution along the x axis ($x1 < x < x2$) will have a strength distribution of

$\mu(x) = \mu 0 + \mu 1(x - x1) + \mu 2(x - x1)^2$

where the doublet elements pointing in the z direction [$\boldsymbol{\mu} = (0, \mu)$] are selected as shown in Fig. 1.31. Since the contribution of the constant and linear strength terms were evaluated in the previous sections only the third term ($\mu(x) = \mu 2 x^2$) is considered and the influence at a point $P(x, z)$ is an integral of the influences of the point elements between $x1$ and $x2$:

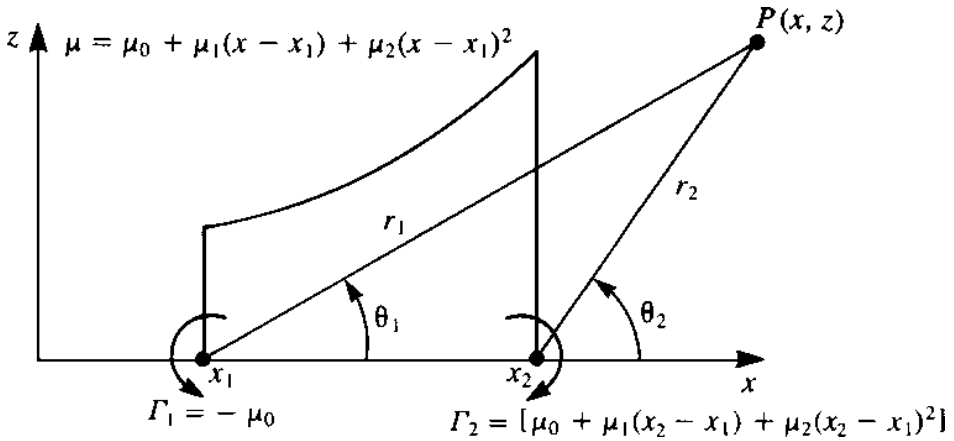

Figure 1.31 Quadratic-strength doublet element.

1.10 Three-Dimensional Constant-Strength Singularity Elements

In the three-dimensional case, as in the two-dimensional case, the discretization process includes two parts: discretization of the geometry and of the singularity element distribution. If these elements are approximated by polynomials (both geometry and singularity strength) then a first-order approximation to the surface can be defined as a quadrilateral[1] panel, a second-order approximation will be based on parabolic curve- fitting, while a third-order approximation may use a third-order polynomial curve-fitting. Similarly, the strength of the singularity distribution can be approximated (discretized) by constant-strength (zero-order), linearly varying (first-order), or by parabolic (second-order) functions.

The simplest and most basic three-dimensional element will have a quadrilateral geometry and a constant-strength singularity. When the strength of this element (a constant) is unknown a panel code using N panels can be constructed to solve for these N constants. In the following section, such constant-strength elements will be described.

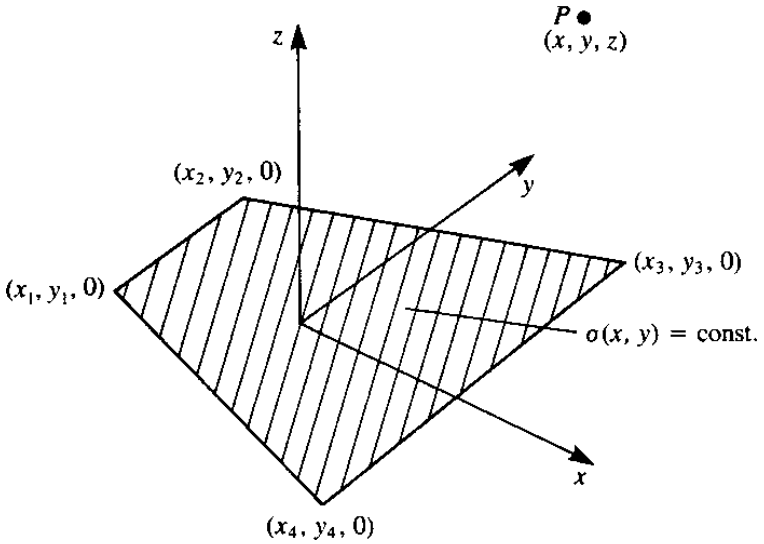

Figure 1.32 Quadrilateral constant-strength source element.

The derivation is again performed in a local frame of reference, and for a global coordinate system a coordinate transformation is required.

UNIT-II
METHOD OF CHARACTERISTICS, BOUNDARY CONDITIONS

2.1 Introduction

The method of characteristics has been used for many years to compute supersonic irrotational flows. Although the method has a strong analytical basis, its practical implementation is, essentially, always numerical and it is then used to compute the values of the flow variables at a series of distinct points in the flow rather than continuously throughout the flow field. Let's consider a general steady two-dimensional irrotational flow field. We have already derived the velocity potential (φ) equation for such flow field.

$$\left(1-\frac{u^2}{a^2}\right)\frac{\partial^2\phi}{\partial x^2}+\left(1-\frac{v^2}{a^2}\right)\frac{\partial^2\phi}{\partial y^2}-\frac{2uv}{a^2}\frac{\partial^2\phi}{\partial x\partial y}=0 \quad \text{----- (2.1)}$$

Consider the change in any flow variable,*f*, *df* which can be determined by small changes in the coordinates *dx* and *dy* as illustrated in Fig.1.2. The change in the variable, *df*,

$$df=\frac{\partial f}{\partial x}dx+\frac{\partial f}{\partial y}dy$$

If $f=\partial\phi/\partial x$ then this will give:

$$d\left(\frac{\partial\phi}{\partial x}\right)=\frac{\partial^2\phi}{\partial x^2}dx+\frac{\partial^2\phi}{\partial x\partial y}dy$$

But $u=\partial\phi/\partial y$ so this equation gives:

$$du=\frac{\partial^2\phi}{\partial x^2}dx+\frac{\partial^2\phi}{\partial x\partial y}dy \quad \text{----- (2.2)}$$

Similarly if $f=\partial\phi/\partial y$ then this will give:

$$d\left(\frac{\partial\phi}{\partial y}\right)=\frac{\partial^2\phi}{\partial x\partial y}dx+\frac{\partial^2\phi}{\partial y^2}dy$$

But $v=\partial\phi/\partial y$ so this equation gives:

$$dv=\frac{\partial^2\phi}{\partial x\partial y}dx+\frac{\partial^2\phi}{\partial y^2}dy \quad \text{----- (2.3)}$$

Now consider eqs. 2.1, 2.2 and 2.3 which involve second derivatives of φ and can be solved using Cramer's Rule.

For example

$$\frac{\partial^2\phi}{\partial x\partial y}=\frac{(1-u^2/a^2)dudy+(1-v^2/a^2)dvdx}{(1-u^2/a^2)(dy)^2+(2uv/a^2)dxdy+(1-v^2/a^2)(dx)^2} \quad \text{----------(2.4)}$$

In general, this equation can be solved for any chosen values of dx and dy, i.e., for any chosen direction, to give $\partial^2\phi/\partial x\partial y$ at a selected point in the flow. However, it is possible to have $\partial^2\phi/\partial x\partial y$ indeterminate in certain directions. More over this differential is expected to be finite at that point. Hence in these directions,

eq. 2.4 must give an indeterminate value.

$$\frac{\partial^2 \phi}{\partial x \partial y} = \frac{0}{0}$$

Let's consider the denominator of eq 32.4 since along a particular direction $\partial^2\phi / \partial x \partial y$ is indeterminate. Hence the denominator should be zero, as:

$$\left(1 - \frac{u^2}{a^2}\right)(dy)^2 + \frac{2uv}{a^2} dx dy + \left(1 - \frac{v^2}{a^2}\right)(dx)^2 = 0$$

Dividing by $(dx)^2$ gives:

$$\left(1 - \frac{u^2}{a^2}\right)\left(\frac{dy}{dx}\right)^2 + \frac{2uv}{a^2}\frac{dy}{dx} + \left(1 - \frac{v^2}{a^2}\right) = 0$$

The subscript on *dy/dx* indicates that the slope of the characteristic line or a specific direction is being considered along which differentials are indeterminate. Solving above equation we get:

$$\left(\frac{dy}{dx}\right)_{ch} = \frac{-\left(\frac{uv}{a^2}\right) \pm \sqrt{\frac{(u^2+v^2)}{a^2} - 1}}{\left(1 - \frac{u^2}{a^2}\right)}$$

Lets represent the component of velocities in terms of velocity vector and angle made by the streamline with co-ordinate axes as,

$$V^2 = u^2 + v^2$$

$$u = V \cos\theta$$

$$v = V \sin\theta$$

Hence, we get the same equation for slope as,

$$\left(\frac{dy}{dx}\right)_{ch} = \frac{-M^2 \cos\theta \sin\theta \pm \sqrt{M^2 - 1}}{(1 - M^2 \cos^2\theta)}$$

where, M=V/a.

We can introduce the local Mach angle, *a*, where ($M = 1/\sin\alpha,\ \sqrt{M^2 - 1} = 1/\tan\alpha$) by replacing Mach number as,

$$\left(\frac{dy}{dx}\right)_{ch} = \frac{\cos\theta \sin\theta \pm \cos\alpha \sin\alpha}{\sin^2\alpha - \cos^2\alpha}$$

After much manipulation and rearrangement, it can be shown that this equation gives:

$$\left(\frac{dy}{dx}\right)_{ch} = \tan(\theta \pm \alpha)$$

----------(2.5)

There are two characteristic lines. This clearly means that the characteristic lines or lines along which derivatives are indeterminate makes Mach angle with the streamline. Hence the net angle made by the characteristic line with the x-axis is the summation of the angle made by the streamline with x-axis and angle made by the Mach wave with streamline. Hence Mach waves are the character lines.

2.2 Governing Equation

We know about the direction of the characteristic line obtained from the indeterminacy of the eq. (2.4) for zero denominators. However finiteness of the differential compels the zero value of the numerator. This condition evolves the equation to be solved along the characteristic lines.

Hence for the numerator eq. (2.4) we have,

$$(1 - u^2/a^2)dudy+(1 - v^2/a^2)dvdx = 0$$

i.e.:

$$\frac{dv}{du} = \frac{(1-u^2/v^2)}{(1-v^2/a^2)(dy/dx)}$$

Substituting for slope (dy/dx) of the characteristic lines from eq. (2.5) that gives:

$$\frac{dv}{du} = \frac{uv/a^2 \pm \sqrt{(u^2+v^2)/a^2 - 1}}{(1-v^2/a^2)}$$

Using the velocity relation we have,

$$\frac{dv}{du} = \frac{M^2 \sin\theta\cos\theta \pm \sqrt{M^2-1}}{1-M^2\sin^2\theta}$$

However,

$$\frac{dv}{du} = \frac{d(V\sin\theta)}{d(V\cos\theta)} = \frac{\sin\theta dV + V\cos\theta d\theta}{\cos\theta dV - V\sin\theta d\theta}$$
$$\Rightarrow \frac{dv}{du} = \frac{d(V\sin\theta)}{d(V\cos\theta)} = \frac{\sin\theta(dV/V)+\cos\theta d\theta}{\cos\theta(dV/V)-\sin\theta d\theta}$$

Substituting this expression in eq. 2.1 we get,

$$\frac{\sin\theta(dV/V)+\cos\theta d\theta}{\cos\theta(dV/V)-\sin\theta d\theta} = \frac{M^2\sin\theta\cos\theta \pm \sqrt{M^2-1}}{1-M^2\sin^2\theta}$$

i.e. $$\sin\theta\left(\frac{dV}{V}\right)+\cos\theta d\theta - M^2\sin^3\theta\left(\frac{dV}{V}\right) - M^2\sin^2\theta\cos\theta d\theta$$
$$= M^2\sin\theta\cos^2\theta\left(\frac{dV}{V}\right) \pm \sqrt{M^2-1}\cos\theta\left(\frac{dV}{V}\right)$$
$$- M^2\sin^2\theta\cos\theta d\theta \pm \sqrt{M^2-1}\sin\theta d\theta$$

i.e. $$[\cos\theta \pm \sqrt{M^2-1}\sin\theta]$$
$$= [-\sin\theta + M^2\sin\theta(\sin^2\theta+\cos^2\theta) \pm \sqrt{M^2-1}\cos\theta]\left(\frac{dV}{V}\right)$$

i.e. $$d\theta = -\left[\frac{\sin\theta(M^2-1) \pm \sqrt{M^2-1}\cos\theta}{\pm\sqrt{M^2-1}\sin\theta - \cos\theta}\right]\left(\frac{dV}{V}\right)$$

$$i.e. \qquad d\theta = -\left[\frac{\sqrt{M^2-1}\sin\theta \pm \cos\theta}{\pm\sqrt{M^2-1}\sin\theta - \cos\theta}\right]\sqrt{M^2-1}\left(\frac{dV}{V}\right)$$

$$d\theta = \pm\sqrt{M^2-1}\,\frac{dV}{V}$$

This is the equation governing the changes in the variables along the characteristic lines. It can be noted that it is an ordinary differential equation whereas the original equation, velocity potential equation, was a partial differential equation

We have already seen the solution for equation during consideration of expansion fan (2.4). On the similar line, the integration equation of leads to,

$$\int d\theta \pm \int \sqrt{M^2-1}\,\frac{dV}{V} = \text{constant}$$

and the $\int \sqrt{M^2-1}\,\frac{dV}{V}$ is the Prandtl Mayer function,

$$\nu(M) = \int_0^M \frac{\sqrt{M^2-1}}{[1+(\gamma-1)M^2/2]}\,\frac{dM}{M}$$

Hence,

$$\theta \pm \nu = constant$$

This is the simple algebraic equation which we will have to solve along the characteristic line.
Following figure represents the details of the characteristic lines.

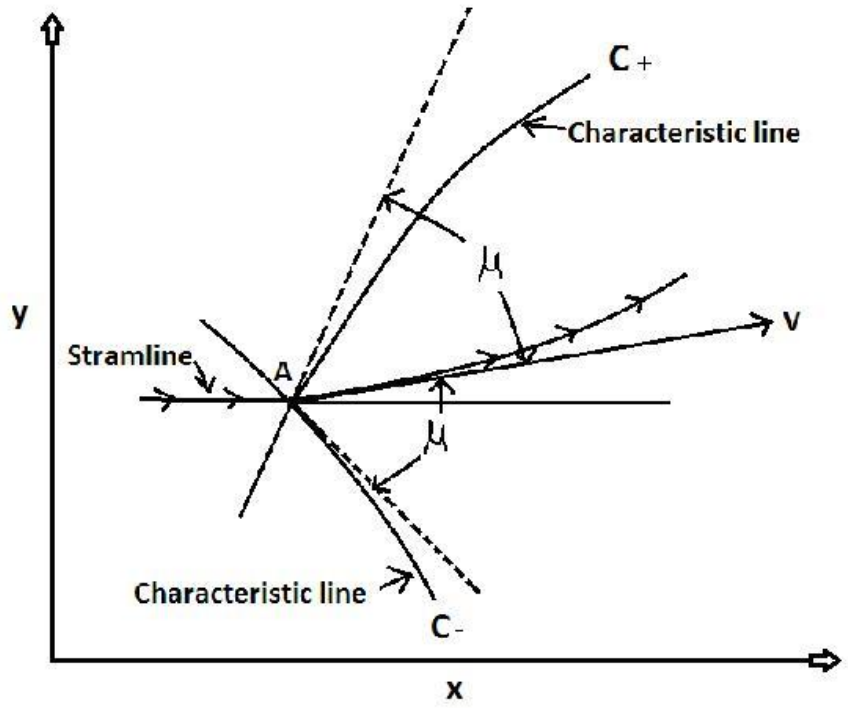

Fig. 2.1. Schematic representation of the details of the characteristic line

We know that there are two characteristic lines from eq. 2.5.
For C+ characteristics line of Fig.2.1:

$$\left(\frac{dy}{dx}\right)_{ch} = \tan(\theta + \alpha)$$

$$\theta - \vartheta = K^{+}$$

For C- characteristics line of Fig.33.1:

$$\left(\frac{dy}{dx}\right)_{ch} = \tan(\theta - \alpha)$$

$$\theta + \vartheta = K^{-}$$

K+ and K - are constants along the + and - characteristic lines.

2.3 Strategy to solve numerically along the characteristic line

Consider any point 3 in the flow field at which properties are to be evaluated. Point 1 and 2 supposed to the points of known properties. Consider C+ characteristic line passing through point 2 and C- passing through 1 intersecting at point 3. Hence point 3 lies on both the characteristic lines. Therefore for point 1 and 3 we have,

$$\theta_1 + \vartheta_1 = (K^{-})_1 = \theta_3 + \vartheta_3 = (K^{-})_3$$

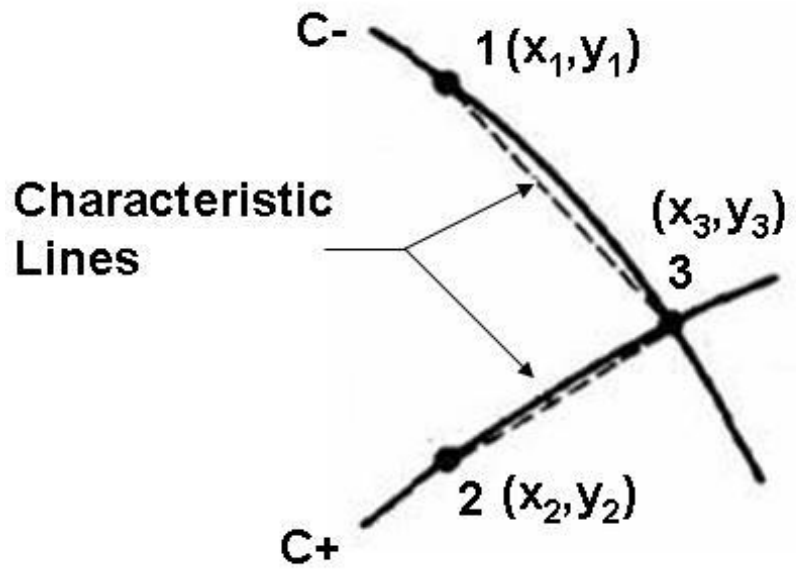

Fig. 2.2. Solution strategy at a point in the flow field.

Similarly for the point 2 and 3

$$\theta_2 - \vartheta_2 = (K^{+})_2 = \theta_3 + \vartheta_3 = (K^{+})_3$$

Hence,

$$\theta_3 + \vartheta_3 = (K^{-})_1$$

$$\theta_3 - \vartheta_3 = (K^{+})_2$$

First adding these two equations and then subtracting them gives:

$$\theta_3 = [(K^-)_1 + (K^+)_2]/2$$

$$\vartheta_3 = [(K^-)_1 - (K^+)_2]/2$$

which can be also written as:

$$\theta_3 = ((\theta_1 + \theta_2)/2) + ((\vartheta_1 - \vartheta_2)/2)$$

$$\vartheta_3 = ((\theta_1 - \theta_2)/2) + ((\vartheta_1 + \vartheta_2)/2)$$

This helps in finding θ_3 and ν_3 from known properties. Since ν_3 depends only on M, this allows $M_3$and hence a_3 can be evaluated. Since the stagnation pressure and temperature are constant throughout the flow field therefore using M_3 we can calculate P_3, T_3, a_3, and ρ_3 and then V_3. The characteristic lines are, in general, curved. Their local slope depends on the local values of ν and θ. However, if points 1 and 3 and 2 and 3 are close together, the characteristic lines can be assumed to be straight with a slope equal to the average of the values at the end points.

$$[(\theta_1 - \alpha_1) + (\theta_3 - \alpha_3)]/2 = \tan^{-1}\left[\frac{y_3 - y_1}{x_3 - x_1}\right]$$

$$[(\theta_2 + \alpha_2) + (\theta_3 + \alpha_3)]/2 = \tan^{-1}\left[\frac{y_3 - y_2}{x_3 - x_2}\right]$$

Since θ_3 and a_3 are determined by solving above two equations we can determine x_3 and y_3.

The procedure discussed above was for an "internal" point, i.e., a point 3 in the flow field that did not lie on a boundary. If a point lies on the boundary, the flow direction at this point will be determined by the slope of the boundary, e.g., consider the point 5 shown in Fig. 2.3 which lies on a solid wall. The flow direction at this point θ_5 is equal to the slope of the wall as indicated. Consider the characteristic line between points 4 and 5 as shown in the same figure. Since (K -)4 = (K -)5 it follows that:

$$\theta_4 + \nu_4 = \theta_5 + \nu_5$$

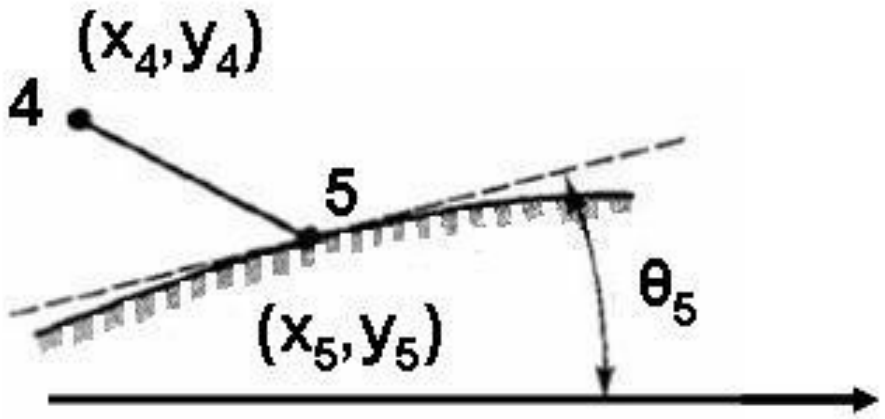

Fig. 2.3. Demonstration of wall boundary condition.

However, θ_5 is known, hence ν_5 is given by:

$$\nu_5 = \theta_4 - \theta_5 + \nu_4$$

With ν_5 determined, the values of all the flow properties at 5 can be determined as discussed before. The characteristic line between 4 and 5 is, of course, assumed to be straight which determines the position of the point 5.

2.4 Irrotational Euler Equation

Irrotationality of the flow can be evident in the compressible flow field for weak or zero entropy gradients as per the Croco's theorem. Supersonic flows shocked in the presence of weakly curved oblique shocks can be treated as irrotational flows. Let's consider such irrotational flow. We know that the curl of velocity vector being zero is the irrotationality condition. Hence,

$$\nabla \times \mathrm{V} = \begin{vmatrix} i & j & k \\ \frac{\partial}{\partial x} & \frac{\partial}{\partial y} & \frac{\partial}{\partial z} \\ u & v & w \end{vmatrix}$$

$$\mathrm{i}\left(\frac{\partial w}{\partial y} - \frac{\partial v}{\partial z}\right) - j\left(\frac{\partial w}{\partial x} - \frac{\partial u}{\partial z}\right) + \mathrm{k}\left(\frac{\partial v}{\partial x} - \frac{\partial u}{\partial y}\right) = 0$$

Component wise equality gives,

$$\frac{\partial w}{\partial y} = \frac{\partial v}{\partial z} \qquad \frac{\partial w}{\partial x} = \frac{\partial u}{\partial z} \qquad \frac{\partial v}{\partial x} = \frac{\partial u}{\partial y}$$

This gradient equality will be used for simplifying the momentum equation. The momentum equation for the in viscid compressible can be written as,

$$\rho \frac{DV}{Dt} = -\nabla P$$

The u-momentum or x-directional momentum equation is,

$$\rho u \frac{\partial u}{\partial x} + \rho v \frac{\partial u}{\partial y} + \rho w \frac{\partial u}{\partial z} = -\frac{\partial \mathrm{p}}{\partial x}$$

Multiplication of d_x on either side gives,

$$-\frac{\partial \mathrm{p}}{\partial x} dx = \rho u \frac{\partial u}{\partial x} dx + \rho v \frac{\partial u}{\partial y} dx + \rho w \frac{\partial u}{\partial z} dx$$

However, from the irrotationality condition, we know that,

$$\frac{\partial u}{\partial y} = \frac{\partial v}{\partial x} \quad and \quad \frac{\partial u}{\partial z} = \frac{\partial w}{\partial x}$$

Using this, u-momentum equation gets modified as,

$$-\frac{\partial \mathrm{p}}{\partial x} dx = \rho u \frac{\partial u}{\partial x} dx + \rho v \frac{\partial v}{\partial x} dx + \rho w \frac{\partial w}{\partial x} dx$$

Further simplification of this equation leads to,

$$-\frac{\partial \mathrm{p}}{\partial x} dx = \frac{1}{2}\rho \frac{\partial u^2}{\partial x} dx + \frac{1}{2}\rho \frac{\partial v^2}{\partial x} dx + \frac{1}{2}\rho \frac{\partial w^2}{\partial x} dx$$

Similarly, v and w momentum equations can be obtained,

$$-\frac{\partial \mathrm{p}}{\partial y} dy = \frac{1}{2}\rho \frac{\partial u^2}{\partial y} dy + \frac{1}{2}\rho \frac{\partial v^2}{\partial y} dy + \frac{1}{2}\rho \frac{\partial w^2}{\partial y} dy$$

$$-\frac{\partial \mathrm{p}}{\partial z} dz = \frac{1}{2}\rho \frac{\partial u^2}{\partial z} dz + \frac{1}{2}\rho \frac{\partial v^2}{\partial z} dz + \frac{1}{2}\rho \frac{\partial w^2}{\partial z} dz$$

Adding all the momentum equations, we get,

$$-\left(\frac{\partial \mathrm{p}}{\partial x} dx + \frac{\partial \mathrm{p}}{\partial y} dy + \frac{\partial \mathrm{p}}{\partial z} dz\right) = \frac{1}{2}\rho \frac{\partial \mathrm{V}^2}{\partial z} dz + \frac{1}{2}\rho \frac{\partial \mathrm{V}^2}{\partial z} dz + \frac{1}{2}\rho \frac{\partial \mathrm{V}^2}{\partial z} dz$$

Where $V^2 = u^2 + v^2 + w^2$

This leads to the irrotational form of the Euler equation as,

$$-dp = \frac{1}{2}\rho d(V^2)$$

$$dp = -\rho V\, dV \quad \text{----------(2.8)}$$

2.5 Velocity Potential Equation

We know that, if curl of any vector field is zero then the corresponding vector field can be represented by gradient of scalar as,

$$\nabla \times A = 0$$

$$\nabla \times \nabla\zeta = 0$$

In view of the same, velocity field can be represented by gradient of potential for the irrotationalitty condition.

$$V \equiv \nabla\Phi$$

However we know that,

$$V = ui + vj + wk$$

and

$$\nabla\Phi = \frac{\partial\Phi}{\partial x}i + \frac{\partial\Phi}{\partial y}j + \frac{\partial\Phi}{\partial z}k$$

Therefore the components of velocities can be represented by corresponding potential gradients as,

$$u = \frac{\partial\Phi}{\partial x} \qquad v = \frac{\partial\Phi}{\partial y} \qquad w = \frac{\partial\Phi}{\partial z}$$

The mass conservation equation for the steady state condition is,

$$\nabla.(\rho V) = 0$$

$$\frac{\partial(\rho u)}{\partial x} + \frac{\partial(\rho v)}{\partial y} + \frac{\partial(\rho w)}{\partial z} = 0$$

Replacing the components of velocities we get,

$$\frac{\partial}{\partial x}\rho\Phi_x + \frac{\partial}{\partial y}\rho\Phi_y + \frac{\partial}{\partial z}\rho\Phi_z = 0$$

$$\rho\left(\Phi_{xx} + \Phi_{yy} + \Phi_{zz}\right) + \Phi_x\frac{\partial\rho}{\partial x} + \Phi_y\frac{\partial\rho}{\partial y} + \Phi_z\frac{\partial\rho}{\partial z} = 0 \quad \text{----------(2.9)}$$

However we have already derived the irrotational form of the Euler equation which can be used to replace the density gradients of above equations,

$$dp = -\rho V\, dV = \frac{1}{2}\rho d(V^2) = \frac{1}{2}\rho d(u^2 + v^2 + w^2)$$

$$dp = -\rho d\left(\frac{\Phi_x{}^2 + \Phi_y{}^2 + \Phi_z{}^2}{2}\right) \quad \text{----------(2.10)}$$

The definition of sound speed leads to,

$$\frac{dp}{d\rho} = \left(\frac{\partial p}{\partial\rho}\right)_s = a$$

$$d\rho = \frac{dp}{a^2}$$

Replacing dp of above equation using Eq. 2.10 we get,

$$d\rho = -\frac{\rho}{a^2} d\left(\frac{{\Phi_x}^2 + {\Phi_y}^2 + {\Phi_z}^2}{2}\right)$$

Hence, partial differentials of density are,

$$\frac{\partial \rho}{\partial x} = -\frac{\rho}{a^2}\frac{\partial}{\partial x}\left(\frac{{\Phi_x}^2 + {\Phi_y}^2 + {\Phi_z}^2}{2}\right)$$

$$\frac{\partial \rho}{\partial x} = -\frac{\rho}{a^2}\left(\Phi_x \Phi_{xx} + \Phi_y \Phi_{yx} + \Phi_z \Phi_{zx}\right)$$

$$\frac{\partial \rho}{\partial y} = -\frac{\rho}{a^2}\left(\Phi_x \Phi_{xy} + \Phi_y \Phi_{yy} + \Phi_z \Phi_{zy}\right)$$

$$\frac{\partial \rho}{\partial z} = -\frac{\rho}{a^2}\left(\Phi_x \Phi_{xz} + \Phi_y \Phi_{yz} + \Phi_z \Phi_{zz}\right)$$

The partial derivatives of density can be used to simplify the Eq. 28.2 as,

$$\left(1 - \frac{{\Phi_x}^2}{a^2}\Phi_{xx}\right) + \left(1 - \frac{{\Phi_y}^2}{a^2}\Phi_{yy}\right) + \left(1 - \frac{{\Phi_z}^2}{a^2}\Phi_{zz}\right) - \frac{2\Phi_x\Phi_y}{a^2}\Phi_{xy} - \frac{2\Phi_x\Phi_z}{a^2}\Phi_{xz} - \frac{2\Phi_y\Phi_z}{a^2}\Phi_{yz} = 0$$

---(28.4)

This equation is called as velocity potential equation. This equation is derived for steady irrotational flows from mass and momentum equations. This equation has two unknowns via velocity potential and acoustic speed or speed of sound. However the speed of sound seen in above equation can also are represented by velocity potential using energy equation. Let's consider that the total enthalpy is constant in the flowfield.

$h_\circ = constt.$

$$C_p T + \frac{V^2}{2} = C_p T_0$$

$$\frac{\gamma RT}{\gamma - 1} + \frac{V^2}{2} = \frac{\gamma RT_0}{\gamma - 1}$$

$$\frac{a^2}{\gamma - 1} + \frac{V^2}{2} = \frac{a_0^2}{\gamma - 1}$$

$$a_0^2 = a^2 - \frac{\gamma - 1}{2}V^2 = a^2 - \frac{\gamma - 1}{2}(u^2 + v^2 + w^2)$$

$$a_0^2 = a^2 - \frac{\gamma - 1}{2}\left({\Phi_x}^2 + {\Phi_y}^2 + {\Phi_z}^2\right)$$ ---- (28.5)

Simultaneous solution of Equations 28.4 and 28.5 gives the velocity potential. Using this we can get the velocity field using the potential gradients. However direct solution of these equation is not possible. Hence linearization of these equations is essential.

2.6 Linearization of Velocity Potential Equation

Consider the steady irrotational flow around the thin aerofoil as shown in **Fig. 2.4**. At location A, velocity is only in x direction. However, presence of body perturbs the components of velocity at location B.

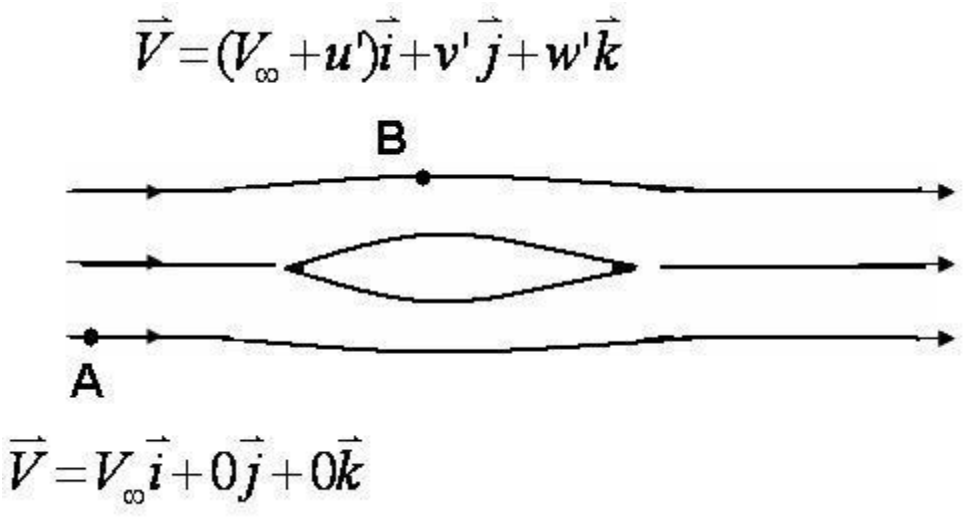

Fig. 2.4. Schematic of the perturbed velocity field.

Lets represent the general velocity field as,

$$\vec{V}=V_x\vec{i}+V_y\vec{j}+V_z\vec{k}$$

here, $V_x=V_\infty+u'$ and u', v', w' are the perturbed velocities in the x, y and z directions respectively such that.

$$V_y=v'$$

$$V_z=w'$$

Since the velocity field is irrotational, we can represent the velocity field using gradient of velocity potential as,

$$\nabla\Phi=\vec{V}=(V_\infty+u')\vec{i}+v'\vec{j}+w'\vec{k}$$

Let the perturbed velocity field be presented by perturbed velocity potential, ϕ. Hence,

$$\frac{\partial\phi}{\partial x}=u' \quad \frac{\partial\phi}{\partial y}=v' \quad \frac{\partial\phi}{\partial z}=w'$$

Therefore,

$$\Phi(x,y,z)=V_\infty x+\phi(x,y,z)$$

Such that,

$$V_x=\frac{\partial\Phi}{\partial x}=V_\infty x+u'=V_\infty x+\frac{\partial\phi}{\partial x}$$

$$V_y=\frac{\partial\Phi}{\partial y}=\frac{\partial\phi}{\partial y}=v'$$

$$V_z = \frac{\partial \Phi}{\partial z} = \frac{\partial \phi}{\partial z} = w'$$

and

$$\Phi_{xx} = \frac{\partial^2 \phi}{\partial x^2} = \phi_{xx}, \quad \Phi_{yy} = \frac{\partial^2 \phi}{\partial y^2} = \phi_{yy}, \quad \Phi_{zz} = \frac{\partial^2 \phi}{\partial z^2} = \phi_{zz}$$

We can use these expressions in the known velocity potential equation.

$$\left(1 - \frac{\Phi_x^2}{a^2}\right)\Phi_{xx} + \left(1 - \frac{\Phi_y^2}{a^2}\right)\Phi_{yy} + \left(1 - \frac{\Phi_z^2}{a^2}\right)\Phi_{zz}$$
$$-2\frac{\Phi_x \Phi_y}{a^2}\Phi_{xy} - 2\frac{\Phi_x \Phi_z}{a^2}\Phi_{xz} - 2\frac{\Phi_y \Phi_z}{a^2}\Phi_{yz} = 0$$

This expression in the form of perturbed velocity potential can be written as,

$$\left[a^2 - \left(V_\infty + \frac{\partial \phi}{\partial x}\right)^2\right]\frac{\partial^2 \phi}{\partial x^2} + \left[a^2 - \left(\frac{\partial \phi}{\partial y}\right)^2\right]\frac{\partial^2 \phi}{\partial y^2} + \left[a^2 - \left(\frac{\partial \phi}{\partial z}\right)^2\right]\frac{\partial^2 \phi}{\partial z^2}$$
$$-2\left(V_\infty + \frac{\partial \phi}{\partial x}\right)\frac{\partial \phi}{\partial y}\frac{\partial^2 \phi}{\partial x \partial y} - 2\left(V_\infty + \frac{\partial \phi}{\partial x}\right)\frac{\partial \phi}{\partial z}\frac{\partial^2 \phi}{\partial x \partial z} - 2\frac{\partial \phi}{\partial y}\frac{\partial \phi}{\partial z}\frac{\partial^2 \phi}{\partial y \partial z} = 0$$

or,

$$\left[a^2 - (V_\infty + u')^2\right]\frac{\partial u'}{\partial x} + \left[a^2 - v'^2\right]\frac{\partial v'}{\partial y} + \left[a^2 - w'^2\right]\frac{\partial w'}{\partial z}$$
$$-2(V_\infty + u')v'\frac{\partial v'}{\partial y} - 2(V_\infty + u')w'\frac{\partial u'}{\partial z} - 2v'w'\frac{\partial v'}{\partial z} = 0 \qquad \text{--- (2.11)}$$

But we know that, total enthalpy is constant in flow field. We can use this fact to represent the speed of sound encountered in the above equation as,

$\because h_0 = const.$

$$h_0 = h_\infty + \frac{V_\infty^2}{2} = h + \frac{V^2}{2} = h + \frac{(V_\infty + u')^2 + v'^2 + w'^2}{2}$$

$$\frac{a_\infty^2}{\gamma - 1} + \frac{V_\infty^2}{2} = \frac{a^2}{\gamma - 1} + \frac{(V_\infty + u')^2 + v'^2 + w'^2}{2}$$

$$a^2 = a_\infty^2 - \frac{\gamma - 1}{2}\left(2u'V_\infty + u'^2 + v'^2 + w'^2\right)$$

Using this expression and further simplification, Eq. 2.11 can be written as,

$$\left(1 - M_\infty^2\right)\frac{\partial u'}{\partial x} + \frac{\partial v'}{\partial y} + \frac{\partial w'}{\partial z}$$

$$= M_\infty^2\left[(\gamma+1)\frac{u'}{V_\infty}+\left(\frac{\gamma+1}{2}\right)\frac{u'^2}{V_\infty^2}+\left(\frac{\gamma-1}{2}\right)\left(\frac{v'^2+w'^2}{V_\infty^2}\right)\right]\frac{\partial u'}{\partial x}$$

$$+M_\infty^2\left[(\gamma-1)\frac{u'}{V_\infty}+\left(\frac{\gamma+1}{2}\right)\frac{v'^2}{V_\infty^2}+\left(\frac{\gamma-1}{2}\right)\left(\frac{w'^2+u'^2}{V_\infty^2}\right)\right]\frac{\partial v'}{\partial x}$$

$$+M_\infty^2\left[(\gamma-1)\frac{u'}{V_\infty}+\left(\frac{\gamma+1}{2}\right)\frac{w'^2}{V_\infty^2}+\left(\frac{\gamma-1}{2}\right)\left(\frac{u'^2+v'^2}{V_\infty^2}\right)\right]\frac{\partial w'}{\partial x}$$

$$+M_\infty^2\left[\frac{v'}{V_\infty}\left(1+\frac{u'}{V_\infty}\right)\left(\frac{\partial u'}{\partial y}+\frac{\partial v'}{\partial x}\right)+\frac{w'}{V_\infty}\left(1+\frac{u'}{V_\infty}\right)\left(\frac{\partial u'}{\partial z}+\frac{\partial w'}{\partial x}\right)+\frac{u'w'}{V_\infty}\left(\frac{\partial w'}{\partial y}+\frac{\partial v'}{\partial z}\right)\right]\frac{\partial v'}{\partial x}$$ --- (2.12)

The equation (2.1) is the exact equation for steady irrotational flow around the thin configurations.

We can simplify this equation, since the perturbed velocities, u', v' and w' are small in comparison with the freestream velocity V_∞.

Hence,

$\frac{u'}{V_\infty}$, $\frac{v'}{V_\infty}$ and $\frac{w'}{V_\infty}$ <<1

So, $\left(\frac{u'}{V_\infty}\right)^2\left(\frac{v'}{V_\infty}\right)^2\left(\frac{w'}{V_\infty}\right)^2$ <<<1

This approximations leads to two facts,

1. Except for the Transonic flows (Flows having Mach number in the range 0.8 to 1.2)

$$M_\infty^2\left[(\gamma+1)\frac{u'}{V_\infty}+\cdots\right]\frac{\partial u'}{\partial x} << \left(1-M_\infty^2\right)\frac{\partial u'}{\partial x}$$

2. If Mach number of the flow is less than 5.0

$$M_\infty^2\left[(\gamma+1)\frac{u'}{V_\infty}+\cdots\right]\frac{\partial u'}{\partial x} << \left(1-M_\infty^2\right)\frac{\partial u'}{\partial x}$$

$$M_\infty^2\left[(\gamma-1)\frac{u'}{V_\infty}+\cdots\right]\frac{\partial v'}{\partial y} << \frac{\partial v'}{\partial y}, \quad M_\infty^2\left[(\gamma-1)\frac{u'}{V_\infty}+\cdots\right]\frac{\partial w'}{\partial z} << \frac{\partial w'}{\partial z}$$

$$M_\infty^2\left[(\gamma-1)\frac{v'}{V_\infty}\left(1+\frac{u'}{V_\infty}\right)\left(\frac{\partial u'}{\partial y}+\frac{\partial v'}{\partial x}\right)+\cdots\right] << 1 \quad (\approx 0)$$

For these two facts we get,

$$\left(1-M_\infty^2\right)\frac{\partial u'}{\partial x}+\frac{\partial v'}{\partial y}+\frac{\partial w'}{\partial z}=0$$

Or,

$$\left(1-M_\infty^2\right)\frac{\partial^2\phi}{\partial x^2}+\frac{\partial^2\phi}{\partial y^2}+\frac{\partial^2\phi}{\partial z^2}=0$$

This is the linear equation and this approximation is valid for steady irrotational subsonic and supersonic flows under the assumption of small perturbation.

2.7 Supersonic flow over a cone

2.7.1 Introduction

The flow over a cone is a two-dimensional axisymmetric problem. It is also referred to as "Quasi-Two dimensional Problem". This is so, because, the cone under consideration is aligned symmetrically about the z-axis or along the direction of V_∞ , as shown in the **Fig.2.5**

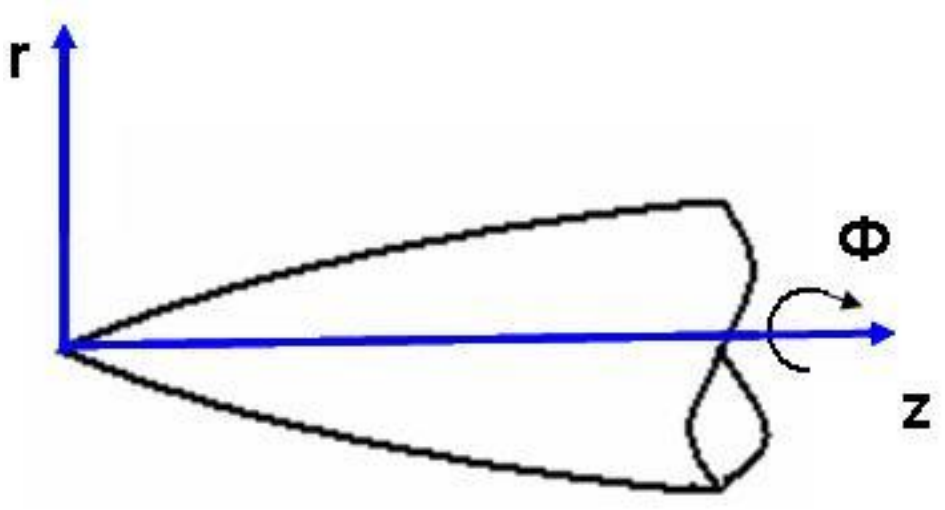

Fig. 2.5: Geometry in consideration and the fluid flow direction

The supersonic flow over a cone is of great practical importance in applied aerodynamics. The nose cones of many high-speed missiles and projectiles are approximately conical, are the nose regions of the fuselages of most supersonic airplanes.
In the particular problem of supersonic flow over a cone, consideration is given to a sharp right circular cone with zero angle of attack. Consider a cone on the (r, ϕ, z) co-ordinate system, as shown in **Fig. 2.5** which is symmetric about the Z axis and extends to infinity with a semi-vertex cone angle θ. The supersonic flow with free stream velocity V_∞ is considered along the Z axis, such that the angle of attack is 0^o. Typical flow field for supersonic flow over cone is as shown in **Fig. 2.6**. For such a supersonic flow over the surface of the cone, it is expected that a oblique shock wave attached to the tip of the cone is formed. Further, the shape of the shock wave formed is also conical.

A streamline from the supersonic free stream discontinuously deflects as it passes through the shock, and then curves continuously downstream of the shock, becoming parallel to the cone surface asymptotically at infinity. Further, it is also assumed that the pressure and all the other flow properties are constant along the surface of the cone. Since the cone surface is simply a ray from the vertex, consider other such rays between the cone surface and the shock wave, as shown by the dashed line in **Fig 2.6**. Hence assumption of constancy of flow properties can be extended along these rays as well. Therefore properties variation takes place as the fluid moves from one ray to the next.

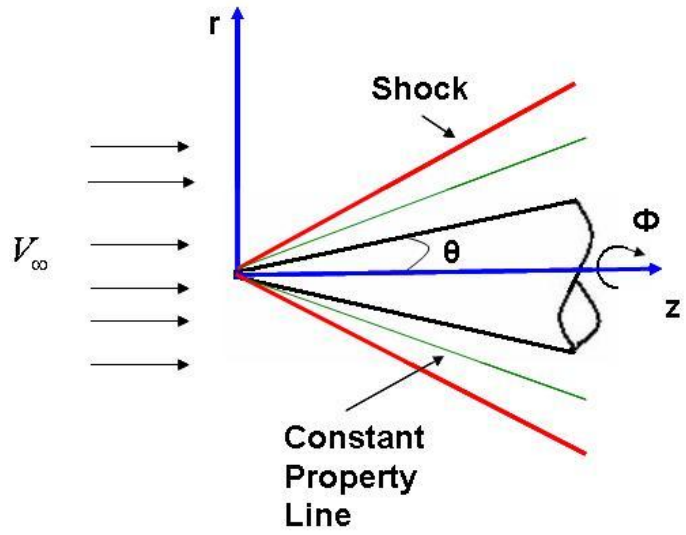

Fig.2.6: Flow field in the presence of supersonic flow over a cone.

2.7.2 Mathematical Formulation for Supersonic flow over cone

Consider **Fig. 2.7.** For the terminologies of the derivation in concerned with supersonic flow over cone. At any angular location in the flow field, the radial and normal components of velocity are V_r and V_θ, respectively. Understanding the flow field around the cone necessarily means solving for the flow field between the body and the shock wave by calculating these velocity components. Since the flow field is symmetric about the *z* axis all properties are independent of Φ.

So,

$$\frac{\partial}{\partial \phi} = 0$$

Further, since we have assumed that the flow properties are constant along a ray from the vertex

$$\frac{\partial}{\partial r} = 0$$

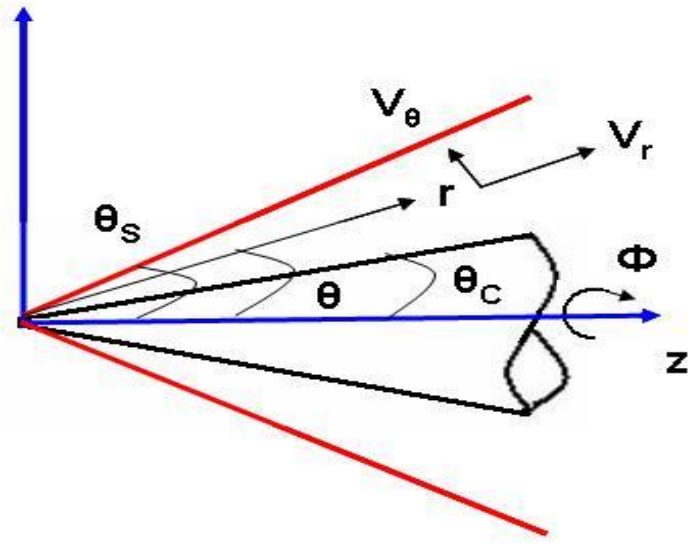

Fig. 2.7: Schematic for terminologies regarding derivation for supersonic flow over cone.

From the equation of continuity, we get

$$\nabla.(\rho V) = 0$$

But, since the geometry is symmetric about the z axis and extends to infinity, the scale on the Z-axis can be neglected while considering the spherical co-ordinate system to analyze the problem. Hence the mass conservation equation can be written as,

$$\nabla.\rho(V) = \frac{1}{r^2}\frac{\partial}{\partial r}(r^2\rho V_r) + \frac{1}{r\sin\theta}\frac{\partial}{\partial\theta}(\rho V_\theta \sin\theta) + \frac{1}{r\sin\theta}\frac{\partial(\rho V_\phi)}{\partial\phi} = 0$$

$$\frac{1}{r^2}[r^2\frac{\partial(\rho V_r)}{\partial r} + (\rho V_r)(2r)] + \frac{1}{r\sin\theta}[\rho V_\theta\cos\theta + \sin\theta\frac{\partial(\rho V_\theta)}{\partial\theta}] + \frac{1}{r\sin\theta}\frac{\partial(\rho V_\theta)}{\partial\phi} = 0$$

$$\frac{2\rho V_r}{r} + \frac{\rho V_\theta}{r}\cot\theta + \frac{1}{r}(\rho\frac{\partial V_\theta}{\partial\theta} + V_\theta\frac{\partial\rho}{\partial\theta}) = 0$$

$$2\rho V_r + \rho V_\theta\cot\theta + (\rho\frac{\partial V_\theta}{\partial\theta} + V_\theta\frac{\partial\rho}{\partial\theta}) = 0 \quad \text{----------(2.13)}$$

This is the continuity equation for the axisymmetric flow over the cone.

For this axisymmetric flow, there is increase in the entropy across the shock, but the change in entropy is zero in the region between the shock and the cone since post shock flow is isentropic, i.e, $\nabla s = 0$ .Further, the flow in this region is steady and adiabatic, hence $\Delta h_0 = 0$ .Therefore, from Crocco's equation, $V\times(\nabla\times V) = \nabla h_0 - T\times\nabla s$,we find that $V\times(\nabla\times V) = 0$ i.e., the conical flow field is irrotational. Hence,

$$\nabla\times\mathbf{V} = \frac{1}{r^2\sin\theta}\begin{vmatrix} \mathbf{e}_r & r\mathbf{e}_\theta & (r\sin\theta)\mathbf{e}_\phi \\ \frac{\partial}{\partial r} & \frac{\partial}{\partial\theta} & \frac{\partial}{\partial\phi} \\ V_r & rV_\theta & (r\sin\theta)V_\phi \end{vmatrix} = 0$$

$$\nabla\times V = \frac{1}{r^2\sin\theta}\{e_r[\frac{\partial}{\partial\theta}(rV_\phi\sin\theta) - \frac{\partial}{\partial\phi}(rV_\theta)] - re_\theta[\frac{\partial}{\partial r}(rV_\phi\sin\theta) - \frac{\partial(V_r)}{\partial\phi}] + (r\sin\theta)e_\phi[\frac{\partial}{\partial r}(rV_\theta) - \frac{\partial V_r}{\partial\theta}]\} = 0$$

Applying the axisymmetric conical flow constant as, $\frac{\partial}{\partial\phi} = 0$ and, we can get as

$$\frac{\partial}{\partial r}(rV_\phi\sin\theta) - \frac{\partial(V_r)}{\partial\phi} = 0$$

$$r\frac{\partial}{\partial r}(V_\phi\sin\theta) = 0$$

This simplifies the irrotatinality constant to,

$$V_\theta = \frac{\partial V_r}{\partial\theta} \quad \text{----------(2.14)}$$

2.7.2 Unit process is one or more grouped operations in a manufacturing system that can be defined and separated from others.

2.8 Flow through duct.

The procedure for using the method of characteristic lines are to numerically calculate the flow in a duct is as follows:

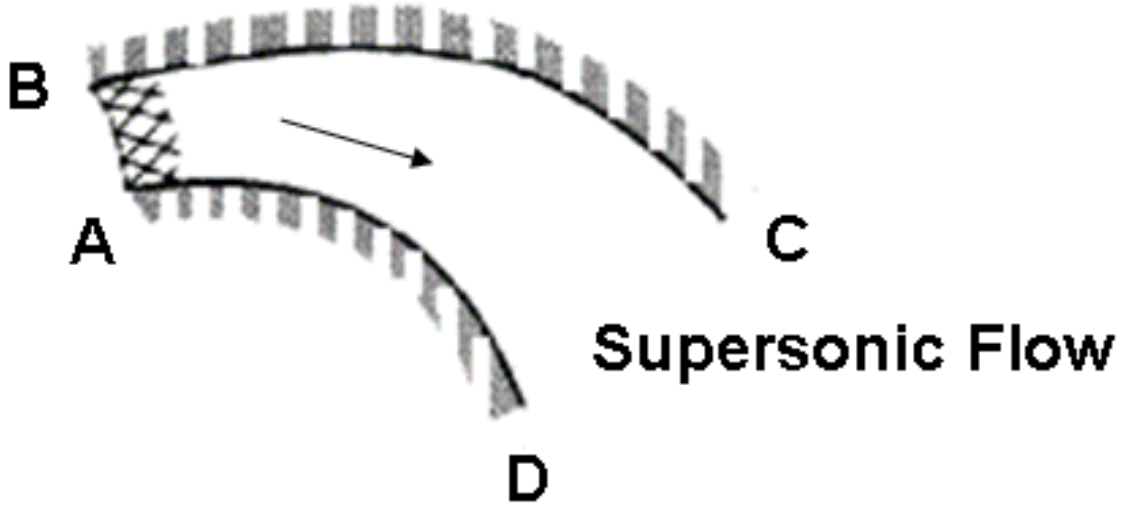

Fig. 2.8. Supersonic flow through duct

1. The conditions on some initial line must be specified, e.g., conditions on the line AB in Fig. 2.8 must be specified.
2. The shape of the walls, e.g., AD and BC in Fig. 2.8, must be known.
3. Using the initial values of the variables on line A, determine the stagnation pressure, temperature, etc.
4. Starting with a series of chosen points on line AB, march the solution forward to the points defined by the intersection of characteristics with each other or with the wall as indicated.
5. At each point, use the calculated values of ν and θ to get flow variables.

A computer program based on this procedure can be easily developed.

2.8.1 Nozzle Design

Supersonic nozzles are used in a variety of engineering applications to expand a flow to desired supersonic conditions. Supersonic nozzles can be divided into two different types: gradual-expansion nozzles and minimum-length nozzles (Fig. 2.9). Gradual-expansion nozzles are typically used in applications where maintaining a high-quality flow at the desired exit conditions is of importance (e.g., supersonic wind tunnels). For other types of applications (e.g., rocket nozzles), the large weight and length penalties associated with gradual-expansion nozzles make them unrealistic; therefore minimum-length nozzles, which utilize a sharp corner to provide the initial expansion, are commonly used.

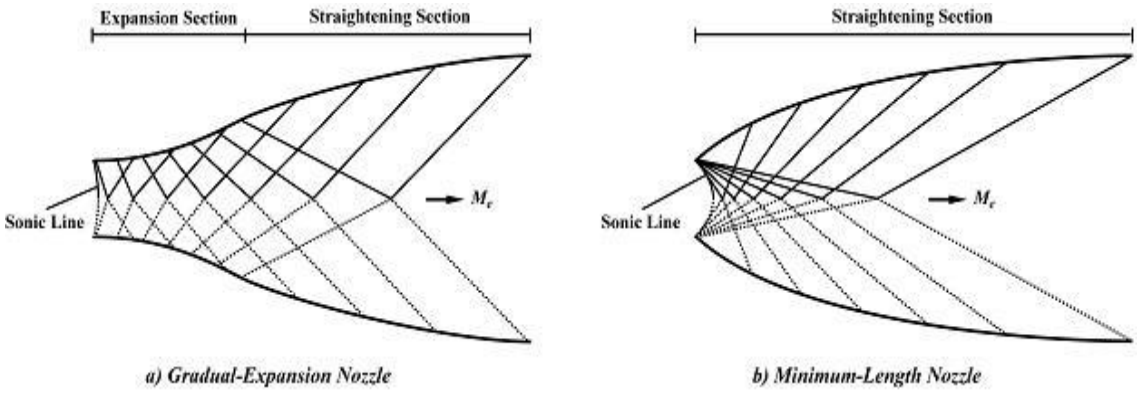

Fig. 2.9 Types of nozzles.

For both gradual-expansion and minimum-length nozzles, the flow can be divided into simple and non-simple regions. A non-simple region is characterized by Mach wave reflections and intersections. In order to meet the requirement of uniform conditions at the nozzle exit, it is desirable to minimize the non-simple region as much as possible. This can be performed by designing the nozzle surface such that Mach waves (e.g., characteristics) are not produced or reflected while the flow is straightened.

The Method of Characteristics is therefore applied to allow the design of a supersonic nozzle which meets these requirements. In the present work, design of both gradual-expansion nozzle and minimum-length nozzle is demonstrated.

The boundary layer on the nozzle and side walls has a displacing effect which reduces the effective height and width of the nozzle. Allowance for this is to be made by adding a correction for boundary layer. The side walls should also diverge to allow for their boundary layers.

2.8.2 Method of characteristics is & Method of waves

The method of characteristics deals with a continuous velocity field, the computation being made at the lattice points of a network of characteristics. The wave method deals with a patch work field of cells of uniform flow, with discontinuities between them. Accuracies in the two methods are similar, being dependent on the fineness of the mesh

Computation with waves is convenient only in plane flow, since it depends on the theorem that the strength of a wave does not change after intersections and reflections. In axially symmetric flow and in general 3-D flow the strength of a wave varies continuously.

The wave method is more intuitive in plane flow than the characteristic method and is usually preferred. In some problem it is more convenient – because of the idea of wave cancellation to determine a boundary shape.

2.9 Design of Minimum-Length Nozzle (MLN)

It should be noted that for this two-dimensional nozzle configuration, flow symmetry implies that only half of the nozzle is physically required, assuming that the characteristic reflections in the non-simple region are maintained. Therefore, we can make the assumption of a half-symmetric minimum-length nozzle, in which a nozzle flap is extended from the symmetry plane such that it meets the length requirement for the last characteristic intersecting the nozzle surface (Fig.2.10).

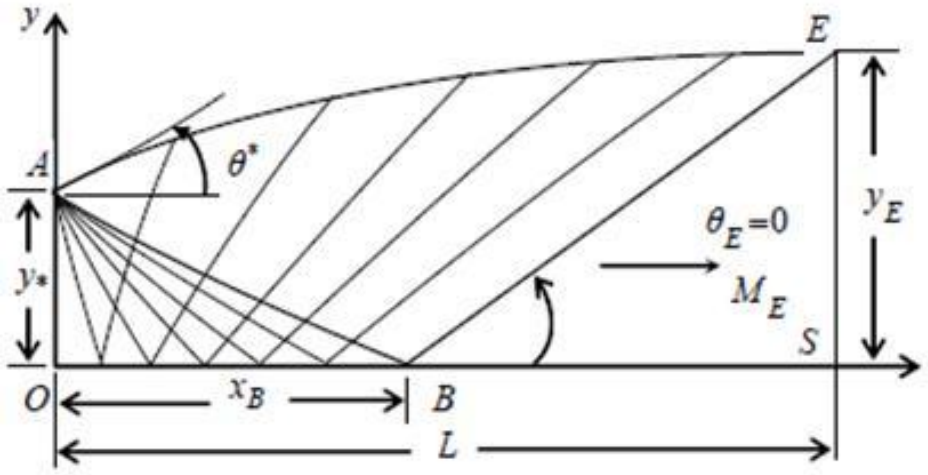

Fig. 2.10. Schematic of characteristic lines for MLN.

2.9.1 Implementation of Method of Characteristics

The two-dimensional Method of Characteristics is a relatively simple analytical model for analyzing supersonic two-dimensional flow. This analysis is performed by considering the characteristic lines in the flow. Points along each characteristic have five important properties: M (Mach number), θ (flow angle), ν (Prandtl-Meyer function), and x and y (position). For the assumption of steady, supersonic, we know that,

$$\theta \pm \vartheta = Constant$$

The constant for summation can be said to be K+ and for subtraction to be K-. These constants are the Riemann invariants, which are constant along the characteristics C+ and C-.

2.9.2 Design of Gradual expansion nozzle

The steps involved in this calculation are precisely same as those used for the minimum length nozzle except for the fact that the expansion fan at the sharp corner is now replaced by a series of right running characteristic characteristic lines originating from the arc of the circle. One major assumption that has been made here is that a characteristic originating from any point on the expansion section is always reflected from the axis in such a way that it reaches the straightening portion of the nozzle. Multiple reflections of characteristic lines within the smooth expansion portion of the nozzle would make the problem much complicated without really improving the results much.

UNIT- III
NUMERICAL SOLUTION OF TRANSONIC SMALL DISTURBANCE EQUATION

3.1 THE TRANSONIC SMALL DISTURBANCE EQUATION

We consider the techniques for numerically the transonic flow over airfoils and bodies of revolution. Our ultimate interest is in techniques for predicting the pressure distribution Cp and the loads (lift Cl, drag Cd and the pitching moment about the quarter chord cm) over these geometries. For simplicity, we extensively discuss only 2-D planar flows. From the previous chapter, we recall that the governing equations are:

$$\boxed{\left(\rho\phi_x\right)_x + \left(\rho\phi_y\right)_y = 0} \tag{3.1}$$

It is possible to eliminate the explicit appearance of density r from equation and arrive at the following quasi-linear form of the full potential equation:

$$\boxed{\left(a^2 - u^2\right)\phi_{xx} - 2uv\phi_{xy} + \left(a^2 - v^2\right)\phi_{yy} = 0} \tag{3.2}$$

Equation 3.2 is called quasi-linear because it is linear in its highest derivatives. It is, of course, nonlinear . It is this nonlinearity that allows us to model shock waves, a very non-linear phenomenon. From a mathematical theory called the method of characteristics, one can show that equation (3.2)

3.1.1 Loads over the Airfoil

The airloads over the airfoil may be found once Cp is known as follows:

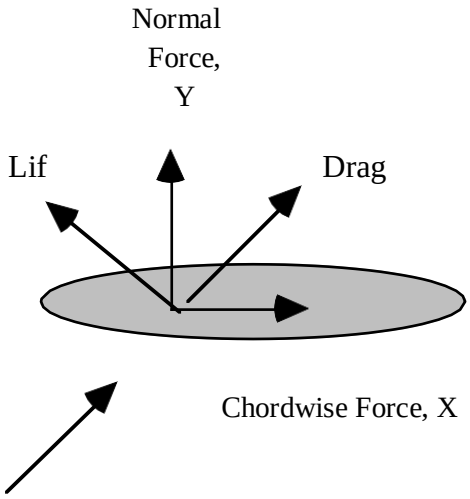

where Y(x) is the airfoil shape

We are interested in the solution of the governing equations, in the entire region between the airfoil and infinity. Because of the nonlinearity of the governing equations, we can not analytically solve the governing equations except in some highly simplified cases. Thus, our approach is necessarily numerical, and is based on CFD techniques.

3.1.2 Small Disturbance Assumptions

In this, we attempt to simplify the problem by making some physically acceptable assumptions. In the next chapter, we will discard these restrictive assumptions and will solve equation set 3.1 and 3.2 directly.

The assumptions we make are:

1. The body is thin, has a small angle of attack, and has only a mild camber. As a result, the body slope dY/dx, in a coordinate system attached to the free stream (known as the wind tunnel coordinate system) is small.
2. As a consequence, we assume that the local flow velocity components u and v are not significantly different from their free stream values.

It must be noted that the above assumption and the resulting analysis known as the transonic small disturbance (TSD) theory are, to some extent, only of historical interest. Today, most real world problems are solved by directly solving equations 3.1 and 3.2, known as the full potential equations (FPE). Nevertheless, the TSD theory provides a useful starting point for the more accurate FPE approach.

Disturbance Potential :

We introduce a disturbance potential, φ, related to the full potential ϕ as follows:

It must be remembered that in this chapter we are using the wind tunnel coordinate system, and the freestream velocity is parallel to the x- axis.

$$\boxed{\begin{aligned} u &= \phi_x = V_\infty + \varphi_x \\ v &= \phi_y = \varphi_y \end{aligned}} \qquad (3.3)$$

3.2 Mathematical Characteristics of the TSD Equation:

The transonic small disturbance equation is still nonlinear, in spite of the approximations that were made to arrive at this equation. It is this nonlinearity which makes formation of shock waves possible. To see why, consider the following equation which is similar in form to equation

These two solutions may occur across a jump (a shock wave) as shown below:

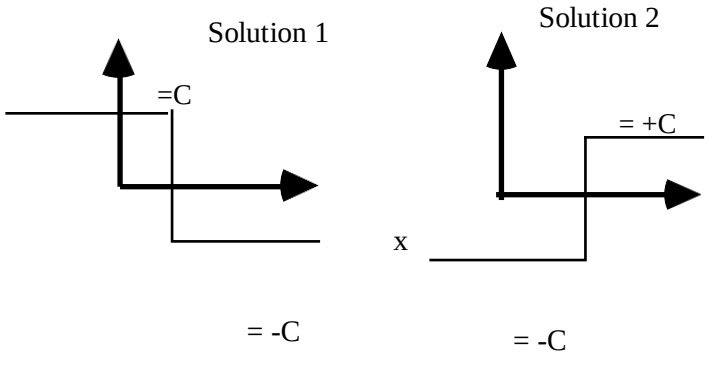

Note that the flow will slow down across the first jump, as the disturbance velocity changes in magnitude from a positive value to a negative value. This type of jump is classified as a compression shock. The second jump, on the other hand, corresponds to an expansion shock, across which the flow abruptly increases in velocity. We therefore conclude that our TSD equation can give rise to compression shocks as well as expansion shocks. Expansion shocks violate the second law of Thermodynamics, and should be excluded, as part of the numerical solution procedure. When A is positive, there are no real characteristics, and the equation is elliptic. When A is zero, the equation is called parabolic, with characteristic lines that are parallel to the y- axis. Finally, when A is negative, two distinct characteristics exist, and the equation is hyperbolic.

At any point P in space, these two characteristics will have slopes that are equal in magnitude and opposite in sign, and will be symmetric about the x- axis, as shown. The region in front of the point P enclosed by the characteristics is known as the domain of dependence of point P. The region downstream of P, enclosed within the characteristics is influenced by point P and known as the domain of influence of P.

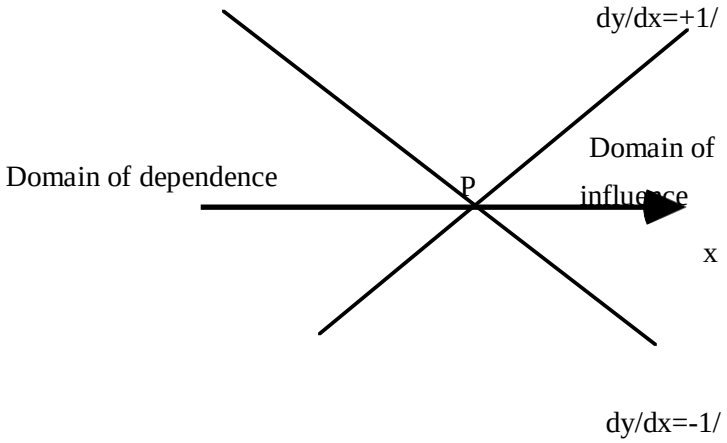

In a general transonic flow, the quantity A can change sign from point to point. Thus, the TSD equation may be elliptic in some (subsonic) regions of the flow, parabolic on sonic lines, and supersonic and hyperbolic in other regions:

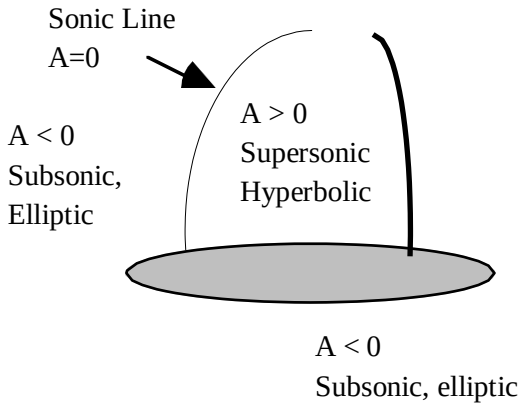

Any numerical scheme must account for the fact that these three regions may simultaneously exist in a transonic flow. The numerical scheme must be properly designed, so that a point P depends on its entire surrounding when the point is in an elliptic region. The numerical scheme must also ensure that the point P depends only on its domain of dependence in hyperbolic regions. Finally, the numerical scheme must capture the sonic line where the equation is parabolic, and the shock wave, across which the flow is discontinuous. Simplifying, the following small disturbance approximation to surface pressure coefficient results:

Boundary Conditions

Before the transonic small disturbance equation may be solved, we need to specify the boundary conditions. Of course, the boundary conditions must take into account the physics of the problem, and the mathematical characteristics of the equation.

Boundary Conditions at the Solid Boundary:

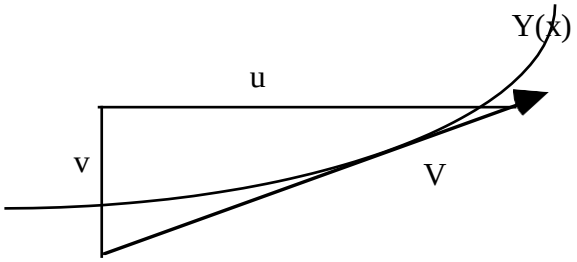

At any point on the body surface, the flow must be tangential to the body.

r

In other words, the slope of the velocity vector *V* must equal the body slope.

$$\varphi_y \approx V_\infty \frac{dY}{dx} \tag{3.4}$$

Where this boundary condition should be applied? We have two choices. This boundary condition may be applied either at the actual airfoil surface, or on a slit along the chord line, located on the x- axis. The latter choice makes the solution procedure simpler because we can use a Cartesian coordinate system, rather than a curvilinear coordinate system that is wrapped around the body. Within the assumptions built into the small disturbance theory, these two approaches may be shown to be equivalent. Note that this slit is a discontinuity, across which both the disturbance velocity potential and its y- derivative are discontinuous.

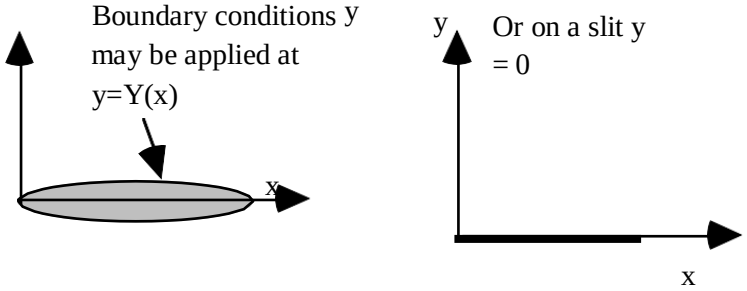

Boundary Conditions along a cut downstream of the airfoil trailing edge: Consider an airfoil at an angle of attack, producing lift. Then, in a potential flow, the following line integral over any contour enclosing the airfoil will produce a nonzero result, known as the circulation.

In the above integral, *dS* is an infinitesimal line segment vector, tangential to the contour. If this contour does not enclose the airfoil, then, using Stokes' theorem the above line integral may be shown to be equivalent to the following area integral:

$$\underset{\text{Not enclosing the airfoil}}{\int} V \bullet dS = \underset{\text{Area enclosed by the contour}}{\iint} \left(\nabla \times V\right) \bullet \hat{n}\, dA = 0$$

The area integral is zero because the curl of the velocity vector is zero in a potential flow.

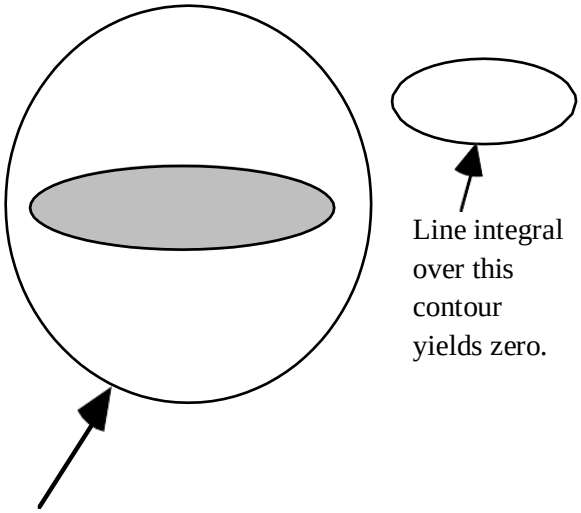

Line integral over this contour yields a non-zero result.

$$\begin{aligned}\vec{V} \bullet d\vec{S} &= \vec{\nabla}\phi \bullet d\vec{S} \\ &= \left(\phi_x \vec{i} + \phi_y \vec{j}\right) \bullet \left(dx\, \vec{i} + dy\, \vec{j}\right) \\ &= \frac{\partial \phi}{\partial x} dx + \frac{\partial \phi}{\partial y} dy \\ &= d\phi\end{aligned}$$

Thus, the circulation in equation is related to the jump in the velocity potential (or the jump in the disturbance potential):

The jump in the value of the velocity potential or the disturbance potential implies that these are not single valued functions. Somewhere in the x-y plane, these functions must experience an abrupt jump in their value, by an amount equal to the circulation, G. The location where the jump occurs may, however, be chosen to suit our convenience. In our analysis, we will assume that the disturbance potential jumps by an unknown amount along a cut that starts at airfoil trailing edge, and ends at downstream infinity.

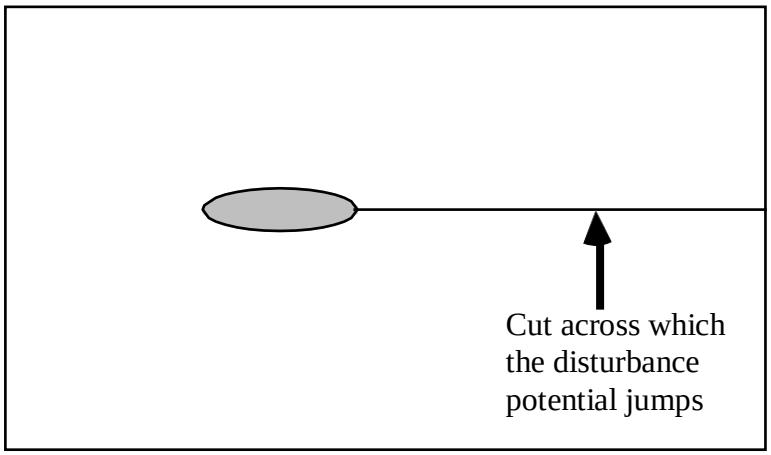

3.3 Far Field Boundary Conditions:

All numerical calculations are necessarily done on a finite domain. This means the outermost boundary where the disturbance velocity potential is solved for, ends at a finite distance from the airfoil. Boundary conditions consistent with the physics of the flow must be specified on this problem, and over-specification of the boundary conditions must be avoided. The specification of boundary conditions is different for subsonic free stream (M< 1) and supersonic free stream (M >1).

Subsonic free stream:

In this case, the disturbance velocity vanishes at the farfield boundary and the potential flow satisfies the linearized velocity potential equation. Since this equation is linear, it may be solved by superposition of sources, sinks, doublets (sources and sinks placed in close proximity with the product of their strength times the separation distance is a constant) and vortices.

For closed bodies, no mass may be generated within the airfoil, or in the flow. Therefore, we should not use source or sink singularities. A doublet (source-sink combination) may be placed somewhere on the airfoil chord line to represent the airfoil thickness effects and the lateral displacement of streamlines. A vortex may also be placed somewhere along the airfoil chord (usually at the quarter chord) to simulate the lift effects.

Now, from incompressible flow, a doublet of strength A produces the following disturbance potential at the far field boundary, at a distance r from the doublet:

Because this quantity rapidly goes to zero at large distances from the airfoil, the doublet effects (i.e. the airfoil thickness effects) are usually not included in the farfield boundaries.

The vortex of strength placed somewhere on the airfoil chord line introduces the following disturbance:

This expression may be shown to satisfy equation. The distances x and y must be measured from the location of the vortex. Note that the above expression reduces to the familiar incompressible form associated with point vortices, when the Mach number is zero.

3.3.1 Supersonic Free stream:

When the free stream is supersonic, the uses of sources, sinks and doublets are not appropriate, because signals from the airfoil cannot travel upstream. The proper boundary conditions are as follows.

Upstream Boundary: At this boundary, is set to zero.

Downstream Boundary: On this boundary, it is not appropriate to specify any boundary conditions, because in supersonic flow information can only flow downstream. In other words, the behavior of is determined by the flow over the airfoil itself. Thus, we should determine from the nonlinear governing equation or its linearized form.

Lateral Boundaries: At these boundaries, the linearized potential equation may be examined to arrive at the proper boundary conditions. From the mathematical theory of characteristics, this equation has two characteristics, and two corresponding compatibility conditions that must be satisfied along the characteristics. These are:

These characteristic equations and their compatibility equations must be applied at the lateral boundaries. Equation set, which corresponds to a characteristic that starts in the interior of the flow out proceeds upwards and outwards is applied at the top boundary. Equation corresponds to a characteristic with a negative slope, which starts at the interior and proceeds down towards the lower lateral boundary. Therefore, this equation is applied at the bottom boundary.

dy/dx=+1/

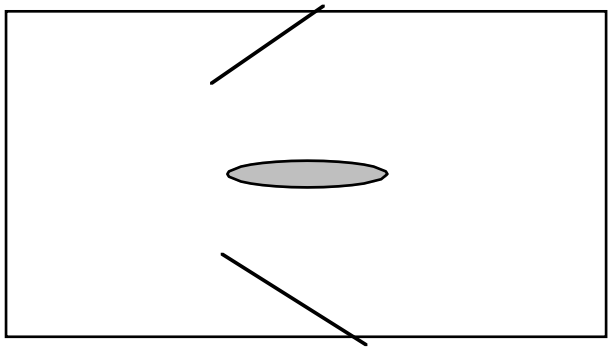

dy/dx= - 1/

One can apply the method o f characteristic at the downstream boundary as well to solve it is far easier to solve the governing equations at this boundary, in a manner identical to that used in the interior.

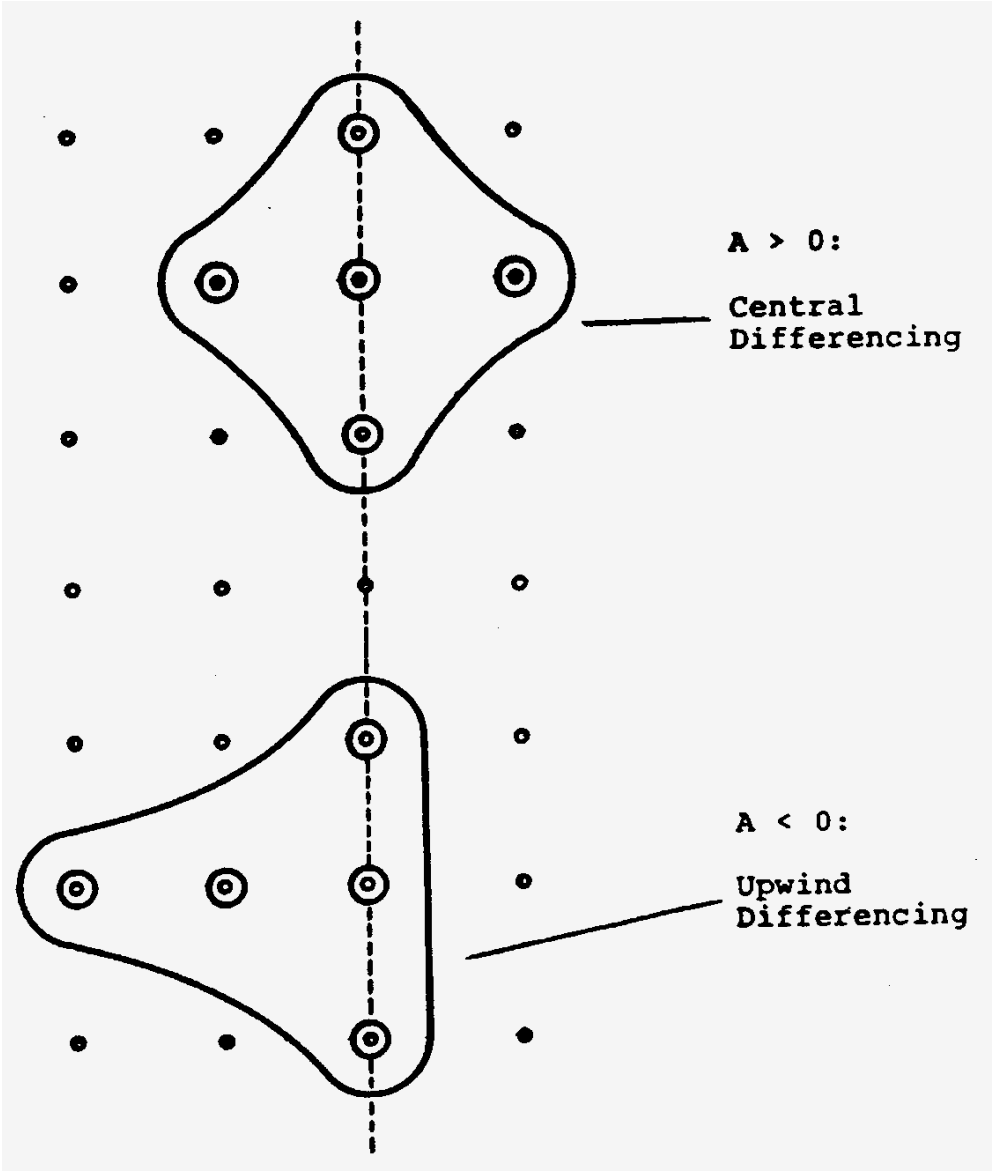

Murman-Cole Difference Scheme: $Av_{xx} + v_{yy} = 0$

UNIT - IV
NUMERICAL METHODS FOR EULER EQUATIONS, BOUNDARY LAYER EQUATIONS

4.1 Solution of the Euler Equations

4.1.1 Formulation

The results of potential flow calculations have proved accurate enough to be used as the basis of the wing design of the latest generation of transport aircraft, such as the Boeing 767 and Airbus A 310. Nevertheless, the assumption of potential flow is not strictly correct when shock waves are present, and this inconsistency must set a limit to the accuracy that could be obtained even if the discretion errors were entirely eliminated. To provide a correct description of inviscid transonic flow we must solve the Euler equations. The widespread use of Euler codes has so far been impeded by large numerical errors (leading, for example, to generation of, spurious vorticity), and excessively slow convergence (often no convergence). Recent developments promise to correct this situation.

The emphasis here will be on the calculation of steady state solutions. While other iterative methods can be conceived, most of the methods so far developed are based on the concept of integrating the equations in time until they reach a steady state. An exterior problem can reach a steady state as a result of the propagation of disturbances away to infinity. This mechanism of convergence by expulsion of errors is effective as long as out- going disturbances are not too strongly reflected back into the interior and boundary conditions must therefore be treated with care. Since the time dependent terms are used merely as a device for generating an iterative scheme, they may be modified to increase the rate of convergence. The time dependent formulation is similar in principle to the Jacobi method. When applied to Laplace's equation, for example, the Jacobi method is equivalent to integrating the heat equation

$\upsilon_t = \upsilon_{xx} + \upsilon_{yy}$

until it reaches a steady state.

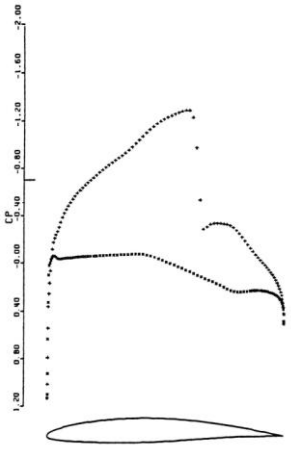

Figure 4.1: Transonic flow solution obtained with 3 multigrid cycles NACA 640410, Mach .720, $\alpha = 0^\circ$, CL=.6640, CD=.0031, 192 × 32 grid Residual .58010−6

An advantage of the time dependent formulation is that it brings the problem within the frame work of the mathematical theory of difference methods for hyperbolic equations. Stemming from the early work of Courant, Von Neumann, and Lax, this theory is by now highly developed.

A stability theory for the initial boundary value problem has been formulated and refined by Kreiss, Gustaffson and Sundstrom, and the application of this theory has been worked out for a variety of discretization schemes. Procedures have also been developed for the construction of boundary conditions designed to allow outgoing waves to pass through the outer boundary. The availability of this body of theory provides a solid foundation for the development of codes to treat practical aerodynamic problems.
A special case occurs when the flow is everywhere supersonic. The steady state equations then constitute a hyperbolic system in which the stream wise coordinate plays the role of the time like variable, and the entire flow field can be calculated in a single sweep, marching downstream.

4.1.2 Semi-Discrete Finite Volume Schemes

A convenient way to assure a steady state solution independent of the time step is to separate completely the space and time discretization procedures. In the scheme proposed by Jameson, Schmidt and Turkel one begins by applying a semi-discretization in which only the spatial derivatives are approximated. The resulting ordinary differential equations are then solved by a multi-stage time stepping procedure.
The space discretization scheme can be developed by writing the Euler equations in the integral form. The computational domain is divided into quadrilateral cells denoted by the subscripts *i, j* as, sketched in Figure 4.1

4.1.2.1 Adaptive Dissipation

The finite volume scheme defined by equations is not dissipative, allowing undamped oscillations with alternate sign at odd and even mesh points. In order to eliminate spurious oscillations, which will be triggered by discontinuities in the solution, one can follow either of two strategies. The first is to begin with a non-dissipative scheme, and to attempt to add just enough dissipation where it is needed to control the tendency to produce spurious oscillations. The second approach is to try to construct a scheme which is guaranteed to prevent oscillations by preserving the monotonicity of an initially monotone profile, typically through the use of one-sided upwind differencing.

In this section I describe an adaptive scheme for adding dissipation which has proved effective in practice. The idea of the adaptive scheme is to add third order dissipative terms throughout the domain to provide a base level of dissipation sufficient to prevent nonlinear instability, but not sufficient to prevent oscillations in the neighborhood of shock waves. In order to capture shock waves additional first order dissipative terms are added locally by a sensor designed to detect discontinuities.

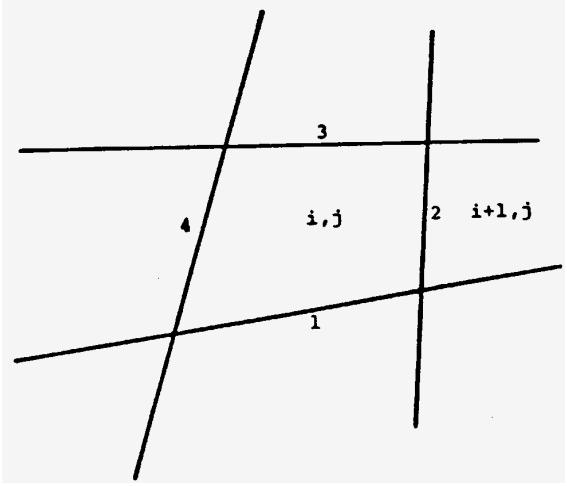

Figure 4.2: Finite Volume Scheme

4.1.2.2 Upwind Differencing, Total Variation Diminishing Schemes, and Flux vector Splitting

It is not easy to simulate a propagating discontinuity by a numerical method. The simplest model of convection is provided by the one dimensional wave equation

$u_t + u_x = 0$

This equation can be approximated by the one sided scheme

$u_i^{n+1} = u_i^n - \lambda(u_i^n - u_{i-1}^n)$

where λ is the Courant number $\Delta t/\Delta x$. This scheme is stable for $0 < \lambda < 1$ and it is appealing for two reasons:

1. It simulates the physical process of wave propagation by looking back- wards along the direction of propagation: if $\lambda = 1$, it exactly represents propagation along characteristics.
2. It has the property of preserving the monoticity of an initially mono- tone profile: this excludes the possibility of generating an overshoot behind a shock wave.

These observations have motivated numerous studies of one sided schemes, dating back to the early work of Courant, Isaacson and Rees. There has recently been a revival of interest in the use of one sided differencing for compressible flow calculations, beginning with the nonconservative λ scheme of Moretti, and the conservative scheme of Steger and Warming.
There is by now a rather extensive theory of difference schemes for the treatment of a scalar conservation law.

4.1.2.3 Boundary Conditions

The pressure at the wall is then estimated by extrapolation from the pressure at the adjacent cell centers, using the known value.
The rate of convergence to a steady state will be impaired if outgoing waves are reflected back into the flow from the outer boundaries. The treatment of the far field boundary condition is based on the introduction of Riemann invariants for a one dimensional flow normal to the boundary. Let subscripts and e denote free stream values and values extrapolated from the interior cells adjacent to the boundary and let q_n and c be the velocity component normal to the boundary and the speed of sound. Assuming that the flow is subsonic at infinity.

4.2.1 Explicit Time Stepping Schemes

Multi-stage schemes for the numerical solution of ordinary differential equations are usually designed to give a high order of accuracy. Since the present objective is simply to obtain a steady state as rapidly as possible, the order of accuracy is not important. This allows the use of schemes selected purely for their properties of stability and damping.

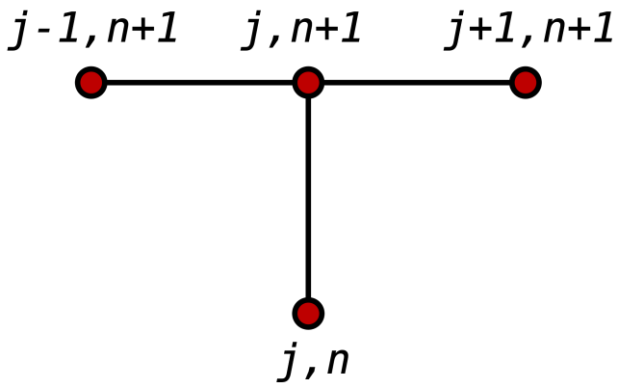

Figure 4.3: Explicit Scheme

For this purpose it pays to distinguish the hyperbolic and parabolic parts stemming respectively from the convective and dissipative terms, and to treat them differently. This leads to a new class of hybrid multi-stage schemes.

Let w^n be the value of w after n time steps. Dropping the subscripts i, j the general $m/$ stage hybrid scheme to advance a time step Δt can be written as

$$\begin{aligned} w(0) &= w^n \\ w(1) &= w(0) - \alpha_1 \Delta t R(0) \\ &\ldots \end{aligned}$$

In order to assess the properties of these schemes it is useful to consider the model problem

$$u_t + u_x + \mu \Delta x^3 u_{xxxx} = 0$$

In the absence of the third order dissipative term this equation describes the propagation of a disturbance without distortion at unit speed. With centered differences the residual has the form

$$\Delta t R i = \lambda (u_{i+1} - u_{i-1}) + \lambda\mu(u_{i+2} - 4u_{i+1} + 6u_i - 4u_{i-1} + u_{i-2})$$

where $\lambda = \Delta t/\Delta x$ is the Courant number. If we consider a Fourier mode

$$\hat{u} = e^{ipx} \text{ the discretization in space yields}$$

where z is the Fourier symbol of the residual. Setting $\xi = p\Delta x$, this is

$$z = -\lambda i \sin\xi - 4\lambda\mu(1 - \cos\xi)^2$$

A single step of the multistage scheme yields

$$\hat{u}^{n+1} = g(z)\hat{u}^n$$

where $g(z)$ is the amplification factor. The stability region of the scheme is given by those values of z for which $g(z) \leq 1$.

Schemes of this subclass have been analyzed in a book by van der Houwen, and more recently in papers by Sonneveld and van Leer, and Roe and Pike. They are second order accurate in time for both linear and nonlinear problems if $\alpha m-1 = 1/2$. An efficient 4 stage scheme, which is also fourth order accurate for linear problems, has the coefficients

$$\alpha 1 = 1/4, \quad \alpha 2 = 1/3, \quad \alpha 3 = 1/2$$

The amplification factor of this scheme is given by the polynomial

$$g(z) = 1 + z + \frac{z2}{2} + \frac{z3}{6} + \frac{z4}{24}$$

where D_x and D_y are difference operators approximating.The scheme is second order accurate in time if $\beta = 1/2$, and in the linear scalar case it will be unconditionally stable for all $\Delta t > 0$ if $\beta > 1/2$.

In this form the scheme is too expensive, since it calls for the solution of coupled nonlinear equations at each time step.

4.2.2 Implicit Schemes

An obvious way to accelerate convergence to a steady state is to increase the time step. The time step of an explicit scheme is limited by the Courant Friedrichs Lewy condition, which requires that the region of dependence of the difference scheme must at least contain the region of dependence of the differential equation. This motivates the introduction of implicit schemes.

The celebrated paper of Beam and Warming give an elegant formulation of implicit schemes for nonlinear hyperbolic equations.
A prototype implicit scheme for a system of equations such as the Euler equations (2.5), can be formulated as

$$w^{n+1} = w^n - \beta\Delta t[D_x \boldsymbol{f}(w^n) + D_y g(w^n)] \\ (1-\beta)\Delta t[D_x \boldsymbol{f}(w^{n+1} + D_y g(w^{n+1}))]$$

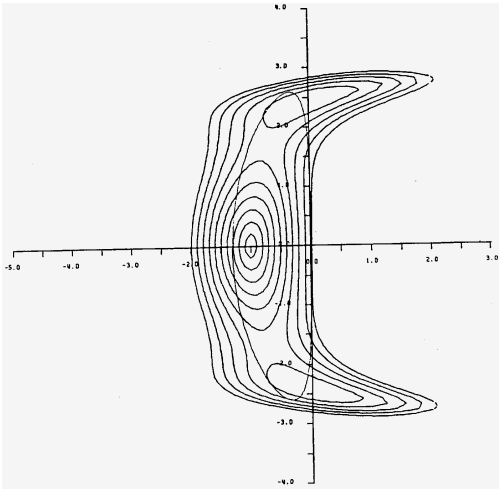

Figure 4.4(a) Stability region of standard 4 stage scheme Contour lines $|g|$ = 1., .9, .8, . . . and locus of $z(\zeta)$ for $\lambda = 2.6$, $\mu = 1/32$
Coefficients $\alpha 1 = 1/4$, $\alpha 2 = 1/2$, $\alpha 3 = ½$

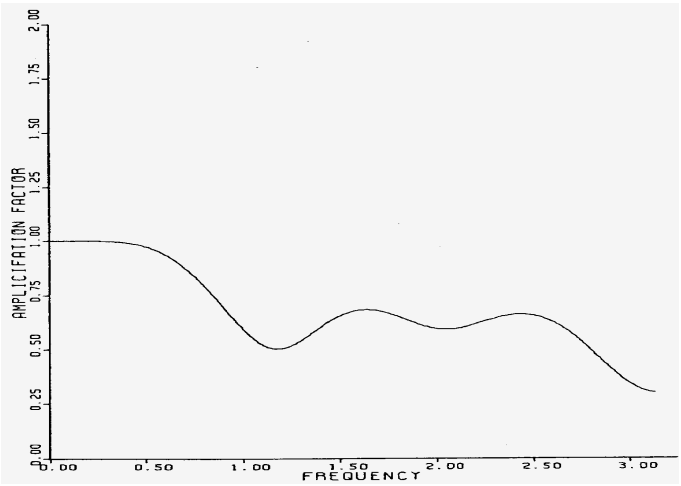

Figure 4.4(b) Amplification factor $|g|$ of standard 4 stage scheme for $\lambda = 2.6, \mu = 1/32$
Coefficients $\alpha 1 = 1/4,\ \alpha 2 = 1/2,\ \alpha 3 = 1/2$

If $\beta = 1/2$ the scheme remains second order accurate because $||\delta w|| = O(n^4)$ operations for inversion. Because of this rapid growth of the operation count with n, the Newton method appears to be uncompetitive except on very coarse meshes.

Beam and Warming derive a relatively inexpensive scheme by replacing the operator on the left side of equation by a product of two one dimensional operators:

$$(I + \beta \Delta t D_X A)(I + \beta \Delta t D_Y B)\delta w + \Delta t R = 0$$

Equation can be inverted in two steps

$$(I + \beta \Delta t D_X A)\delta w^* + \Delta t R = 0$$

$$(I + \beta \Delta t D_Y B)\delta w = \delta w^*$$

Equation remains second order accurate if $\beta = 1/2$, and unconditionally stable for the linear scalar case if $\beta > 1/2$. It also has the desirable feature for steady state calculations that the steady state is independent of Δt. The corresponding scheme in three dimensions is unstable.

This reduction of an implicit scheme to an alternating direction scheme was originally introduced by Mitchell and Gourlay. Briley and Mac- Donald have also developed an equivalent alternating direction procedure for solving nonlinear hyerbolic equations. The alternating direction method has been used for transonic flow calculations by Steger and Pulliam.

An alternative reduction is to replace the operator on the left hand side of equation by a product of factors with upwind and downwind differencing, leading to an LU implicit scheme. Care must then be taken to ensure that the operators in the two factors have respectively positive and negative eigen values. This scheme has been used to calculate transonic flows through cascades by Buratynski and Caughey.

Another approach to Increasing the time step is to replace the residual at each point by a weighted average of residuals at neighboring points. Consider the multi-stage scheme described by equation (5.30). In the one dimensional case one might replace the residual R_i by the average at each stage of the scheme.

$$\bar{R}_i = sR_{i-1} + (1-2s)R_i + sR_{i+1}$$

This smooths the residuals and also increases the support of the scheme, thus relaxing the restriction on the time step imposed by the Courant Friedrichs Lewy condition. If $s > 1/4$, however, there are Fourier modes such that $\bar{R}_i = 0$ when $R_i \neq 0$. To avoid this restriction it is better to perform the averaging implicitly by setting

$$s\bar{R}_{i-1} + (1-2s)\bar{R}_i - s\bar{R}_{i+1} = R_i$$

Foran infinite interval this equation has the explicit solution

$$R_i = \frac{1-r}{1+r} \sum_{q=-\infty} r^q R_{i+q}$$

Thus the effect of the implicit smoothing is to collect information from residuals at all points in the field, with an influence coefficient which decays by factor r at each additional mesh interval from the point of interest

$$1 + r > \lambda$$

$$\frac{}{1-r} \quad \frac{}{\lambda *}$$

4.2.3 Multigrid Scheme

While the available theorems in the theory of multi grid methods generally assume ellipticity, it seems that it ought to be possible to accelerate the evolution of a hyperbolic system to a steady state by using large time steps on coarse grids, so that disturbances will be more rapidly expelled through the outer boundary. The interpolation of corrections back to the fine grid will introduce errors, however, which cannot be rapidly expelled from the fine grid, and ought to be locally damped, if a fast rate of convergence is to be attained. Thus it remains important that the driving scheme should have the property of rapidly damping out high frequency modes.

In a novel multigrid scheme proposed by Ni, the flow variables are stored at mesh nodes, and the rates of change of mass, momentum and energy in each mesh cell are estimated from the flux integral appearing in equation. The corresponding change 6wo associated with the cell is then distributed unequally between the nodes at its four corners by the rule where δw_o is the correction at a corner, and A and B are the Jacobian matrices. The signs are varied in such a way that the accumulated corrections at each node correspond to the first two terms of a Taylor series in time, like a Lax Wendroff scheme. As it stands, this scheme does not damp oscillations between odd and even points. Ni introduces artificial viscosity by adding a further correction proportional to the difference between the value at each corner and the average of the values at the four corners of the cell. Residuals on the coarse grid are formed by taking weighted averages of the corrections at neighboring nodes of the fine grid, and corrections are then

assigned to the corners of coarse grid cells by the same distribution rule. When several grid levels are used, the distribution rule is applied once on each grid down to the coarsest grid, and the corrections are then interpolated back to the fine grid. Using 3 or 4 grid levels, Ni obtained a mean rate of convergence of about .95, measured by the average reduction of the residuals in a multigrid cycle. The performance of the scheme seems to depend critically on the presence of the added dissipative terms to provide the necessary damping of high frequency modes. In Ni's published version of the scheme these introduce an error of first order.

The flexibility in the formulation of the hybrid multi-stage schemes allows them to be designed to provide effective damping of high frequency modes with higher order dissipative terms. This makes it possible to devise rapidly convergent multigrid schemes without any need to compromise the accuracy through the introduction of excessive levels of dissipation.
In order to adapt the multi-stage scheme for a multigrid algorithm, auxiliary meshes are introduced by doubling the mesh spacing. Values of the flow variables are transferred to a coarser grid by the rule, where the subscripts denote values of the mesh spacing parameter, *S* is the cell area, and the sum is over the 4 cells on the fine grid composing each cell on the coarse grid. This rule conserves mass, momentum and energy. With the result that the evolution on the coarse grid is driven by the residuals on the fine grid. This process is repeated on successively coarser grids. Finally the correction calculated on each grid is passed back to the next finer grid by bilinear interpolation.

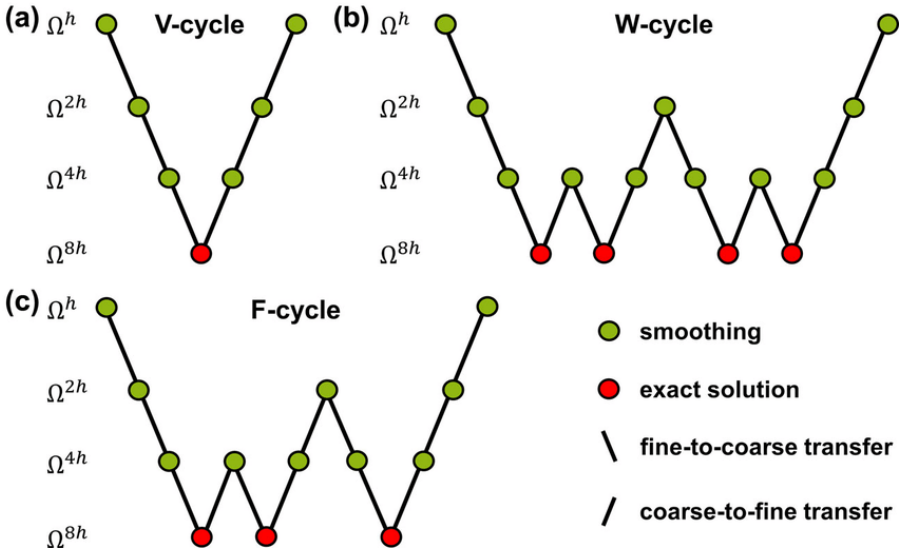

Figure 4.5 Multigrid Scheme

Since the evolution on a coarse grid is driven by residuals collected from the next finer grid, the final solution on the fine grid is independent of the choice of boundary conditions on the coarse grids. The surface boundary condition is treated in the same way on every grid, by using the normal pressure gradient to extrapolate the surface pressure from the pressure-in the cells adjacent to the wall. The far field conditions can either be transferred from the fine grid, or recalculated by the procedure.

It is also possible to use different dissipative terms on the coarse grids. In practice the best convergence rates have been obtained by using second differences. It turns out than an effective multigrid strategy is to use a simple saw tooth cycle (as illustrated in Figure 4.6), in which a transfer is made from each grid to the next coarser grid after a single time step. After reaching

the coarsest grid the corrections are then, successively interpolated back from each grid to the next finer grid without any intermediate Euler calculations. On each grid the time step is varied locally to yield a fixed Courant number, and the same Courant number is generally used on all grids, so that progressively larger time steps are used after each transfer to a coarser grid. In comparison with a single time step of the Euler scheme on the fine grid, the total computational effort in one multigrid cycle is

1 1 4
1 +
+ _____
4 16 + . . . ≤ 3

Plus the additional work of calculating the forcing functions P, and interpolating the corrections.

It is important that the time stepping scheme should be effective at damping the high frequency modes. One can fairly easily devise 3 and 4 stage schemes in the class defined by which meet this requirement.
An effective 3 stage scheme is given by the coefficients

$\alpha 1 = .6, \alpha 2 = .6$

Additional flexibility is provided by a class of schemes in which the dissipative terms are evaluated twice. This may be used to make a further improvement in the high frequency damping properties, or else to extend the stability region along the real axis to allow more margin for the dissipation Introduced by an upwind or TVD scheme of the type described
In the case of pure dissipation ($Q_w = 0$), the amplification factor reduces to

$$g = 1 + x + \alpha 1 \beta z 2$$

The 5 stage scheme combines van der Houwen's optimal coefficients with two evaluations of the dissipative terms to attain a stability interval of 4 along both the imaginary and the real axes.

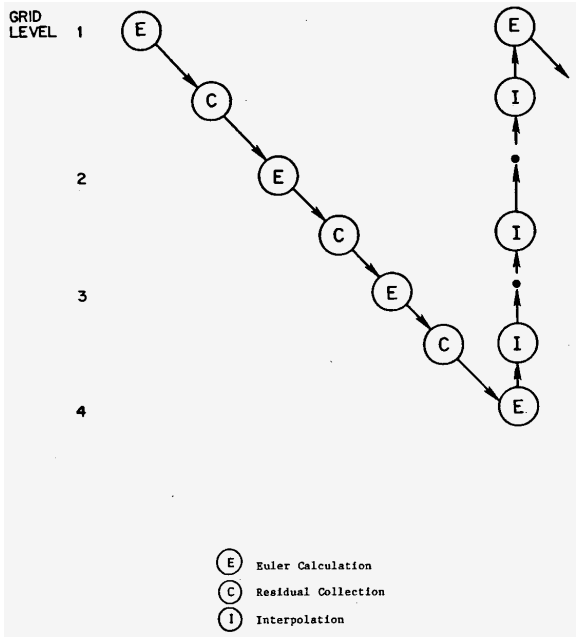

Figure 4.6: Saw Tooth Multigrid Cycle

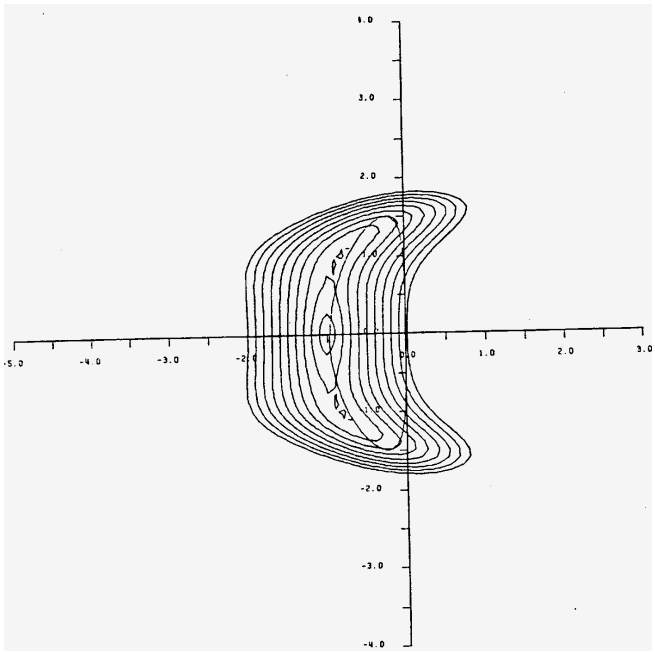

Figure 4.7: Stability region of 3 stage scheme with single evaluation of dissipation Contour lines $|g| = 1., .9, .8, \ldots$ and locus of $z(\xi)$ for $\lambda = 1.5$, $\mu = 0.04$ Coefficients $\alpha 1 = .6$, $\alpha 2 = .6$

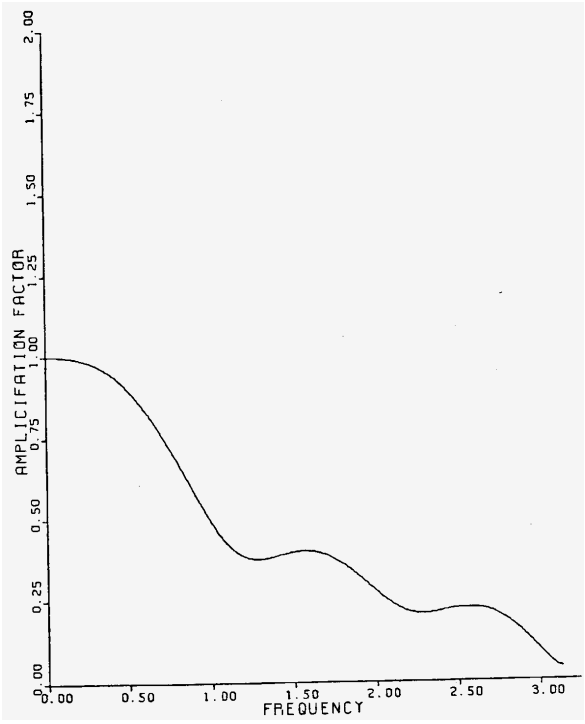

Figure 4.8 Amplification factor $|g|$ of 3 stage scheme with single evaluation of dissipation for $\lambda = 1.5$, $\mu = 1/32$ Coefficients $\alpha 1 = 1/4$, $\alpha 2 = 1/2$, $\alpha 3 = 1/2$

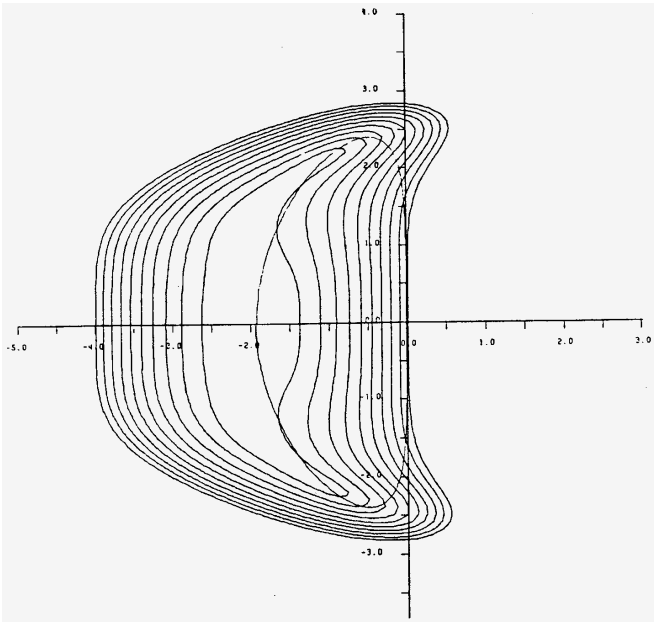

Figure 4.9 Stability region of 4 stage scheme with two evaluations of dissipation Contour lines $|g|$ = 1., .9,.8, . .. and locus of $z(\xi)$ for λ = 2.4, μ = 0.05 Coefficients $\alpha 1$ = 1/4, $\alpha 2$ = 1/3, $\alpha 3$ = 1/2, β = 1

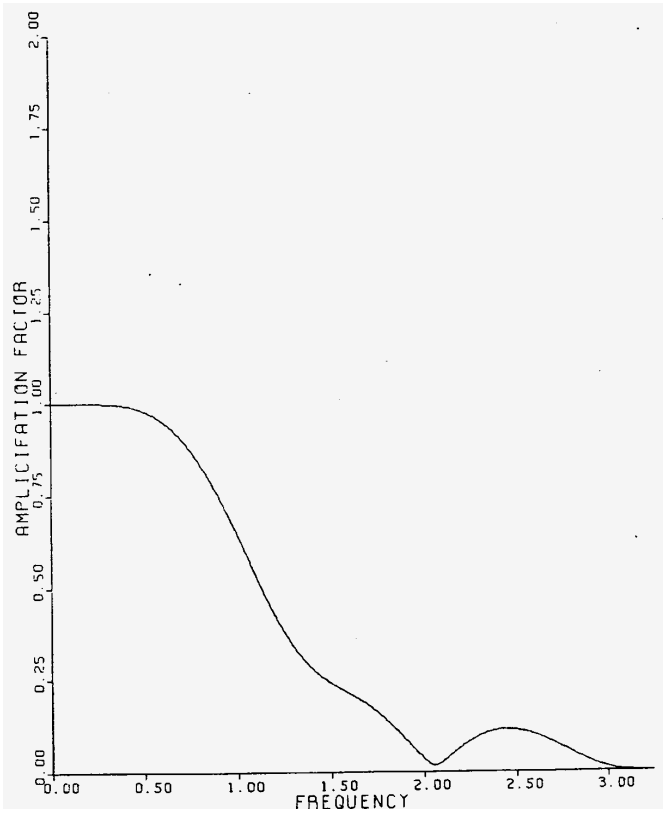

Figure 4.10 Amplification factor 4 stage scheme with two evaluations of dissipation for λ = 2.4, μ = 0.05 Coefficients $\alpha 1$ = 1/4, $\alpha 2$ = 1/3, $\alpha 3$ = 1/2, β = 1

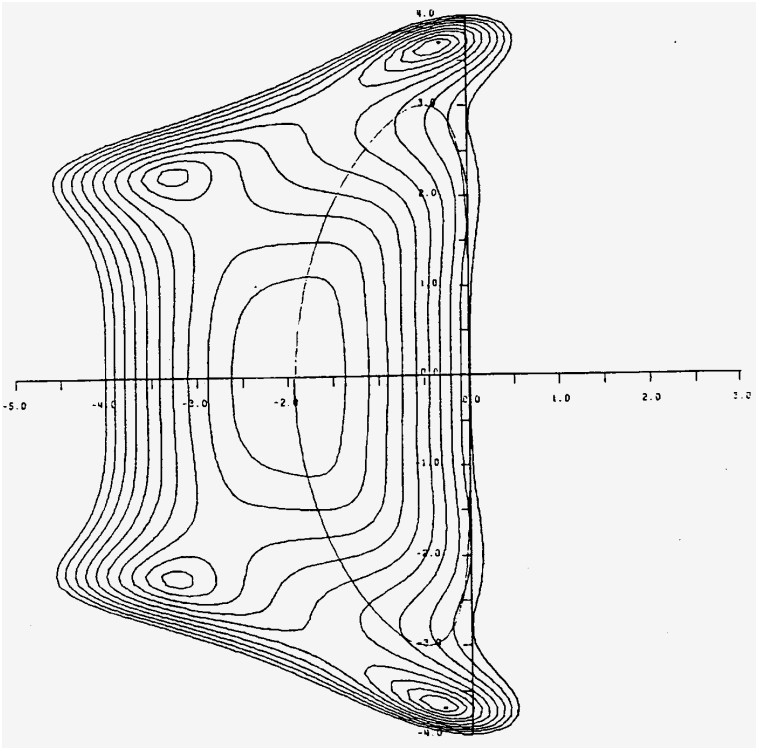

Figure 4.11 Stability region of 5 stage scheme with two evaluations of dissipation Contour lines $|g|$ = .9, .8, .7 . .. and locus of $z(\zeta)$ for λ = 3, μ = 0.04 Coefficients α1 = 1/4, α2 = 1/6, α3 = 3/8, β = 1

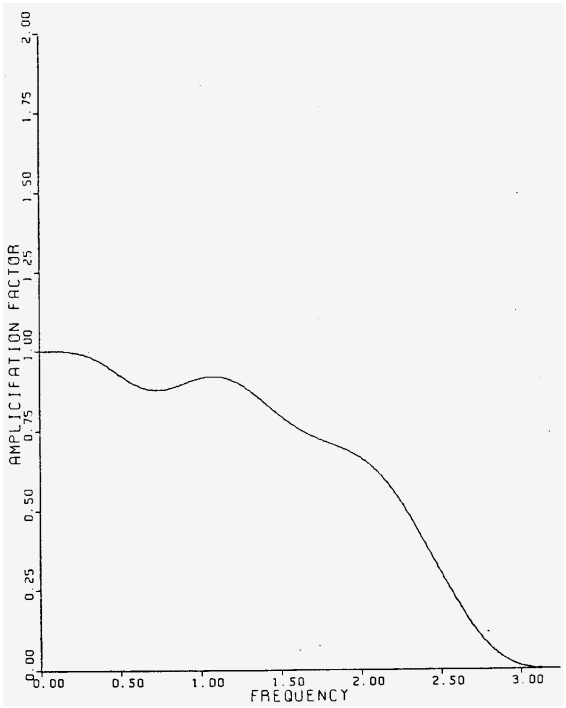

Figure 4.12 Amplification factor 5 stage scheme with two evaluations of dissipation for λ = 3,μ = 0.04 Coefficients α1 = 1/4, α2 = 1/6, α3 = 3/8, β = 1

4.3 Results from the Euler Equations

This section presents some typical results of multigrid calculations of the Euler equations for two-dimensional flow. The 5 stage scheme defined by equation was used in all the examples, and residual averaging was also used to allow steps corresponding to a Courant number of 7.5.
The first example is the flow past a circular cylinder at Mach .50, calculated on a grid with 128 cells in the circumferential direction and 32 cells in the radial direction. The calculation was started from an initial condition of uniform flow.

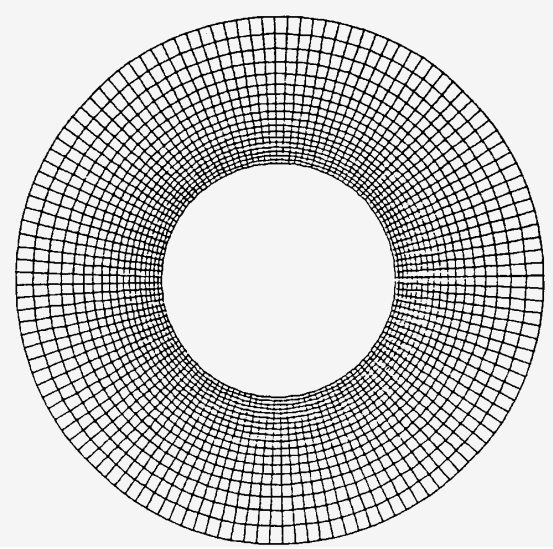

Figure 4.13 Inner part of the grid for 128 X 32 cells

There is a shockwave of moderate strength slightly beyond the crest of the cylinder. One curve shows the decay of the logarithm of the error (measured by the root mean square rate of change of density on the fine grid): the mean rate of convergence is just less than 8 per multigrid cycle. The other curve shows the buildup of the number of grid points in the supersonic zone: it can be seen that the flow field is fully developed in about 30 cycles.

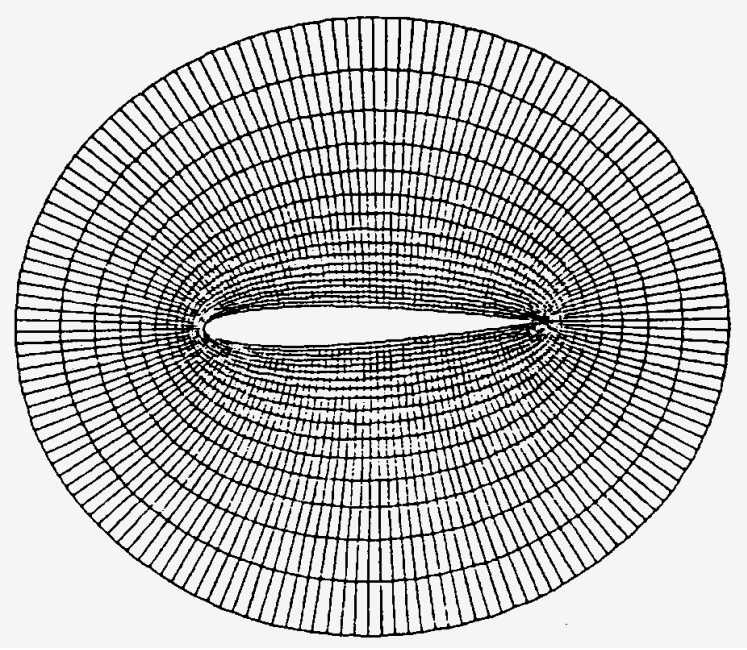

Figure 4.14 Inner part of the grid for NACA 0012 160 X 32 cells

The next examples are transonic flows past airfoils. A 0-mesh was used in these calculations with the outer boundary at a distance of about 50 chords. Each result was obtained with 50 cycles on an 80 x 16 mesh, followed by 50 cycles on a 160 x 32 mesh. This was sufficient for full development of the flow field. The flow past the NACA 0012 airfoil contains a fairly strong shock wave on the upper surface, which is resolved in about 5 mesh cells, and a weak shock wave on the lower surface, which is quite smeared. The Korn airfoil is designed to be shock free at the given Mach number and angle of attack. The result of the Euler calculation is in close agreement with the result of the design calculation.

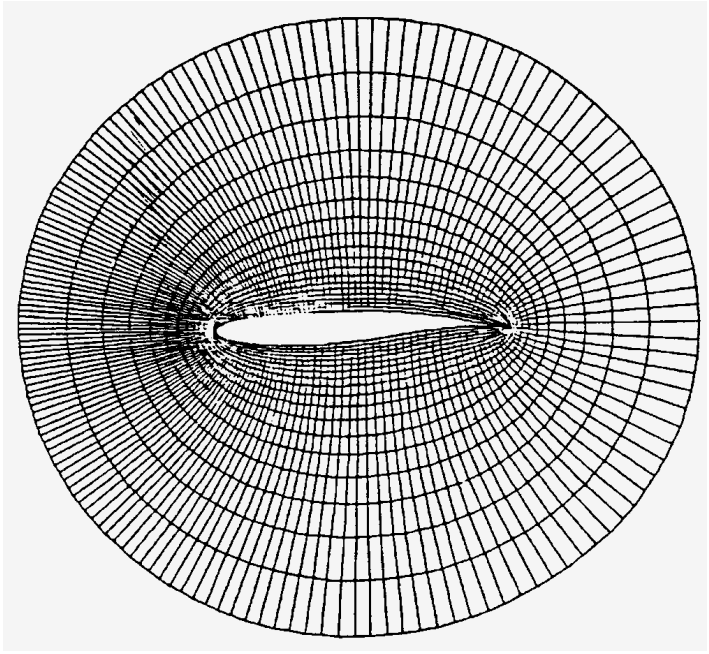

Figure 4.15 Inner part of the grid of Korn airfoil 160 X 32 cells

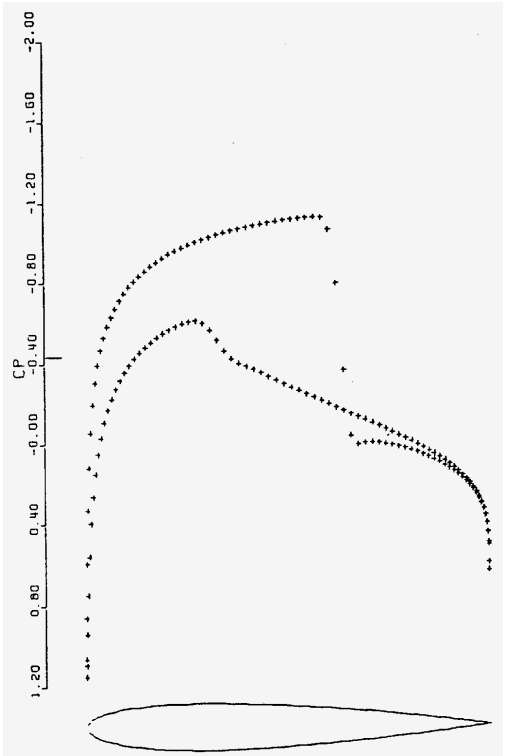

Figure 4.16 Pressure distribution for NACA 0012 Mach .800 α1.25◦ CL .3504 CD .0227 160X32 grid 50 cycles Residual .15210−3

The drag should be zero in a shock free flow, and the calculated value of the drag coefficient *CD* = .0005 is an indication of the level of discretization error. Another measure of error is the entropy, which should also be zero.

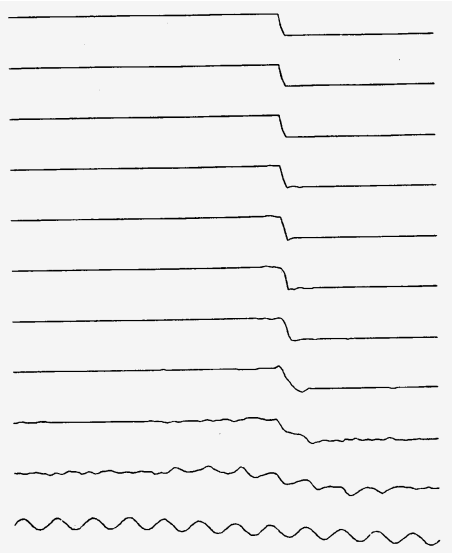

Figure 4.17 Initial state and first 10 cycles in evolution of Burger's equation (reading upwards) Adaptive dissipation(scheme 1a) 128 cells 5 grids $\lambda =$ 2.0

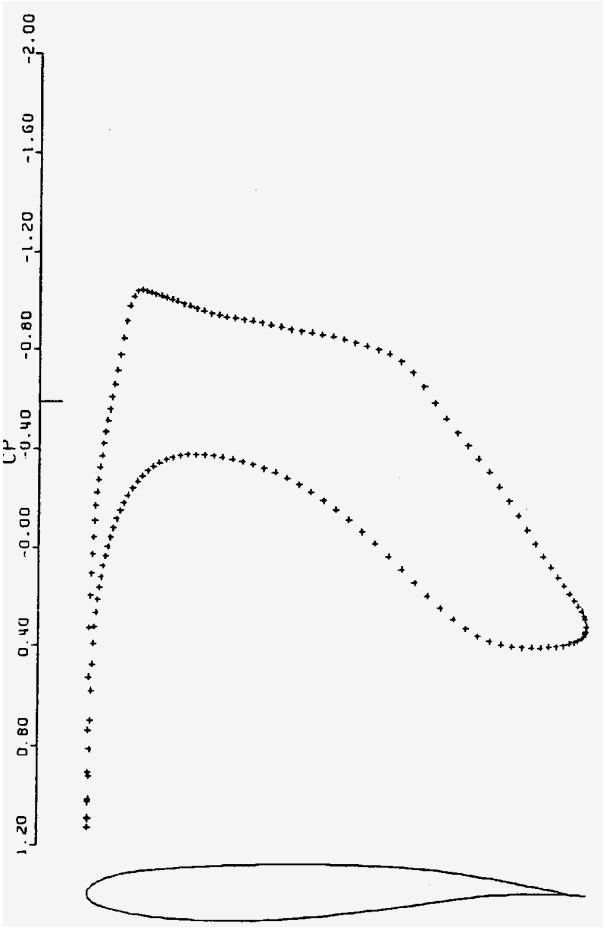

Figure 4.18 Pressure distribution for Korn airfoil Mach .750 α0◦ CL .6254 CD .005 160X32 grid 50 cycles Residual .11210−3

4.4 Viscous Flow Calculations

4.4.1 Boundary Layer Corrections

While it is true that the viscous effects are relatively unimportant outside the boundary layer, the presence of the boundary layer can have a drastic influence on the pattern of the global flow. This will be the case, for example, in the event that the flow separates. The boundary layer can also cause global changes in a lifting flow by changing the circulation. These effects are particularly pronounced in transonic flows. The presence of a boundary layer can cause the location of the shock wave on the upper surface of the wing to shift 20% of the chord.

While we must generally account for the presence of the boundary layer, the accuracy attainable in solutions of the Navier Stokes equations for complete flow fields is severely limited by the extreme disparity between the length scales of the viscous effects, and those of the gross patterns of the global flow. This has encouraged the use of methods in which the equations of viscous flow are solved only in the boundary layer, and the external flow is treated as inviscid. These zonal methods can give very accurate results in many cases of practical concern to the aircraft designer.

In the outer region the real viscous flow is approximated by an equivalent inviscid flow, which has to be matched to the inner viscous flow by an appropriate selection of boundary conditions. In most of the boundary layer the viscous flow equations may consistently be approximated by the boundary layer equations. This is sufficient in regions of weak interaction, in which the viscous effect on the pressure is small. There are, however, regions of strong interaction in which the classical boundary layer formulation fails, because of the appearance of strong normal pressure gradients across the boundary layer. Coupling conditions for the interaction between the inner viscous flow and the outer inviscid flow can be derived from an asymptotic analysis in which the Reynolds number is assumed to become very large. The two solutions could be patched at the outer edge of the boundary layer. It is often more convenient, however, to allow the equivalent inviscid flow to overlap the inner viscous region.

A complete analysis of the viscous flow over an airfoil should include the following principal effects:

1. The displacement effect of the boundary layer over the airfoil
2. The displacement effect of the wake
3. The wake curvature effect induced by the momentum defect in the wake
4. The Interaction of the boundary layer with the trailing edge
5. The interaction of the boundary layer with shock waves

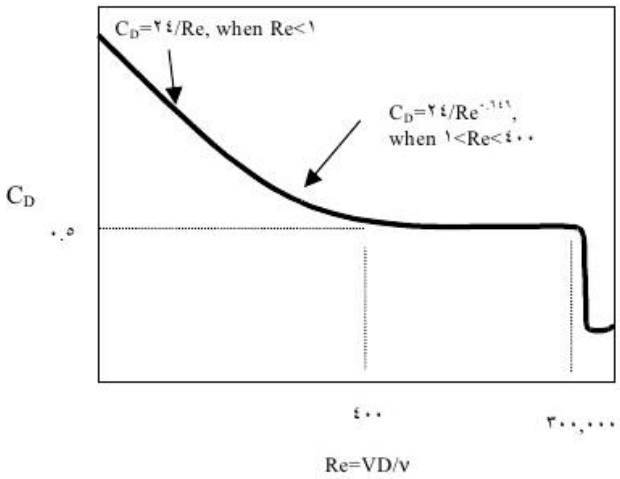

Figure 4. 19 Boundary Layer Corrections

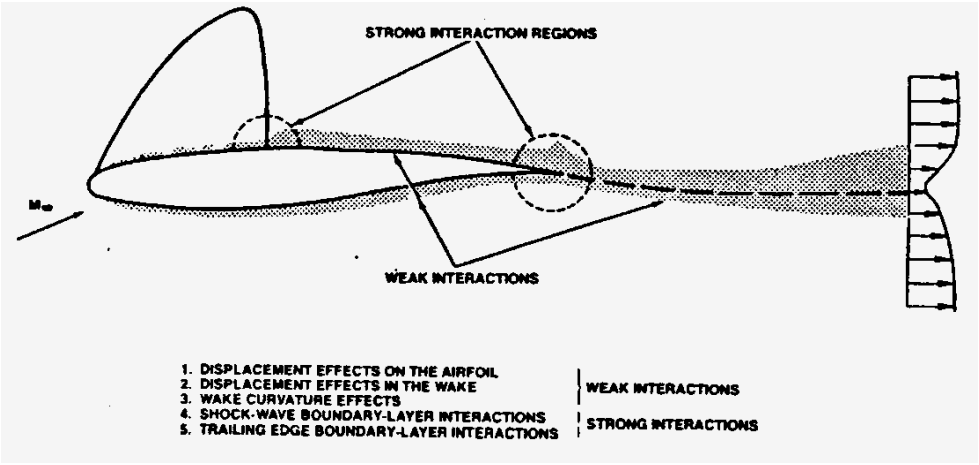

Figure 4.20: Viscid-Inviscid Interactions on Airfoils

The first three of these are weak Interactions, and the last two are strong interactions.

The displacement effect is caused by the outward displacement of the streamlines which results from the reduced mass flow in the boundary layer. This effect can be modeled by adding an equivalent thickness to the body, equal to the displacement thickness of the boundary layer, and applying the flow tangency condition at the surface of the modified body. An alternative formulation, discussed, for example, by Light hill, is to extend the equivalent inviscid flow to the real body, and to apply a transpiration boundary condition. This condition can be derived by considering the defect equation for the difference between the inviscid and viscous flows. By integrating the continuity equation across the boundary layer, and assuming that the inviscid and viscous flows match at the edge of the boundary layer thickness, and the subscript *i* denotes the inviscid flow. This is the boundary condition that is now applied in the calculation of the equivalent inviscid flow.

We can write it as $dQ(\rho v)\text{wall} = ds$

where Q is the mass flux defect defined by the integral in equation (6.1). If the outer inviscid flow is represented by the Euler equations, similar defect equations for the momentum and energy provide the additional boundary conditions that are needed to solve the Euler equations. The displacement effect is usually more pronounced on the upper surface than it is on the lower surface. This leads to an equivalent decambering of the airfoil which acts to reduce the lift.

There is also a displacement effect due to the wake behind the airfoil.

The matching condition for the wake displacement effect is $1[v]\text{wake} = \rho w Q w ds$

where $[v]$ is the jump in the normal velocity across the wake, ρw is the average of the densities in the Inviscid flow on the two sides of the wake, and Qw is the total mass flux defect in the wake. The main result of the wake displacement effect is a reduction in the pressure near the trailing edge, and a corresponding increase in the drag.

The curvature of the wake induces an additional reduction of the lift. Because there is a momentum defect in the wake, it acts like a jet flap with a negative momentum coefficient. The deflection of the wake towards the direction of the outer stream requires a normal pressure gradient, with the result that the pressure at the trailing edge is larger on the upper surface than it is on the lower surface. The Kutta condition for the equivalent inviscid flow must be modified to allow for this difference in the pressures.

The matching condition for the wake curvature effect is $[p]\text{wake} = Cw\kappa w$

where $[p]$ is the jump in the pressure across the wake, Cw is the total momentum defect in the wake and κw is the wake curvature. The magnitude of the wake curvature effect is formally of the same order as that of the displacement effect.

The analysis of the flow in regions of strong interaction is more complicated because of the breakdown of the boundary layer approximation. In the region of the trailing edge the flow in the boundary layer accelerates, and the boundary layer thickness decreases, because the retardation of the flow by skin friction suddenly ceases. Melnik has developed a consistent model of the strong interaction of an un separated turbulent boundary layer with a cusped trailing edge, under the assumption that the Reynolds number is large. As the flow passes through a shockwave, the sharp pressure rise at the foot of the shock wave causes a steep thickening of the boundary layer. As long as the shock wave is not too strong, it turns out, however, that the growth of boundary layer thickness through the shockwave is quite well predicted by boundary layer theory, although the local details of the flow are not accurately modeled. Consequently the coupling condition can still be used to obtain the global flow.

The coupled viscous and inviscid equations are solved iteratively. The simplest procedure is a direct one. The inviscid flow is first solved without a boundary layer, and the boundary layer is calculated using the wall pressure from the inviscid solution as a boundary condition. The inviscid flow is then recalculated with a boundary condition which accounts for the presence of the boundary layer, and the process is repeated until the solution converges. A linearized analysis of this procedure indicates that it will generally be necessary to under-relax the changes in the boundary conditions, and that it will become unstable near a separation point.

This difficulty has led to the introduction of semi-inverse methods in which the transpiration boundary condition is prescribed in both the inviscid flow calculation and the boundary layer calculation. The inviscid flow calculation provides an estimate ue, I of the speed at the edge of the boundary layer. An inverse boundary layer method is used to calculate a corresponding estimate ue, V of the speed at the edge of the boundary layer from the boundary layer equations. In Carter's method, the equivalent mass flux defect Q appearing in the transpiration boundary condition is then multiplied by the correction factor (ue, V)

$$1 + \omega \quad ue, I - 1$$

where ω is a fixed relaxation factor, and the process is repeated. Le Balleur uses a more complicated correction formula with a locally varying relaxation factor. These methods converge for flows containing separated regions. The method of Bauer, Garabedian, Korn and Jameson was the first to incorporate boundary layer corrections into the calculation of transonic potential flow. This method only accounted for displacement effects on the airfoil, and modeled the wake as a parallel semi-infinite strip. Nevertheless, this simple model substantially improved the agreement with experimental data. More complete theoretical models including effects due to the wake thickness and curvature have been developed by Collyer and Lock, Le Balleur, and Melnik, Chow, Mead, and Jameson. Recently Whit field, Thomas, Jameson, and Schmidt have developed a method based on the use of the Euler equations for the inviscid flow. It can be seen that the inclusion of the boundary layer correction shifts the inviscid result into close agreement with the experimental data.

4.4.2Reynolds Averaged Navier Stokes Equations

The simulation of attached flows by zonal methods now rests on a firm theoretical foundation, and has reached a high level of sophistication in practice. The treatment of three-dimensional flows is presently limited by a lack of available boundary layer codes for general configurations. During the last few years there has also emerged the possibility of simulating flows with small separated regions by zonal methods. In cases of massive flow separation, where the flow is often observed to be unsteady, adequate zonal models have yet to be developed. Zonal methods also have the disadvantage that extensions to more general configurations require a separate asymptotic analysis of each component region, such as the corner between a wing and a nacelle pylon, with the result that they can become unmanageable as the complexity of the configuration is increased.

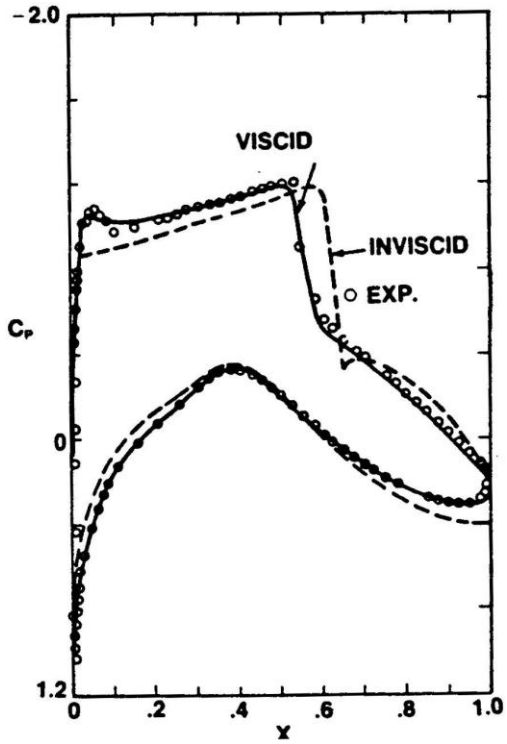

Figure 4.21: Comparisons Between the Viscid and Inviscid Solutions and Experimental Data RAE 2822 Airfoil, Mach .725, CL .743

For these reasons a continuing body of research is directed at the global solution of the Reynolds averaged Navier Stokes equations. The hope is that it will be possible to develop a fairly universal method, which will be able to predict separated flows where the present zonal methods fail, in particular, separated flows that are two-dimensional and unsteady, and three-dimensional separated flows, both steady and unsteady. The present state of the art has been very thoroughly reviewed by Mehta and Lomax [1011. During the past decade the Navier Stokes equations have been the subject of exploratory investigations aimed at establishing the feasibility of their solution, but the methods so far developed have been too expensive to permit their use in a routine production mode.

The principal requirements for a satisfactory solution of the Reynolds averaged Navier Stokes equations are:

1. The reductions of the discretization errors to a level such that any numerically introduced dissipative terms are much smaller than the real viscous terms.
2. The closure of the equations by a turbulence model which accurately represents the turbulent stresses.

The problem of sufficiently reducing the numerical errors is particularly severe in regions of strong interaction, such as the foot of a shock wave, where it may not be possible to attain a high order of accuracy in the difference approximation. The use of a fine enough mesh to overcome this problem has so far been impeded by a lack of powerful enough computers.

The development of the necessary numerical methods is already quite well advanced. The methods described in the previous section can generally be carried over to the Navier Stokes equations. MacCormack has extended both his explicit scheme and his new implicit scheme to the treatment of viscous flows. Diewert has used MacCormack's explicit scheme in his path-finding calculations of viscous flows over airfoils, and Shang and Hankey have recently used the same scheme to calculate the flow past a hypersonic cruiser. Beam and Warming have also made a corresponding extension of their alternating direction implicit scheme to treat viscous flows.

Rapid developments in the speed and memory of computers are steadily improving the prospect of useful simulations of the Reynolds averaged Navier Stokes equations. In the opinion of Mehta and Lomax, the development of reliable turbulence models is now the crucial pacing item. No single turbulence model has been found which can be used in the simulation of a variety of flows. At the present time not much is known about the behavior of turbulence in separated regions, and this has impeded the development of turbulence models for complex three-dimensional flows. It appears that near term improvements in the computational simulation of turbulent flow will probably depend heavily on experimental inputs and checks.

Quite satisfactory methods are now available for the prediction of steady transonic flows using either the potential flow equation or the Euler equations as a mathematical model.
With the advent of a new generation of computers it will be entirely feasible to calculate solutions of the Euler equations for a complete aircraft. A code to solve the Euler equations for wing-body-tail-fin combinations is already operational. The Cray 2, for example, is projected to be at least six times faster than the Cray 1, and will have 256 million words of memory. When a Cray 1 is used to perform calculations with the four- stage scheme, three-dimensional Euler solutions on a 25000 point mesh can be advanced 200 steps in 150 seconds. Assuming that the multigrid acceleration procedure described in Section 5e is introduced, 200 steps should be ample for convergence. Using a grid with one million points, it should therefore be possible to calculate a solution in 20 minutes or less with a Cray 2. One million grid points should be enough for a reasonably accurate representation of an airplane, and the corresponding memory requirement, of the order of 40 million words, would not tax the new machines.
We can also anticipate the routine calculation of unsteady flows for the determination of structural loads. Looking further ahead, we can see on the horizon the increasingly real possibility of simulating the flow past a complete aircraft with the Reynolds averaged Navier Stokes equations.

4.4.2 Steady State Laminar Boundary Layer on a Flat Plate.

We consider a flat plate at $y = 0$ with a stream with constant speed U parallel to the plate. We are interested in the steady state solution. We are not interested in how the flow outside the boundary layer reached the speed U.

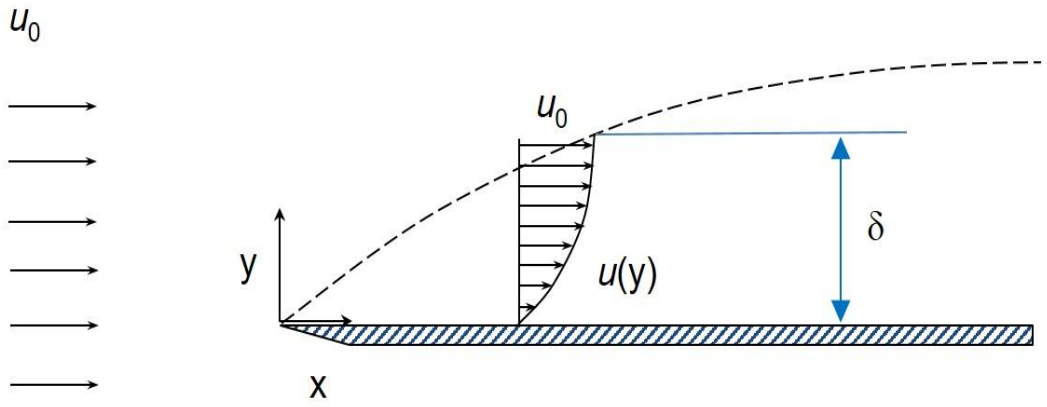

Figure 4.22: Laminar Boundary Layer on a Flat Plate

In this case, we need only to ∂u consider boundary conditions and the equation simplifies since $\partial t = 0$. At the plate surface there is no flow across it, which implies that
$v = 0$ at $y = 0$.

Due to the viscosity we have the no slip condition at the plate. In other words,
$u = 0$ at $y = 0$.
At infinity (outside the boundary layer), away from the plate, we have that
$u \rightarrow U$ as $y \rightarrow \infty$.
For the flow along a flat plate parallel to the stream velocity U, we assume no pressure gradient, soothe momentum equation in the x direction for steady motion in the boundary layer is
$u\partial u + v\ \partial u$
and the appropriate boundary conditions are:

At y = 0, x > 0; u = v =

Ât y → ∞, all x; u = U,

At x = 0;u = U.

These conditions demand an infinite gradient in speed at the leading edge $x = y = 0$, which implies a singularity in the mathematical solution there. However, the assumptions implicit in the boundary layer approximation break down for the region of slow flow around the leading edge. The solution given by the boundary layer approximation is not valid at the leading edge. It is valid downstream of the point $x = 0$.
At $y \rightarrow \infty$, all x; $\partial y = U$.
The boundary value problem admits a similarity solution. We would like to reduce the partial differential equation (3.33) to an ordinary differential equation. We would like to find a change of variables which

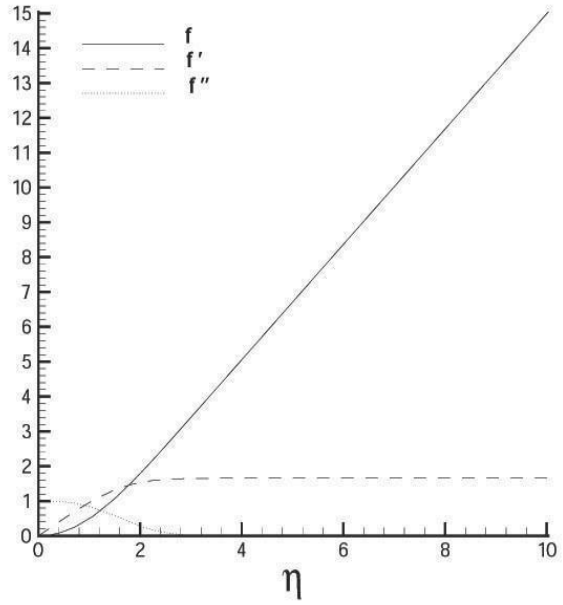

allows us to perform the reduction mentioned above.
Figure 4.23: Functions $f(\eta)$, $ft(\eta)$ and $ftt(\eta)$. The horizontal axis represents the range of values of η considered, and in the vertical axis we have the values of the functions $f(\eta)$, $ft(\eta)$ and $ftt(\eta)$.

Once we have computed numerically $f(\eta)$ and its derivatives up to second order, we can obtain the velocity components (u, v) at any point (x, y) of the flow domain, according to the equations.

4.4.5 Boundary-layer Thickness, Skin friction, and Energy dissipation

According to equation, the pressure across the boundary layer is constant in the boundary-layer approximation, and its value at any point is therefore determined by the corresponding main-stream conditions. If $U(x,t)$ now denotes the main stream velocity.

Elimination of the pressure from equation gives in terms of dimensional variables the boundary layer momentum equation.
In most physical problems the solutions of the boundary layer equations are such that the velocity component u attains its main-stream value U only asymptotically as $R1/2y/L \rightarrow \infty$. The thickness of the layer is therefore indefinite, as there is always some departure from the asymptotic value at any finite distance y from the surface. In practice the approach to the limit is rapid and a point is soon reached beyond which the influence of viscosity is imperceptible. It would therefore be possible to regard the boundary layer thickness as a distance δ from the surface beyond which $u/Y > 0.99$, for example, but this is not sufficiently precise (since $\partial u/\partial y$ is small there) for experimental work, and is not of theoretical significance.

The scale of the boundary layer thickness can, however, is specified adequately by certain lengths capable of precise definition, both for experimental measurement and for theoretical study. These measures of boundary layer thickness are defined as follows:

- Displacement thickness $\delta 1$:
- Momentum thickness $\delta 2$:
- Energy thickness $\delta 3$:

The upper limit of integration is taken as infinity owing to the asymptotic approach of u/U to 1, but in practice the upper limit is the point beyond which the integrand is negligible.
$U\delta 1$ is the diminution, due to the boundary layer, of the volume flux across a normal to the surface; the streamlines of the outer flow are thus displaced away from the surface
Two other quantities related to these boundary layer thickness are the skin friction $\tau\omega$ and the dissipation integral D.

4.5 Turbulent Flat Plate Boundary Layer

A laminar boundary layer over a flat plate eventually becomes turbulent over certain range of Reynolds number. There is no unique value pf Reynolds number, for this change to happen. It mainly depends on the free stream turbulence and surface roughness parameters. With a very fine polished wall and with a quiet free stream, one can delay the transition. A controlling parameter such as the critical *Reynolds number of transition* $Re_{x,\,CR}$ may be defined.
On a flat plate with a sharp leading edge in a typical free stream air flow, the transition occurs between the Reynolds number ranges of 2×10^5 to 3×10^5.
So the transitional Reynolds number is normally taken as $Re_{x,\,CR}=3\times10^5$.

The complex process of transition from laminar to turbulent flow involves the instability in the flow field. The small disturbances imposed on the boundary layer flow will either grow (i.e. instability) or decay (stability) depending on the location where the disturbance is introduced. If the disturbance occurs at a location where $Re_x < Re_{x,\,CR}$, then the boundary layer will return to laminar flow at that location. Disturbances imposed on locations $Re_x > Re_{x,\,CR}$ will grow and the boundary layer flow becomes turbulent from this location. The transition to turbulence involves noticeable change in the shape of boundary layer velocity profile as shown in Fig. 4.24. As compared to laminar profiles, the turbulent velocity profiles are flatter and thicker at the same Reynolds number. Also, they have larger velocity gradient at the wall.
There is no exact theory for turbulent flat plate flow rather many empirical models are available. To begin with the analysis of turbulent boundary layer, let us recall the momentum-integral relation which is valid for both laminar as well as turbulent flows.

$$\tau_w(x) = \rho U^2 \frac{d\theta^*}{dx}$$

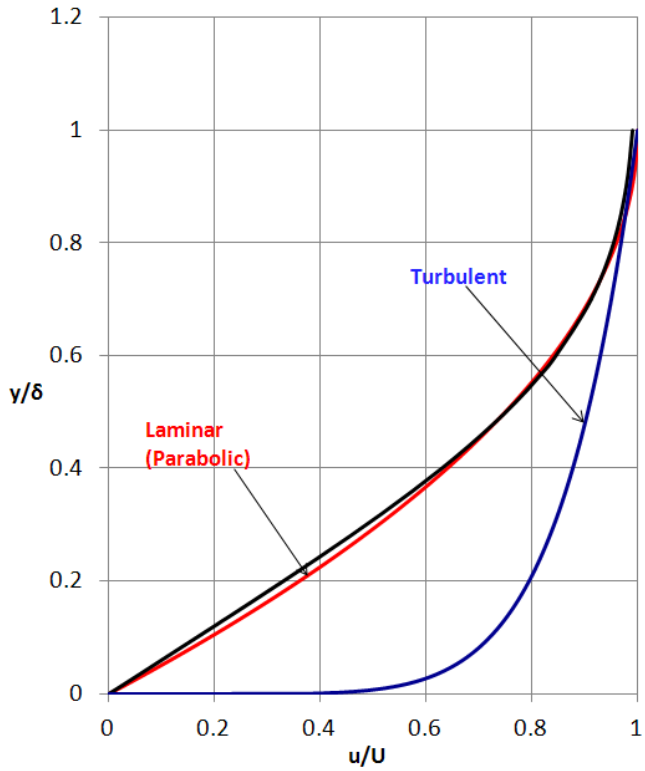

Fig. 4.24: Comparison of laminar and turbulent boundary layer profiles for flat plate.

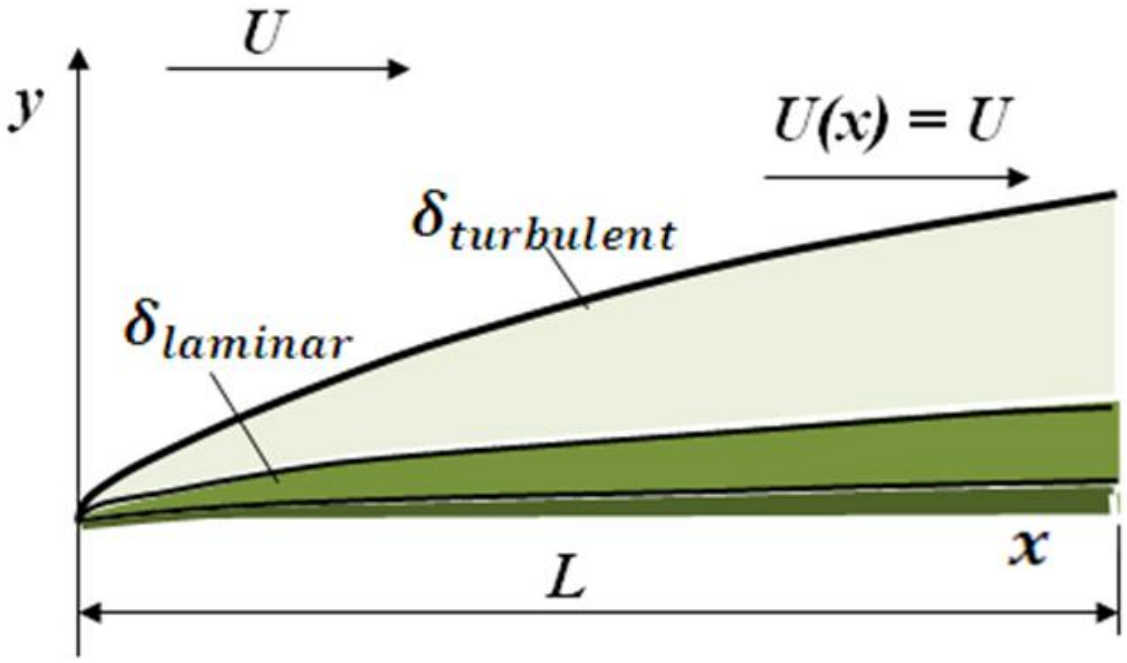

Fig. 4.25: Comparison of laminar and turbulent boundary layer profiles for flat plate.

Parameters	*Laminar (Blasius solution)*	*Turbulent (Prandtl approximation)*
Boundary layer thickness	$\frac{\delta}{x}=\frac{5}{\sqrt{\mathrm{Re}_x}}$	$\frac{\delta}{x}=\frac{0.16}{(\mathrm{Re}_x)^{1/7}}$
Displacement thickness	$\frac{\delta^*}{x}=\frac{1.72}{\sqrt{\mathrm{Re}_x}}$	$\frac{\delta^*}{x}=\frac{0.02}{(\mathrm{Re}_x)^{1/7}}$
Momentum thickness	$\frac{\theta^*}{x}=\frac{0.664}{\sqrt{\mathrm{Re}_x}}$	$\frac{\theta^*}{x}=\frac{0.016}{(\mathrm{Re}_x)^{1/7}}$
Shape factor	$H=\frac{\delta^*}{\theta^*}=2.59$	$H=\frac{\delta^*}{\theta^*}=1.25$
Local skin friction coefficient	$c_f=\frac{0.664}{\sqrt{\mathrm{Re}_x}}$	$c_f=\frac{0.027}{(\mathrm{Re}_x)^{1/7}}$
Wall shear stress	$\tau_w=\frac{0.332\mu^{1/2}\rho^{1/2}U^{3/2}}{x^{1/2}}$	$\tau_w=\frac{0.0135\mu^{1/7}\rho^{6/7}U^{13/7}}{x^{1/7}}$
Drag coefficient	$c_d=\frac{1.328}{\sqrt{\mathrm{Re}_L}}$	$c_d=\frac{0.031}{(\mathrm{Re}_L)^{1/7}}$

4.4.6 Two-dimensional Laminar Jet.

We consider a two-dimensional jet as illustrated in the figure below. *x* is the horizontal coordinate and *y* is the vertical coordinate. *u* and *v* are, respectively, the horizontal and vertical fluid velocities. The jet in the direction of the *x* axis generates a flow where the fluid velocity along the *y* axis tends to zero. We assume that the boundary layer approximation is valid and the governing equation for the fluid motion are equations but with $\partial u/\partial t$. The pressure does not vary in the *y* direction according to equation, soothe pressure is constant across the boundary layer and its gradient is given by the pressure gradient outside the boundary layer.

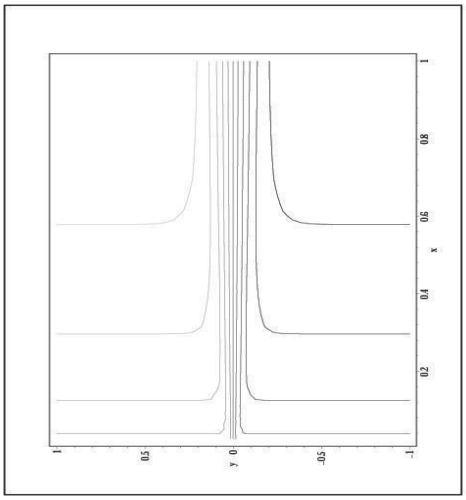

Figure 4.26: Streamlines obtained from equation (8.176) with $M = 1000kg/sec2$, $v = 0.01m2/sec$ and $\rho = 1000kg/m3$.

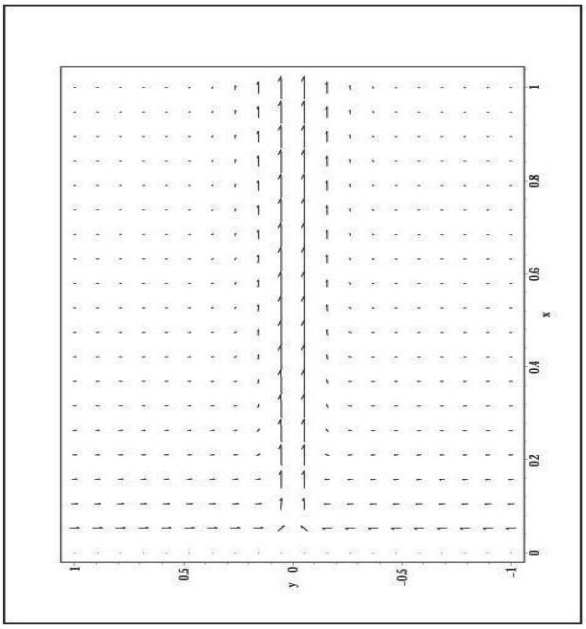

Figure 4.27: Velocity field obtained from equations (8.177) and (8.178) with $M = 1000kg/sec2$, $v = 0.01m2/sec$ and $\rho = 1000kg/m3$.

UNIT-V
TIME DEPENDENT METHODS

5.1 TIME-DEPENDENT METHODS

- The time-dependent scalar-transport equation
- One-step methods for single variables
- One-step methods for CFD
- Multi-step methods
- Uses of time-marching in CFD

5.1.1 The Time-Dependent Scalar-Transport Equation

The time-dependent scalar-transport equation for an arbitrary control volume is

$$\frac{\mathrm{d}}{\mathrm{d}t}(amount) + net\ \ flux = source$$

$$\frac{\mathrm{d}}{\mathrm{d}t}(\rho V \phi_P) + a_P \phi_P - \sum_F a_F \phi_F = b_P$$

As a preliminary we examine numerical methods for the first-order differential equation

$$\frac{\mathrm{d}\phi}{\mathrm{d}t} = F(t, \phi), \qquad \phi(0) = \phi_0$$

Initial-value problems of the form (3) are solved by time-marching. There are two main types of method:

- One-step methods: use the value from the previous time level only;
- Multi-step methods: use values from several previous times.

5.1.2 CFL conditions

In mathematics, the Courant–Friedrichs–Lewy (CFL) condition is a necessary condition for convergence while solving certain partial differential equations (usually hyperbolic PDEs) numerically by the method of finite differences. It arises in the numerical analysis of explicit time integration schemes, when these are used for the numerical solution. As a consequence, the time step must be less than a certain time in many explicit time-marching computer simulations, otherwise the simulation produces incorrect results.

$$\frac{\partial u}{\partial t} + a\frac{\partial u}{\partial x} = 0$$

5.2 FTCS scheme

In numerical analysis, the FTCS (Forward-Time Central-Space) method is a finite difference method used for numerically solving the heat equation and similar parabolic partial differential equations. It is a first-order method in time, explicit in time, and is conditionally stable when applied to the heat equation. When used as a method for advection equations, or more generally hyperbolic partial differential equation, it is unstable unless artificial viscosity is included.

By definition, is explicit because u_I at time step $n + 1$ can be solved explicitly in terms of the known quantities at the previous time step n, thus called an explicit scheme.

Order of accuracy of the scheme is $O(\Delta t, \Delta x^2)$. The method is conditionally stable, and the stability condition is given by $d \leq 0.5$.

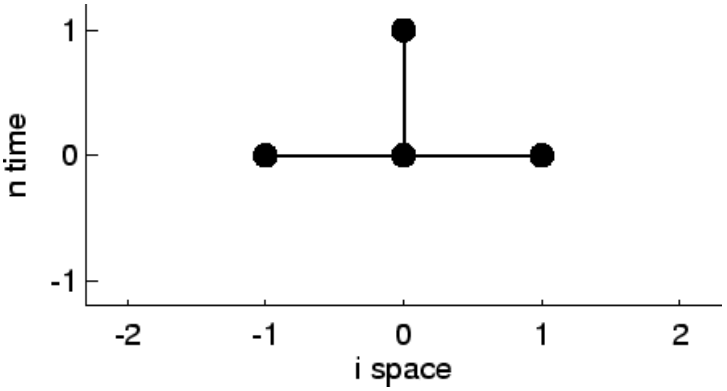

Figure 5.2: Explicit FTCS scheme.

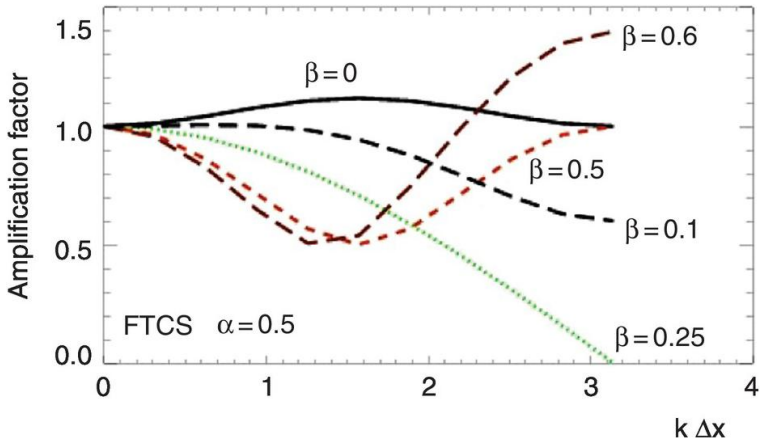

Figure 5.3: Explicit FTCS

5.3 BTCS scheme

Writing this equation for all grid points at n +1 time level, leads to a tridiagonal system and can be solved using TDMA algorithm. The BTCS scheme is also known as the Laasone method. This is unconditionally stable. Order of accuracy of the scheme is $O(\Delta t, \Delta x^2)$.

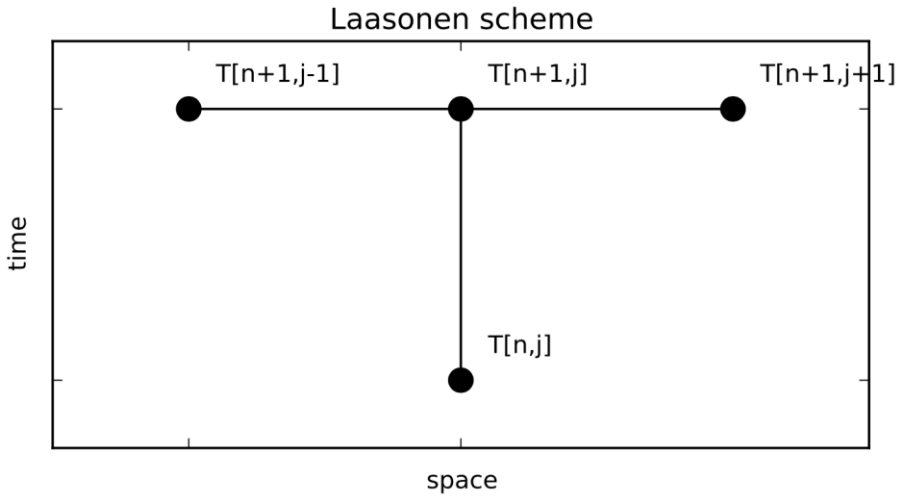

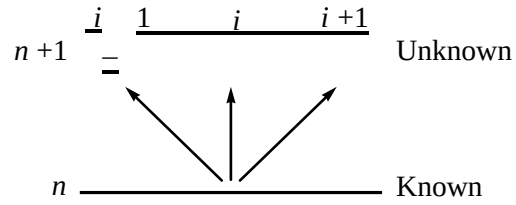

Figure 5.4: Computational molecule for the implicit BTCS scheme.

5.3.1Richardson method

Richardson method is a Central Time Central Space (CTCS) scheme for parabolic type diffusion equations. This is known as the Richardson method. Order of accuracy of the scheme is $O(\Delta t^2, \Delta x^2)$. A stability analysis would show that it is unconditionally unstable, no matter how small t is. Thus, it is of no practical use. It may be noted that the unstable behavior refers to the equation as a whole. It is a stable method for convection equation.

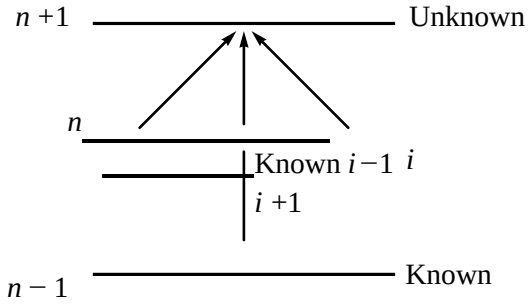

Figure 5.5: Computational molecule for the Richardson Method.

5.3.2 Dufort–Frankel scheme

The Richardson method can be modified to produce a stable algorithm. This is achieved n by replacing u_i on the right-hand side with the time-average of previous and current time values at n − 1 and n + 1. This new formulation is called Dufort–Frankel scheme.

This scheme is explicit and can be shown to be unconditionally stable by the von Neumann stability analysis. Since Dufort–Frankel stencil is constructed on the basis of an ad-hoc modification of the Richardson scheme, its consistency must be examined by computing the modified equation. Note that the Dufort–Frankel method is a two-level method since the stencil contains values of *u* at two time levels other than the current level *n*.

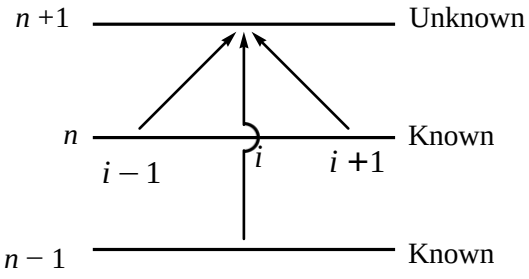

Figure 5.6: Computational molecule for the Dufort–Frankel scheme.

Consequently, to start the computation, values of u at n and $n-1$ are required. Therefore, either two sets of initial data must be available or from a practical point of view, a one-step method may be used as a starter to generate additional data.

Order of accuracy of the scheme is $O(\Delta t^2, \Delta x^2, (\Delta t/\Delta x)^2)$. Even though the method is unconditionally stable, accurate solution will be obtained only if Δt, Δx.

5.3.3 Crank–Nicolson scheme

Both FTCS and BTCS schemes are first-order in time and second-order in space. Since they are first-order accurate in time, the time step Δt must be kept small to ensure acceptable accuracy. A scheme having a second-order accuracy in time for parabolic PDE can be obtained by taking the average of the FTCS and BTCS schemes.

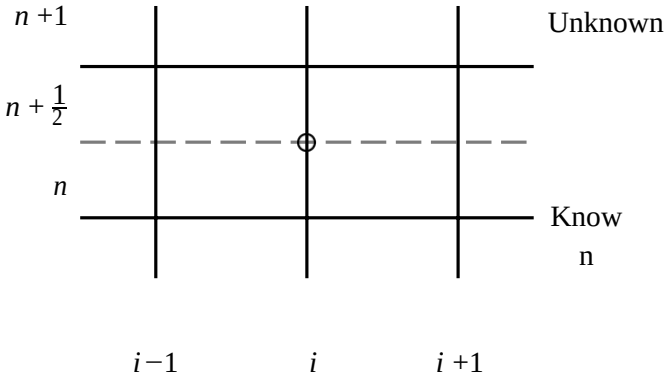

Figure 5.7: Grid points for the Crank–Nicolson scheme.

The new scheme known as the *Crank–Nicolson scheme* or *trapezoidal differencing scheme* named after their inventors John Crank and Phyllis Nicolson.

Where we have expressed u_{xx} at $n + 1/2$ time level by the average of the previous and current time values at n and $n + 1$ respectively. Crank–Nicolson method can also be written as an algorithm. A stability analysis would indicate that this implicit method is unconditionally stable.

5.3.4 Generalized implicit method

A general form of the finite difference approximation for diffusion equation may be obtained from Crank–Nicolson method by expressing space derivative by a weighted average of previous and current time values at n and $n + 1$. Where in practice $0 < \beta < 1$. This is known as the β-method. $\beta = 0$ gives the explicit FTCS scheme, $\beta = 1$ gives the fully implicit BTCS scheme, and $\beta = 1/2$ gives the Crank–Nicolson method. For $1/2 \leq \beta \leq 1$, the method is unconditionally stable, but for $0 \leq \beta < 1/2$

5.3.5 Alternating Direction Implicit (ADI) method

It is clear that, when implicit schemes are applied to multidimensional problems, the resulting implicit matrix system is not tridiagonal anymore as for three point discretizations on one-dimensional equations. Since each discretized equation consists of five unknowns, we obtain a pentadiagonal matrix system. Unfortunately, we do not have an efficient direct solver, such as Thomas algorithm, for the solution of a pentadiagonal matrix system. However, a multidimensional

problem can be split into a series of pseudo-one-dimensional problems and each of which can be solved using Thomas algorithm. More specifically, in a two-dimensional problem, each time step is split into two sub step of equal duration $\Delta t/2$ and approximating the spatial derivative in a partially implicit manner while alternating between x and y directions. This method is called Alternating Direction Implicit (ADI) method. The following are the two steps of ADI method by Peaceman and Rachford.

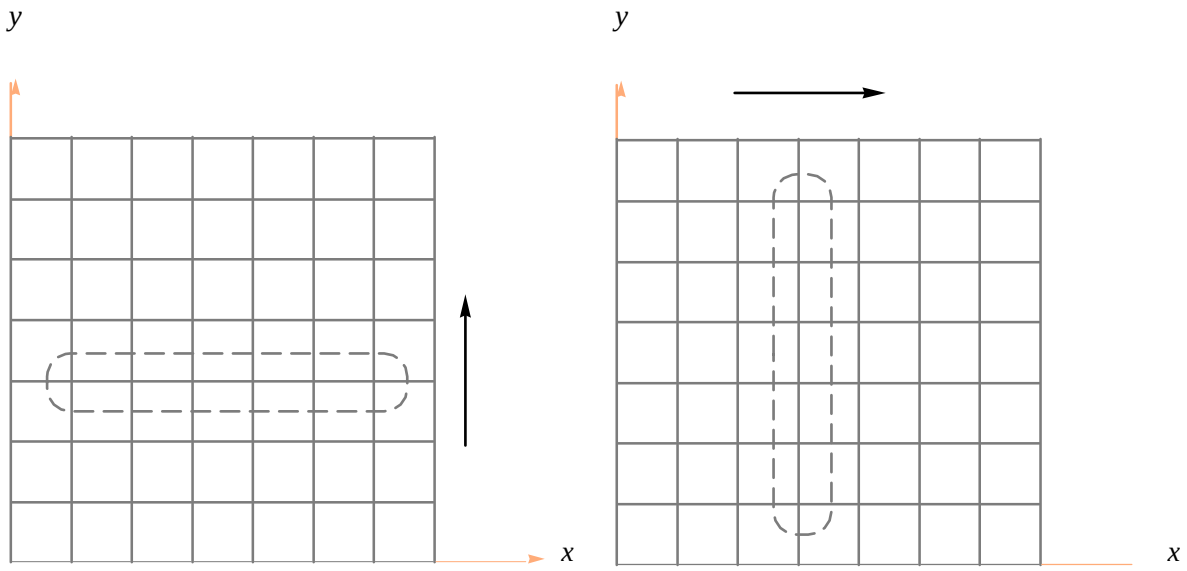

Figure 5.8: Grid system for ADI method.

The ADI formulation can be shown to be an approximate factorization method based on the Crank–Nicolson scheme.

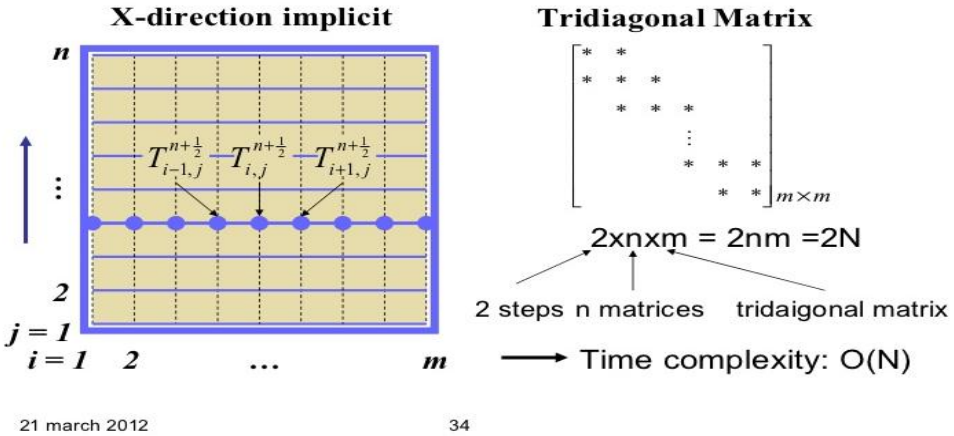

Figure 5.9 Analysis of ADI Method

5.3.6 Splitting or fractional step method

In the fractional step method, introduced by Yanenko, the original multidimensional equation is split into a series of one-dimensional equations and then solve them sequentially TDMA. This formulation can also be considered as a approximate factorization method. The method provides the following discretized equations for two-dimensional diffusion equation. This scheme is of the order of $O\ \Delta t,\ \Delta x^2,\ \Delta y^2$ and is unconditionally stable. The temporal accuracy can be made second-order by using a Crank–Nicolson scheme within each fractional step.

This scheme is of the order of $O^{\cdot}\Delta t^2,\ \Delta x^2,\ \Delta y^{2\cdot}$ and is unconditionally stable.